UNIVERSITA' DEGLI STUDI DI PADOVA

Dipartimento Dipartimento di Ingegneria Industriale DII

Corso di Laurea Magistrale in Ingegneria Energetica

Tesi di Laurea

# Experimental investigation of single and two-phase heat transfer for propylene in a horizontal structured tube

**Relatore**
Prof. Davide Del Col

**Correlatore**
Prof. Andrea Luke

Laureando: Francesco Bolcato

Anno accademico 2020-2021

*Alla mia famiglia*

*E a tutti gli amici che mi hanno sempre sostenuto*

# Contents

# List of Figures

# Nomenclature

**Dimensionless Numbers**

| | |
|---|---|
| $Gr$ | Grashoff number |
| $Nu$ | Nusselt number |
| $Pr$ | Prandtl number |
| $Re$ | Reynolds number |

**Greek Symbls**

| | |
|---|---|
| $\alpha$ | Heat transfer coefficient |
| $\beta$ | Inclination of the tube |
| $\lambda$ | Thermal conductivity |
| $\mu$ | Dinamic viscosity |
| $\rho$ | Density |
| $\tau$ | Shear force |
| $\upsilon$ | Kinematic viscosity |
| $\xi$ | Void fraction |

**Index**

| | |
|---|---|
| $a$ | Accelleration component |
| $ext$ | Outer tube |
| $f$ | Frictional component |

$g$ Gas phase

$gr$ Gravitational component

$HO$ Homogeneous

$in$ Internal surface of the tube

$inlet$ Inlet condition

$ins$ Insulation

$int$ Inner tube

$l$ Liquid phase

$lm$ Logaritmic mean temperature

$local$ Local parameter

$loss$ Losses

$m$ Mean

$mean$ Integral parameter

$oil$ Therminol

$out$ External surface of the tube

$outlet$ Outlet condition

$p$ Propylene

$sat$ Saturation condition

$wall$ Wall of tube

**Latin Symbols**

$\dot{G}$ Specific mass flux

$\dot{Q}$ Heat flux

$\dot{q}$ Heat flux density

$A$ Area

| | |
|---|---|
| $cp$ | Specific heat capacity |
| $d, D$ | Diameter |
| $f$ | Friction factor |
| $g$ | Gravitational accelleration |
| $GWP$ | Global Warming Potential |
| $h$ | Hentalpy |
| $J$ | Surface velocity |
| $L$ | Lenght |
| $l\dot{m}$ | Mass flux |
| $ODP$ | Ozone Depletion Potential |
| $r$ | Radius |
| $RTD$ | Resistance Temperature Detector |
| $T$ | Temperature |
| $TC$ | Thermocouples |
| $U$ | Overall heat trasnfer coefficient |
| $u$ | Velocity |
| $x$ | Vapour quality |
| $z$ | Position along the tube |

**Abstract**

The present work has been developed and performed at the Technical Thermodynamics Faculty of the University of Kassel within the Erasmus exchange program of the University of Padova. Two-phase flows processes are used in a variety of industries and applications. Knowledge of the condensation process of hydrocarbons is limited compared to other fluids such as CFCs or HFCs since the number of studies carried out on the subject is small. Therefore, the Technical Thermodynamics Faculty of the University of Kassel built a test facility to carry out research regarding single and two-phase heat transfer processes of hydrocarbons. For the development of this work several tests were carried out, both with single and two-phase fluids. In the single-phase tests, superheated propylene steam with pressure between 11,4 $bar$ and 27 $bar$, inlet temperatures between 70 $°C$ and 74 $°C$ and Reynolds numbers of 500,000-800,000 was investigated. Measurements for two-phase heat transfer were carried out at pressure between 11,38 and 22,75 $bar$, mass flow densities of $300 - 600\ kg/(m^2 s)$ and a flow steam content of $0.1 - 0.9$. The experimental data showed a confirmation of the trend reported in the literature for the gas cooling processes while for the two-phase condensation tests the pressure loss and heat transfer were reported as a function of the reduced pressure $p_r$, the specific mass flux $\dot{G}$ and the vapour quality $x$.

# Chapter 1

# INTRODUCTION

Many industrial processes are related to two-phase flows, where a phase change occurs, since a high heat flux density $\dot{q}$can be transferred with a low temperature gradient $\Delta T$. Two-phase flows are very complex processes so that a good knowledge in the areas of two-phase heat and momentum transport is required for a full understanding of the processes. For the design of corresponding systems, a calculation method is therefore used with which the two-phase pressure loss and heat transfer can be predicted. However, these existing calculation models show considerable deviations due to physical mechanisms that are not fully understood, so that experimental data of synthetic and non-natural refrigerants are used to adapts the models. Natural refrigerants such as hydrocarbons have only been investigated for a few years due to ongoing resource scarcity, so the database for natural refrigerants still has significant deficiencies [31]. This leads to over dimensioning and thus a waste of resources in the design of heat exchangers. The aim of this work is therefore to gain better knowledge about the two-phase heat transfer and pressure loss during the condensation of natural refrigerants in the horizontal micro-fin pipes. The measurements are carried out with the natural refrigerant propylene, which has a high potential for improvement due to its better transport properties and low GWP and ODP [37]. For this purpose, experimental investigations are carried out for the heat transfer and pressure loss in horizontal flow condensation at a test facility located at the Institute of Technical Thermodynamics. Furthermore, calculation models for heat transfer and pressure drop are presented, which are described for the assumed constraints. The experimental results are discussed and summarized in comparison to calculated values using the presented models. In the Thermodynamics Faculty of Kassel University, a test facility has been built to develop researches on the efficiency during condensation of hydrocarbons. Other plants with a similar aim are composed of a unique path where the working fluid

flows at a defined conditions. The peculiarity of this facility is the multi-phase pump installed to treat the two phases separately. Both liquid and gas phase flows in different paths before entering the test pipe, allowing to have improved control over the conditions of the fluid before the mixing. In this way, it is possible to recreate an artificial two-phase flow that allows performing tests in particular conditions. In the third chapter of this work, a literature review is presented regarding the two-phase flow patterns inside horizontal pipes and the characteristics of the enhanced surfaces. It is also presented an extensive review of the single and two-phase heat transfer and pressure drop. In the fourth chapter, the experimental set up is presented. A description of the test facility is done, focusing on the sensors installed and on the fluids employed. The fifth chapter is about the data reduction used for the data analysis for both local and integral measurement. The uncertainty analysis is also presented in the fifth chapter. In the sixth chapter, the experimental results are presented and analyzed. Finally, in the seventh chapter, the conclusions of this work are presented. The present work, with all the practical tests needed, was developed at the Institute of Technical Thermodynamics of the University of Kassel (Germany) within the Erasmus exchange program of the University of Padova (Italy).

# Chapter 2

# THEORETICAL BASIS

## 2.1 Two phase flow patterns

The processes with phase change are very important in the industrial field. The possible applications of the two-phase flow are numerous and one of the most important appliances are inside the vapour power plant where the two-phase flow is present in the evaporator and the condenser. Another relevant field where the two-phase flow is essential, are the cooling and chemical industries where the condensation and the vaporization of the refrigerants are the crucial processes inside the reverse cycle. Among all the possible two-phase flow the gas-liquid one is the most complex because the interface between the compounds is deformable and one of the two phases, the gaseous one, is compressible. These cause the creation of a big number of possible flow configurations and difficulties on the definition of the two-phase regime map. The classification of two-phase regimes is important because each one is characterized by a specific heat transfer and pressure drop definition and these parameters are fundamental for having a correct identification of the overall process. The principal characteristics that allow us to define the flow regime are:

- The vapour quality $x$ of the two-phase flow

$$x = \frac{\dot{m}_g}{\dot{m}_g + \dot{m}_l} \tag{2.1}$$

  is defined as the ratio between the gas flow $\dot{m}_g$ and the overall flow $\dot{m}$ which is described as the sum of the vapour flow and the liquid flow $\dot{m}_l$.

- The void fraction of the mixture $\xi$ defined as

$$\xi = \frac{A_g}{A} \tag{2.2}$$

is the ratio between the transverse area of the flow occupied by the gas phase $A_g$ and the total transverse area $A$.

- The surface velocities of the gas and liquid phase are described as

$$J_g = \frac{\dot{m} * x}{\rho_g * A} = \frac{G * x}{\rho_g} = \frac{\dot{Q}_g}{A} \tag{2.3}$$

$$J_l = \frac{\dot{m} * (1-x)}{\rho_l * A} = \frac{G * (1-x)}{\rho_l} = \frac{\dot{Q}_l}{A} \tag{2.4}$$

where $G[\frac{kg}{\frac{m^2}{s}}]$ is the specific mass flux defined as the ratio between the total flux and the transverse area of the flux. The sum of the two-surface velocities is described as the surface velocity of the mixture that is also the ratio between the volumetric flow and the transverse area of the flux.

- The mean velocities of the liquid and gas phase are defined as

$$u_g = \frac{\dot{m} * x}{\rho_g * A_g} = \frac{\dot{m} * x}{\rho_g * A * \xi} \tag{2.5}$$

$$u_l = \frac{\dot{m} * (1-x)}{\rho_l * A_l} = \frac{\dot{m} * (1-x)}{\rho_l * A * (1-\xi)} \tag{2.6}$$

where these velocities are defined considering the area occupied by the single phase.

- The density of the mixture defined as

$$\rho_m = \rho_g * \xi + \rho_l * (1-\xi). \tag{2.7}$$

Depending on the inclination of the pipe, the characteristics of the flow regime may vary greatly due to the different interaction between gravity forces and shear forces. The most common orientations in industrial applications are horizontal and vertical ones. Two-phase flow inside horizontal tubes has a lot of industrial applications such as, pipelines for transportation of gas and liquid, condenser and evaporator in finned coil and shell and tube heat exchangers. In a horizontal tube, there are different kinds of flow regimes and the appearance of one of them depends on the intensity with which the different forces act on the fluid. The main forces performing on the fluids are the gravity force and the shear force. The last one can be defined as [1]:

$$\tau = \frac{1}{2} * f_g * \frac{G^2 * x^2}{\rho_g} = \frac{1}{2} * f_l * \frac{(G_l)^2}{\rho_l} \tag{2.8}$$

and, because of the much higher velocity of the gas-phase, the shear stress caused by this phase is higher compared to the one related to the liquid-phase. The coefficient $f_g$ and $f_l$ represent the friction factors for the gas and liquid phase as if they would flow inside the tube as a single phase. In the case of the horizontal pipe, the gravity force acts in a path orthogonal to the direction of the flow, creating a situation of asymmetry distribution in the two phases compare to the case of a vertical pipe where the shear and gravity forces act on the same direction creating an ambient where the distribution is symmetrical along all pipe [1]. In the open literature is possible to find various studies that have tried to classify the different flow regimes according to diverse conditions like pipe inclination, diameter, fluid characteristics and others. In these investigations is possible to find different definitions of flow regime depending on the precise choices made by the authors to describe the characteristics of the flow. Here are reported the most common flow regimes found in the literature. The flow regimes that can occur inside a horizontal pipe are:

- **Dispersed bubble flow**: The gas-phase appears as distinct bubbles in a continuous liquid phase. The bubbles tend to rise to the top of the flow due to buoyancy effects. When the liquid velocity is high, the bubbles may be more uniformly distributed in the liquid.

- **Plug flow**: An increase of quality results in larger gas bubbles size which tend to remain at the top of the flow channel due to buoyancy force.

- **Stratified flow**: With low gas velocity, the gravity force takes over and keeps the liquid phase at the bottom section of the tube while the less dense gas flow in the upper side of the tube creates a well-defined separation between the two phases.

- **Stratified-wavy flow**: As the gas velocity increases in the stratified flow, the shear forces of the gas flow over the liquid cause ripples on the top of the liquid phase and result in the formation of waves on the liquid-gas interface.

- **Slug flow**: The amplitude of the waves increase as the liquid flow rate increases. The crests can span the entire tube, and a bridge starts to develop, separating the slugs from one another. However, a substantial liquid phase remains, and gravity pulls it to the bottom of the flow channel. The top of the flow channel is still wetted by a relatively thin film of liquid.

- **Annular-dispersed flow**: The liquid layer flows near to the inner wall of the tube and the gas flows in the central core. However, the liquid layer

at the bottom is thicker than that on the top of the channel because of the gravitational force

A representation of all this flow regimes is visible in the picture 2.1. In the litera-

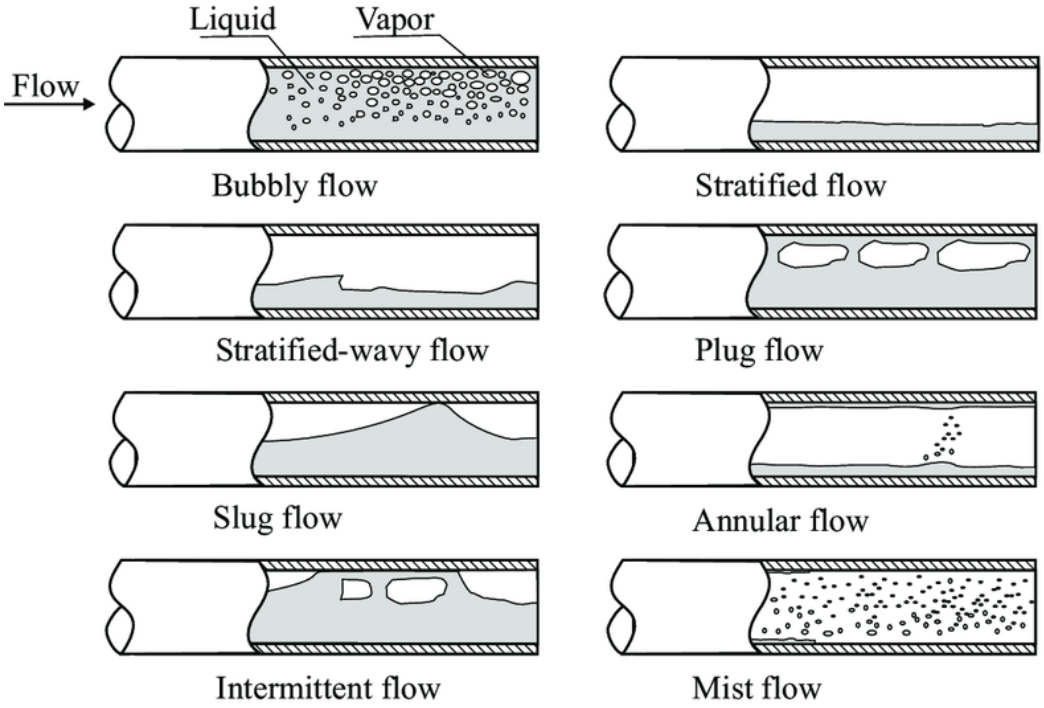


Figure 2.1: Flow regimes in horizontal two-phase flow [36]

ture, there are many different models which can be used to estimate the transitions between flow regimes as a function of the flow parameters, substance-bound variables and pipe geometry. The determination of the flow regime in two-phase flow is done with the help of flow pattern maps. These maps describe the physical phenomena of two-phase flow mostly using empirically determined correlations of the influencing factor. Usually, a distinction is made between flow pattern maps for horizontal and vertical pipe flow, however, some models can account for the entire range of pipe inclinations. A distinction must be made between flow pattern maps for flow in adiabatic conditions and others in diabatic conditions. In the second case, the determination of the flow shape is particularly complex since different flow regimes occur along the pipe due to the varying steam content. One of the most used and known flow pattern map is the one proposed by Taitel and Duckler (1976) [44] [45]. This model was originally developed for flows in adiabatic conditions however, various investigations have shown that the parameters described in that map, can also be used in the case of a flow with phase change. [3] [38]. The

flow pattern map of Taitel and Duckler [45] allows a complete analytical prediction of the flow regimes in a horizontal and slightly inclined pipe with gas-liquid flows. This flow chart is based on physical modelling of the transition mechanism involved [38]. The authors define different dimensionless parameters that describe the transition mechanisms of the flow regimes and differentiate different nearby flow regimes from each other. The figure 2.2 shows the flow pattern map of Taitel and Duckler for horizontal pipe flows. The various adimensional parameters used

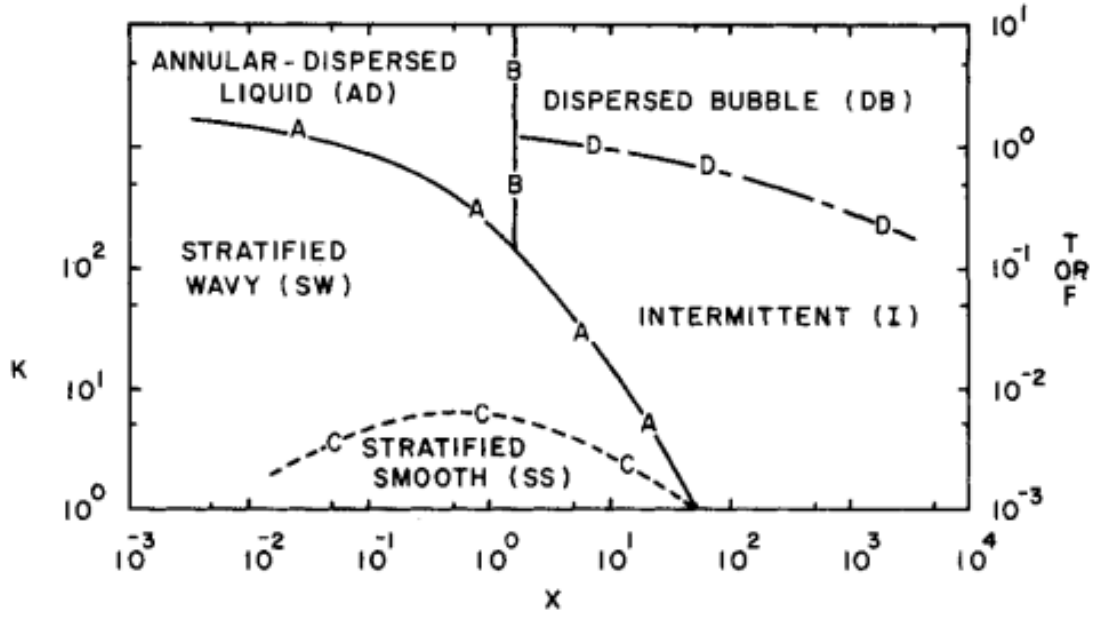


Figure 2.2: Taitel and Duckler flow pattern map [45]

in the map are:

$$F = \frac{J_g \rho_g}{\sqrt{gD \cos\beta \rho_g (\rho_l - \rho_g)}} = \frac{Gx}{\sqrt{gD \cos\beta \rho_g (\rho_l - \rho_g)}} \tag{2.9}$$

$$K = \left\{ \frac{J_g^2 \rho_g}{gD \cos\beta (\rho_l - \rho_g)} \frac{D J_l}{\upsilon_l} \right\}^{0.5} \tag{2.10}$$

$$T = \left\{ \frac{(-\frac{dp}{dz})_{f,l}}{g \cos\beta (\rho_l - \rho_g)} \right\}^{0.5} \tag{2.11}$$

where D is the internal diameter of the pipe, $\beta$ is the inclination angle of the tube axis compared with the horizontal axis and $\frac{dp}{dz}_{f,l}$ is the pressure drop per unit length with only the liquid phase running in the pipe. The transition curves are expressed

as a function of the Martinelli parameter defined as:

$$X = \left\{ \frac{\left(-\frac{dp}{dz}\right)_{f,l}}{\left(-\frac{dp}{dz}\right)_{f,g}} \right\}^{0.5} \tag{2.12}$$

which is the ratio between the pressure gradient of the liquid phase and the one for the gas phase considering as every phase flow alone along the pipe. Although this is the most well known and used flow pattern map, it was created with experimental data obtained using a mixture of water and air, so the model may be inaccurate for synthetic fluid with different proprieties. As explained before, other maps have been created for a better description of the behaviour of a two-phase mixture in different conditions and with diverse liquids. The Taitel and Duckler [45] map was adapted by Breber et. Al. [3] for the condensation. Steiner et al. [42] also developed a more accurate map modifying the transition limit of the Taitel and Duckler [45] one. Other known flow pattern maps are the one from Kattan et al. [25] based on Steiner's model [42], which is suitable for estimating the flow pattern in both adiabatic and diabatic pipe flows and the flow pattern map of El Hajal et al. [19], also based on the Kattan et al. [25] for condensation which includes a new way of defining the void fraction. All the already cited studies are conducted using smooth tubes. Several authors have analyzed the behavior of the two-phase flow for tubes with inner structure. Taitel et al. [43] have analyzed how the method of predicting the flow pattern defined by the Taitel and Duckler map [45] can be extended to rough pipes. They discovered that since the roughness affects both liquid and gas pressure drop, little change in equilibrium liquid level is expected in the pipe. As a result, most transitions between different flow patterns are independent of roughness for structured tubes. The only exception appears for the transitions between intermittent and dispersed bubble because, as described before, this transition occurs when turbulent pressure fluctuation exceeds buoyancy forces. For rough pipes, enhancement of turbulence leads to a transition to a dispersed bubble at a lower liquid flow rate compared to the case of smooth tubes. The condensation inside the tube can be total or partial, depending on the conditions applied. Based on the application, the gas at the inlet can be superheated, with vapour quality grater than one, or not in saturation conditions therefore with vapour quality minor than one. So, the condensation phenomena, can begin with an initial area where cooling is made, then go on with the condensation zone and finish with an area where a subcooling of the condensate happen. Condensation, even with superheated vapour, starts when the temperature of the exchanger surface is lower than the saturation temperature of the gas. During condensation, the vapour quality change while the two-phase flow moves along the tube so that different flow patterns occur inside

the pipe. Palen et al. [34] have illustrated the typical flow pattern when condensation occurs inside a horizontal tube and a graphical representation is reported in figure 2.3. As showed in the figure the authors divide the flow into two major

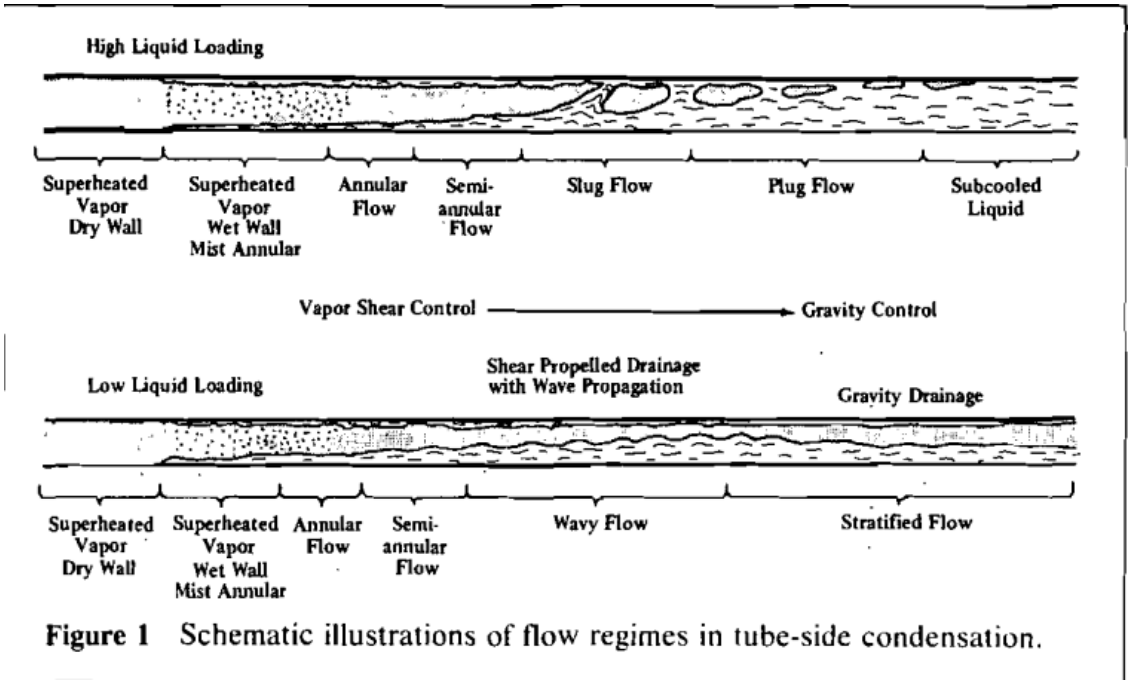


Figure 2.3: Flow pattern during the condensation process [5]

regimes. The first one is the vapour shear-controlled flow where the condensate film thickness is determined by the axial vapour shear force and the condensate interface. In these conditions, annular flow occurs. The other major regime is the gravity-controlled flow where the condensate is not maintained in an annular ring but drains down under the force of gravity and flow along the bottom of the tube. In this situation, the flow regimes can be a wave or stratified depending on the flow velocity, liquid loading and interface conditions [34].

## 2.2 Enhanced surfaces

The new European environmental standards are becoming increasingly stringent requiring, beside the use of refrigerant fluids with low ODP and GWP, also a reduction of the overall quantity of refrigerants in each system. The structured tubes represent a good solution due to their characteristics like the increase of heat transfer coefficient, reduction of occupied spaces and decrease of the refrigerant load. The finned tubes can be categorized into three different classes:

- Micro-fin tubes have a helicoidal fin on the inner surface of the pipe. It is possible to define two kinds of tubes: the low-fin tubes that present a low number of fins and a ratio between the fin height h and the inner diameter of the tube $d_i$ greater than 0,05 ($\frac{h}{d_i} > 0.05$). The other kind is the micro-fin tubes which have a greater number of fins and $\frac{h}{d_i} < 0.05$. Typical micro-fin tubes available for the industrial applications are made of copper and have an outside diameter from 4 to 15 mm, a single set of 50-70 spiral fins with a spiral angle from 6 to 30°, fin height from 0.1 to 0.25 mm and triangular of trapezoidal fin shapes with an apex angle from 25 to 90°. (Figure 2.4)

- Cross-grooved tubes have a second set of groove with the same spiral angle but opposite direction compared to the first one and usually, the second groove has a different depth. (Figure 2.4)

- Herringbone tubes have a herringbone groove-shaped that allows the condensate fluid to be thinner one the sides compared to the bottom and upper area. (Figure 2.5)

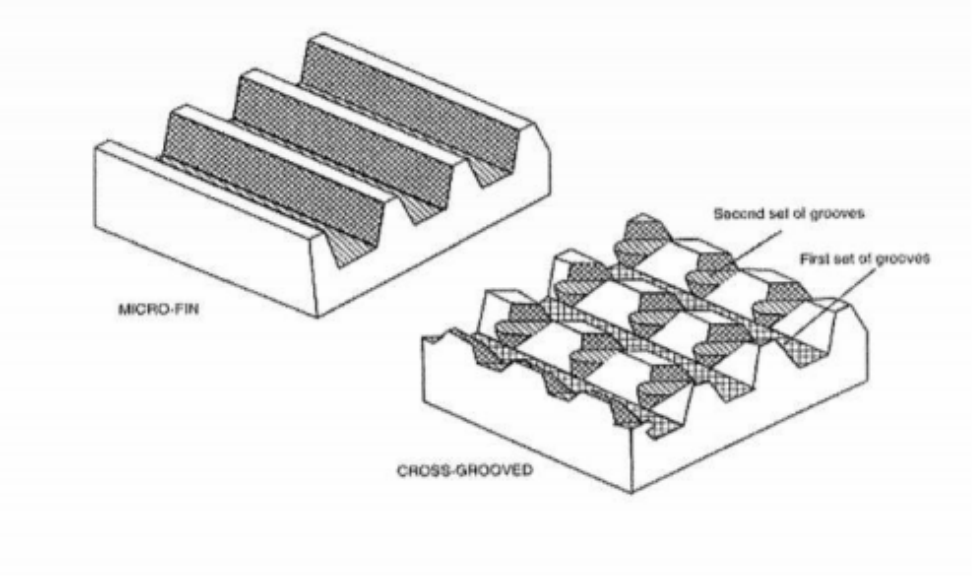


Figure 2.4: Comparison between micro-fin tubes and cross-grooved tubes [36]

Micro-fin tubes are used in a wide area of industrial use due to the enhanced heat transfer performance while increasing the pressure drop in a smaller manner. According to Cavallini et al. [6] the micro-fin tubes show a heat transfer enhancement, compared to smooth tubes under the same operating conditions, from 80 to 180% and over, with a pressure loss increase from 20 to 80%. According to the same authors, cross-grooved tubes give a 25-30% higher heat transfer performance than

micro-fin tubes with a pressure drop only 6-10% higher. The area increase alone is not enough to explain the overall increment of the heat transfer performance of these kinds of tubes. As numerous research has proven, in some conditions, the in-

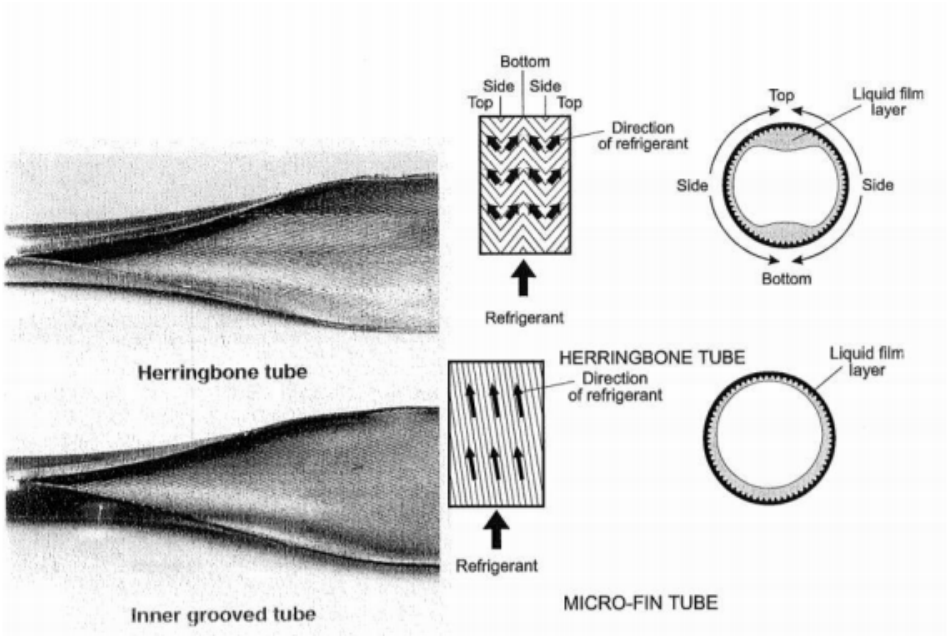


Figure 2.5: Comparison between micro-fin tubes and herringbones tubes [6]

crease of heat transfer coefficient is greater than the increment of the heat exchange area due to the tubes structure. Cavallini et al [6] explain that the heat transfer and pressure drop enhancements are partly due to the simple increase in the effective exchange area, and additionally, to the turbulence induced in the liquid film by the micro fins and to the surface tension effect on the condensate drainage. The combination of these two mechanisms, promote and extend the range of annular flow which is associated with heat transfer coefficients higher than those exhibit in the gravity-controlled flow pattern (stratified and wavy stratified flow) according to Doretti et al. [18]. This effect can be explained because the fins induce a centrifugal effect on the fluid velocity which, together with the superficial tension effect, keep the condensate film adhering to the upper side of the tube even with relatively low vapour velocities. To assess the difference between heat transfer coefficient in a structured tube and a smooth one is possible to define a coefficient called Enhancement Factor EF defined as:

$$EF = \frac{\alpha_{structured}}{\alpha_{smooth}} \tag{2.13}$$

An important aspect, founded in all the already quoted research, is that the enhancement factor of the heat transfer coefficient, referred to as the smooth tube

area, is considerably higher than the increment of the exchange area in a structured tube when the specific flow rate is low, while with a high specific flow rate the EF is considerably lower, as it is possible to see in the figure 2.6. This behavior can be

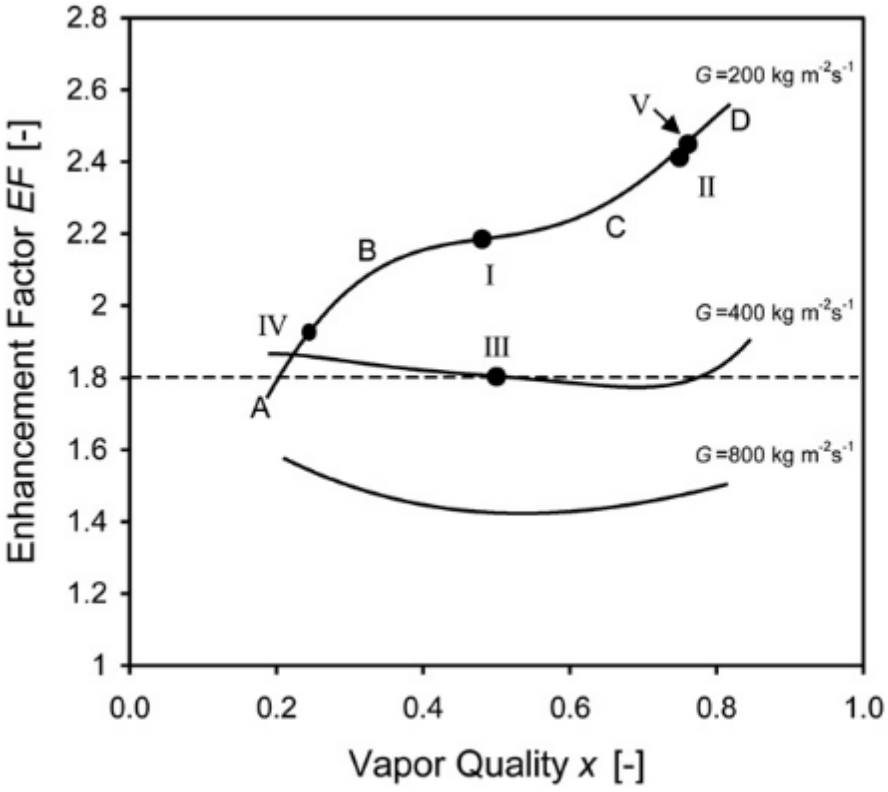


Figure 2.6: Heat transfer enhancement factor plotted against vapour quality for R410 at 40°C of saturation temperature [18]

explained by the effect that the micro fins have on the transition between annular and stratified flow patterns. With low specific flow, in a smooth tube, the flow pattern is stratified, consequently, the heat transfer coefficient is not high compared to the one obtainable with a structured tube. Indeed the adding of micro fins allows to maintain an annular flow configuration even with a low specific flow, creating the conditions, due to higher heat transfer coefficient of the annular flow pattern, for higher heat transfer and so an overall improvement of tube performances. With the decrease of vapour quality, the less present vapour is not enough to sustain the annular flow pattern, even in a micro fin tube, so the enhancement of EF is less pronounced with lower $x$. On the contrary, with the high specific flow and high vapour quality, the annular flow configuration is present even in a smooth tube so, the micro fins are able to increase only the turbulence and the exchange area and consequently the increase of heat transfer performance is moderate. In some

specific conditions, like very high specific flow, the micro-fin structure can even be harmful to the heat transfer performance because the liquid film that the fins retain, is too thick and cover completely the fins, reducing the capacity of the fins tips to remain dry due to the superficial tension. Also, the liquid phase acts like as thermal resistance, neutralizing the effect of the increase of the exchange area.

## 2.3 Heat transfer coefficient

The determination of the heat transfer coefficient is fundamental for the design of the condenser and evaporator. Through the determination of the correct heat transfer coefficient is possible to lay out a more precise heat exchanger and avoid over design problem that leads to inefficiencies and increase of the cost.

### 2.3.1 Single-phase heat transfer coefficient

Since the determination of heat flux density $\dot{q}$ through the use of velocity and temperature field require the knowledge of the characteristics of the flow, heat transfer coefficient is used for the determination of the heat transfer as:

$$\alpha = \frac{\dot{q}}{\Delta T} \tag{2.14}$$

The calculation of the heat transfer according to this formula, requires the knowledge of the temperature filed but this can be determined only through the knowledge of the velocity field inside the tube, so the heat transfer coefficient can be determined in a precise way only in a few situations. Furthermore, the heat transfer is influenced by many factors such as geometrical characteristics of the pipe as well as proprieties of the fluid itself like density $\rho$, viscosity $\mu$, thermal conductivity $\lambda$ and specific heat capacity *cp*. For taking account of all influences it is possible to determine the number of dimensionless parameters which can describe the velocity and temperature fields. These parameters are:

- Nusselt number **Nu**
- Prandtl number **Pr**
- Reynolds number **Re**
- Grashoff number **Gr**

The Nusselt number can be expressed like the following

$$Nu = \frac{\alpha L}{\lambda} \tag{2.15}$$

and it represents the increase of thermal power transmitted through convection in a liquid layer compared to the one transmitted through conduction in the same layer. The Prandtl number is calculated as

$$Pr = \frac{c_p \mu}{\lambda} \tag{2.16}$$

and is defined as the ratio between momentum diffusivity and thermal diffusivity. It is directly bonded to the ratio between the velocity boundary layer and the thermal boundary layer which develops when a viscous fluid is moving among a wall. The Reynolds number is express as follow

$$Re = \frac{\rho u L}{\mu} \tag{2.17}$$

and is defined as the ratio of inertial to viscous forces. Finally the Grashoff number is expressed as

$$Gr = \frac{g \beta \Delta T L^3}{\nu^2} \tag{2.18}$$

and has the same physical meaning of the Reynolds number in the case of free convection. According to the Buckingham theorem, with seven physical variables involving four units of measurement, a convective heat transfer problem can be solved using a set of three non-dimensional parameters. Depending on if the heat transfer is free or forced convection the three parameters used for the determination of the convective heat transfer problem change. The value of the heat transfer coefficient can be calculated with empirical correlations developed in numerous studies available in the open literature. The basic structure of the correlation is the same for both types of convection and is based on the calculation of the number of Nusselt. The differences between the structures are on the dimensionless parameters used for this correlation.

- For free convection the correlation is

$$Nu = C \left(GrPr\right)^n \tag{2.19}$$

  where since both Grashoff and Prandtl numbers have a common exponent is possible to define another dimensionless parameter called Rayleigh number defined as $Ra = GrPr$.

- For forced convection instead the expression is

$$Nu = CRe^m Pr^n \tag{2.20}$$

  where, for both type of convection, $C$,$m$ and $n$ are specific parameters experimentally estimated for each heat transfer configuration.

Since free convection is not common in the industrial process regarding condensation and heat transfer inside tubes, only correlations for forced convection will be analyzed. In the open literature is possible to find several empirical correlations for the determination of the single-phase heat transfer coefficient for forced convection as the one from Petukhov and Popov [35], wherein their study they developed a method of calculating the heat transfer for an not compressible fluid with the arbitrary temperature dependence of its properties. An analytical expression was obtained from the energy and momentum equations and presented a range of validity of $10^4 < Re < 5 * 10^5$ and $0{,}5 < Pr < 200$. Another model developed is the one from Gnielinski [21] that developed a correlation to determine the heat transfer in a fully developed turbulent flow ($Re \geq 10^4$) inside a pipe. The pipe friction coefficient is calculated through the equation of Darcy-Weisbach [21]. The validity range of the model is $3000 < Re < 5 * 10^6$, $0{,}5 < Pr < 2000$ and diameter-length ratio of $(D/L) \leq 1$. Finally one of the most common models used for the determination of the heat transfer coefficient for forced convection is the one developed by Dittus-Böelter [16]. This model is been formulated for fully developed turbulent flow in a smooth circular tube but is applicable also in a structured tube. The Dittus-Böelter equation is less accurate when there is a large temperature difference across the fluid and in case of flow characterized by large propriety variations correction such as the one recommended by Sieder and Tate [16], must be taken into account. The range of validity of this model is $0{,}6 < Pr < 160$, $Re > 10000$ and $(L/D) > 10$.

### 2.3.2 Two-phase heat transfer coefficient

In a horizontal tube, the heat transfer depends greatly on the flow regime that the flow assume. Although numerous correlation exists in the literature for horizontal tub-side condensation, no single correlation can be selected as best for design since every model is developed for different fluids and flow characteristics and with different assumptions. The necessity of diverse correlations is determined also by the fact that while the fluid flow inside the tube, different flow regimes develop from vapour entry to the outlet, requiring so different correlations form corresponding to the locally predominant mechanism. A schematic illustration of the various flow regimes is already showed in figure 2.3. The condensation inside horizontal tubes can be divided into two major regimes [34]:

- **Vapour Shear-controlled flow**
  When the vapour velocity is high, a condition that usually happens with the high specific flow or high vapour quality, the shear force on the vapour is high and the flow regime is annular. The condensate film thickness is determined

| Author | Correlation |
|---|---|
| Petukhov and Popov [35] | $Nu = \frac{(f/8)RePr}{K_1(f)+K_2(Pr)(f/8)^{1/2}(Pr^{2/3}-1)}$ <br> $f = (1{,}82logRe - 1{,}64)^{-2}$ <br> $K_1(f) = 1 + 3{,}4F$ <br> $K_2(Pr) = 11{,}7 + 1{,}8Pr^{-1/3}$ |
| Gnielinski [21] | $Nu = \frac{(f/8)(Re-1000)Pr}{1+12{,}7(f/8)^{1/2}(Pr^{2/3}-1)}$ <br> $f = (1{,}8logRe - 1{,}5)^{-2}$ |
| Dittus-Böelter [16] | $Nu = 0{,}023Re^{0,8}Pr^{0,4}$ |

Table 2.1: Model for calculation of single-phase heat transfer coefficient for turbulent flow

by the axial vapour shear force on the condensate interface. The heat transfer happens as condensation in the interface between the liquid film and the vapour and with forced convection through the film condensate to the pipe wall.

- **Gravity-controlled Flow**
  When the vapour quality is low the flow is gravity controlled and the gas phase occurs as bubbles. The condensate is not maintained in an annular ring, but drains down under the force of gravity and flows along the bottom of the tube. The flow regime can be a wave or stratified depending on the flow velocity, liquid loading and interface condition. Heat transfer prediction is complex because of the great difference between the resistance of the draining film and one of the condensate layer. The heat transfer coefficient is calculated by combining the Nusselt theory that describes the phenomena of the draining in the upper part of the tube and the correlation related to the heat transfer for forced convection present in the liquid part at the bottom of the tube. In some cases, usually with very low mass velocities, the liquid thickness is so big that the heat transfer related to forced convection can be assumed as zero and so in this case the only contribution to the heat transfer coefficient is the one related to the upper part of the pipe.

An approach to determine whether shear or gravity forces are controlling the flow is to set up a force balance equating these forces [3]. The forces in the balance are the following:

- Vapour Shear axial gradient defined as $F_a = \frac{dP_s}{dL} = \frac{4 f_g G_g^2}{D_i 2 \rho_g}$ where $f_g$ is the friction factor for gas phase and $G_g$ is the vapour mass velocity.
- Gravity radial gradient defined as $F_r = \frac{dP_g}{dD_i} = g(\rho_l - \rho_g)$ .

so the ratio of $F_a$ ti $F_r$ is:

$$\frac{F_a}{F_r} = \frac{2 f_g G_g^2}{D_i g \rho_g (\rho_l - \rho_g)} \tag{2.21}$$

As described by Palen et al. [34] the force balance approach leads to a dimensionless group called dimensionless gas velocity $j_g^*$

$$j_g^* = \frac{y G_t}{\sqrt{D_i g \rho_G (\rho_l - \rho_g)}} = \left[ \left( \frac{F_a}{F_r} \right) \left( \frac{1}{2 f_g} \right) \right]^{0,5} \tag{2.22}$$

. Several condensation heat transfer models have been published in the open literature. Each correlation is given with a suitable validity range of parameters within which it can be used to calculate the heat transfer coefficient. Very few models are general and cover the entire map of two-phase regimes. For the vapour shear-controlled flow the model developed by Cavallini and Zecchin [11], Shah [39], Traviss et al. [47] and other are available. These studies developed theoretical analyses based on the analogy between momentum transport and heat transfer. For these models, the heat transfer coefficient is a function of the interfacial vapour-liquid shear stress and the liquid film thickness. The shear stress is computed from the frictional pressure gradient, which can be experimentally measured or calculated from an empirical equation [4]. The model suggested by Cavallini and Zecchin [11] was developed for the prediction of the heat transfer coefficient in annular flow and it is based on the model of single-phase heat transfer correlation where is calculated the local Nusselt number. In stratifying flow processes the heat transfer through the thin film is usually analyzed by the classical Nusselt theory and the average heat transfer coefficient over the entire circumferential tube wall can be consistently computed by the following expression:

$$\alpha = \Omega \left[ \frac{\lambda_L^3 \rho_L^2 g h_{LG}}{\mu_L d \Delta T} \right]^{1/4} \tag{2.23}$$

where $\Omega$ is a parameter defined in different ways depending on the model, $h_{LG}$ is the isobaric latent heat of condensation and $\Delta T = (T_{saturation} - T_{tubewall})$.

The first model that suggested the use of Nusselt theory was the one developed by Jaster and Kosky [23] where they neglected the heat transfer that occurs in the liquid pool at the bottom of the tube. In their study, Dobson and Chato [17] discovered that the hypothesis is reasonable only at very low mass velocities but the heat transfer in the liquid layer might not be ignored at high mass velocity and low quality where wavy or stratified flow could prevail with convective heat transfer at the bottom of the pipe. The model developed by Dobson and Chato [17] cover both shear and gravity controlled condensation phenomena inside smooth tubes. They developed two equations that cover the entire range of possible two-phase flow regimes and suggest their application depending on the value of mass velocity and a specifically defined parameter $Fr_{So}$. Another model developed to cover the entire range of two-phase flow regimes is the one presented by Cavallini et al. [8] . This method is based upon a large data bank and can be used for condensation of halogenated refrigerants inside tubes with an internal diameter $d > 3mm$ and reduced pressure $p_R < 0{,}75$. For the annular flow is used as a basis, the model of Kosky and Staub [28] where the heat transfer coefficient is correlated to the frictional pressure gradient through the interfacial shear stress. A new equation for the frictional pressure gradient during annular flow was presented based on the Friedel parameter [20]. The heat transfer is the sum of two components, the first one is calculated from the Nusselt type equation and is relative to the upper side of the tube while the second component is given as a convective term and refers to the lower part of the pipe. Another model developed for the determination of the heat transfer coefficient for smooth tubes is the one proposed by Cavallini et al. [10]. The model presented includes a simple and objective criterion for the definition of the transition between two different flow categories, depending on whether the heat transfer coefficient is dependent or independent on the temperature difference $\Delta T$. In a horizontal tube, dependence on $\Delta T$ occurs only when gravity is the prevailing force. In the open literature, the data relative to condensation of pure refrigerants inside enhanced horizontal tubes are not numerous. In their research Cavallini et al. [9] presented a heat transfer coefficient measured during condensation of R22 and R407C inside micro-fin tubes. They established that the heat transfer enhancement factor *EF*, defined in equation 2.13 as the ratio of the heat transfer coefficient in the micro-fin tube to the one in an equivalent smooth tube with the same internal diameter equal to the fin tip diameter of the enhanced one, depends on mass velocity and vapour quality. They found also that exists an optimal value of mass velocity that maximizes the heat transfer EF of a micro-fin tube. This is may due to the different flow pattern present with the structured tubes compared to the smooth ones especially because of the different transition conditions from annular to stratified flow. One of the first correlations for the definition of a model for the

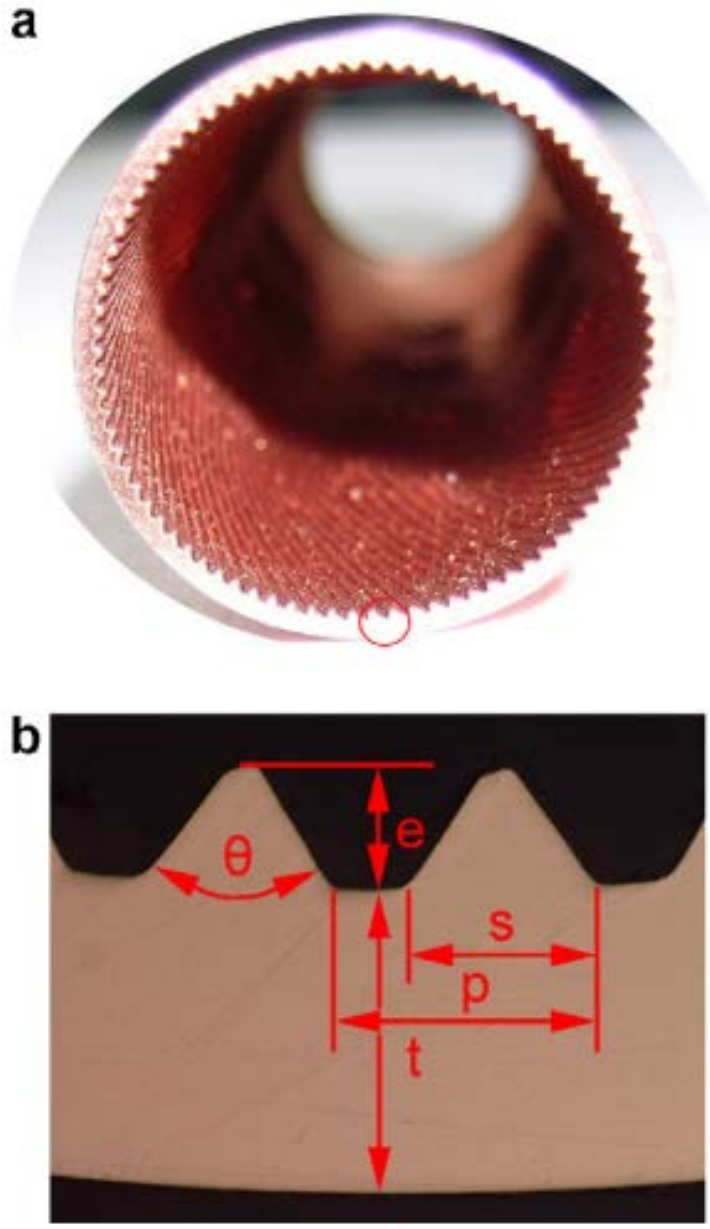


Figure 2.7: Internal structure of a micro-fin tube [29]

calculation of the heat transfer coefficient in a structured tube is the one developed by Cavallini et al. [5]. It is based on the Cavallini and Zecchin [11] equation for smooth tubes, where they add two additional non dimensional groups to account for the effect of the heat transfer area increase and the effect of the surface tension. Another model developed for the calculation of heat transfer coefficient in micro-fin tubes is the one presented by Yu and Koyama [49], where the heat transfer area can

be calculated from an asymptotic equation between forced convective condensation component and a natural convective condensation component od the Nusselt number. This correlation takes account for the effect of inside geometry by referring to the heat transfer coefficient to the total inside heat transfer area. Kedzierski and Goncalves [26] presented a correlation for the condensation of pure refrigerants in micro-fin tubes obtained by regression of their data. The heat transfer coefficient was defined on the actual inner surface area and the geometry effect was taken into account by considering the hydraulic diameter. The authors state that micro fins enhance the heat transfer with a combination of liquid-vapour interface mixing and condensate turbulence mixing near the wall. The finned surface acts as a roughness on the enhancement of heat transfer. In their study, Yang and Webb [48], defined a semi-empirical model to predict the condensation coefficient inside small hydraulic diameter tubes with microgrooves. They assumed that surface tension forces enhance the condensation coefficient when the fins tips are not flooded by the condensate that is mainly at low mass velocity and high vapour quality. At high mass velocity, the flow is vapour shear controlled and the surface tension is less effective Shikazono et al. [40] developed a general analytical model to predict the condensation heat transfer coefficient of pure refrigerants in horizontal micro-fin tubes. The total condensation coefficient is obtained from the forced convective term $\alpha_F$ and the film contribution as $\alpha = \left(\alpha_F^2 + c^2\alpha_B^2\right)^{0,5}$ where $c$ is the enhancement factor and $\alpha_B$ the film condensation coefficient. The enhancement factor is defined as the ratio of the unflooded area of the micro-fin tube and that of an equivalent smooth tube.

Table 2.2: Models for calculation of the heat transfer coefficient for two-phase flow in smooth tubes

| **Author** | **Correlation** |
|---|---|
| Jaster and Kosky [23] | $\alpha = 0{,}728\xi^{3/4}\left[\frac{\lambda_L^3\rho_L(\rho_L-\rho_G)gh_{LG}}{\mu_L D\Delta T}\right]^{1/4}$ <br> $\xi = \left\{1+\left(\frac{\rho_G}{\rho_L}\right)^{2/3}\left[\frac{(1-x)}{x}\right]\right\}^{-1}$ |
| Cavallini et al. [11] | $Nu = \frac{\alpha D}{\lambda_L} = 0{,}05Re_{eq}^{0,8}Pr_L^{1/3}$ <br> $Re_{eq} = \frac{G\,D\left[(1-x)+x\left(\frac{\rho_L}{\rho_G}\right)^{1/2}\right]}{\mu_L}$ <br> $0{,}8 \leq Pr_L \leq 20;\ 5000 \leq Re_{LO} \leq 500000;\ 0{,}1\ \leq x \leq 0{,}9;$ <br> $10 \leq (\rho_L/\rho_G)2000;\ 0{,}01 \leq (\mu_G/\mu_L) \leq 0{,}1;\ 0{,}01 \leq Ph_L \leq 0{,}2$ |

*Continued on next page*

Table 2.2 – *Continued from previous page*

| Author | Correlation |
|---|---|
| | $15 \leq [(G/\rho_G)/(gD)^{0,5}] \leq 4000;\ Ph_L(\rho_L/\rho_G) \leq 25;\ Re_L \geq 1200$ |
| Shah [39] | $Nu = \frac{\alpha D}{\lambda_L} = 0{,}023\left(\frac{G\,D}{\mu_L}\right)^{0,8} Pr_L^{0,4}\left[(1-x)^{0,8} + \frac{3{,}8x^{0,76}(1-x)^{0,04}}{p_R^{0,38}}\right]$ $0{,}002 < p_R < 0{,}44;\ 10{,}8 \leq G \leq 1600kg/(m^2s);\ Pr_L > 0{,}5;$ $Re_{LO} > 350;\ 7 \leq D \leq 40mm;\ 3 \leq G/\rho_G \leq 300m/s;\ 0 \leq x \leq 1$ |
| Dobson and Chato [17] | $Nu = \frac{\alpha D}{\lambda_L} = 0{,}023Re_L^{0,8}Pr_L^{0,4}(1 + 2{,}22/X_{tt}^{0,889})$ $for\ G > 500kg/(m^2s)\ or\ G < 500kg/(m^2s)\ and\ Fr_{So} > 20$ $Nu = \frac{\alpha D}{\lambda_L} = Nu_{fl} + Nu_{fc}(1 - \Theta/\phi))$ $for\ G < 500kg/(m^2s)\ or\ G < 500kg/(m^2s)\ and\ Fr_{So} < 20$ $Nu_{fl} = 0{,}23ReGO^{0,12}(Ga_L Pr_L/Ph_l)^{0,25}/(1 + 11X_{tt}^{0,58})$ $Nu_{fc} = 0{,}0195Re_L^{0,8}Pr_L^{0,4}(1{,}376 + C_1/X_{tt}^{C_2})^{0,5}$ $C_1 = 4{,}172 + 5{,}48Fr_L - 1{,}564Fr_L^2; C_2 = 1{,}773 - 0{,}169Fr_L$ $for\ Fr_L = (G/\rho_L)^2/(g/D) < 0{,}7$ $C_1 = 7{,}242;\ C_2 = 1{,}655\ for\ Fr_L = (G/\rho_L)^2/(gD) \geq 0{,}7$ $\Theta_L = \phi arcos(2\xi - 1)$ |
| Cavallini et al. [10] | $\alpha_A = \alpha_{LO}[1 + 1{,}128x^{0,8170}(\rho_L/\rho_G)^{0,3685} * \ldots$ $*(\mu_L/\mu_G)^0{,}2363(1 - \mu_G/\mu_L)^{2,144}Pr_L - 0{,}1]$ $for\ J_G > J_G^T \Delta T\ indipendent\ flow\ regime$ $\alpha_{LO} = 0{,}023Re_{LO}^{0,8}Pr_L^{0,4}\lambda_L/D$ $\alpha_D = \left[\alpha_A(J_G^T/J_G)^{0,8} - \alpha_{STRAT}\right](J_G^T/J_G) + \alpha_{STRAT}$ $\alpha_{STRAT} = 0{,}725\{1 + 0{,}741[(1-x)x]^{0,3321}\}^{-1} * \ldots$ $*[\lambda^3\rho_L(\rho_L - \rho_G)gh_{LG}/(\mu_L D\Delta T)]^{0,25}(1 - x^{0,087})\alpha_{LO}$ $for\ J_G \leq J_G^T \Delta T\ dependent\ flow\ regime$ $J_G^T = \{[7{,}5/(4{,}3X_{tt}^{1,111} + 1)]^{-3} + C_T^{-3}\}^{-1/3}$ |

*Continued on next page*

Table 2.2 – *Continued from previous page*

| Author | Correlation |
|---|---|
| | $C_T = 1{,}6\ hydrocarbons; C_T = 2{,}6\ others$ |
| Thome et al. [46] | $\alpha_{film}\ for\ given\ temperature\ difference\ \Delta T$ |
| | $\alpha_{tot} = \frac{\alpha_f r\theta + (2\pi - \theta) r \alpha_c}{2\pi r}$ |
| | $\theta = 0\ for annular,\ \theta = \theta_{strat}\ for\ stratified$ |
| | $\theta = \theta_{strat}\left[\frac{(G_{wavy} - G)}{(G_{wavy} - G_{strat})}\right]^{0,5}$ |
| | $\alpha_c = 0{,}003 Re_L^{0,74} Pr_L^{0,5} \frac{\lambda_L}{\delta} f_i$ |
| | $f_i = 1 + \left(\frac{u_G}{u_L}\right)^{1/2}\left(\frac{(\rho_L - \rho_G) g \delta^2}{\sigma}\right)^{1/4}$ |
| | $\alpha_f = 0{,}728\left[\frac{\rho_L(\rho_L - \rho_G) g h_{LV} \lambda_L^3}{\mu_L d (T_{sat} - T_w)}\right]^{1/4}$ |

Table 2.3: Models for calculation of the heat transfer coefficient for two-phase flow in structured tubes

| Author | Correlation |
|---|---|
| Yu and Koyama [49] | $Nu = \frac{\alpha d}{\lambda_L} = \left(Nu_F^2 + Nu_B^2\right)^{0,5}$ |
| | $Nu_F = 0{,}152(\Theta_G / X_{tt}) Re_L^{0,68}(0{,}3 + 0{,}1 Pr_L^{1,1})$ |
| | $\Theta_G = 1{,}1 + 1{,}3\left\{G^{0,35} X_{tt}^{0,35} / [g d_m \rho_G (\rho_L - \rho_G)]^{0,175}\right\}$ |
| | $Re_L = G(1-x) d_M / \mu_L$ |
| | $Nu_B = 0{,}725 H(\xi)[GaPr_L / (Ph_L \eta_A)]^{0,25}$ |
| | $Ga = g \rho_L^2 d_M^3 / \mu_L^2$ |
| | $H(\xi) = \xi + \left\{10(1-\xi)^{0,1} - 8{,}0\right\}(\xi)^{0,5}\left[1 - (\xi)^{0,5}\right]$ |
| | $\xi^{-1} = 1 + [(1-x)\rho_g / (x \rho_L)]\left\{0{,}4 + \ldots\right.$ |
| | $\left. + 0{,}6[x(\rho_L/\rho_G) + 0{,}4(1-x)]^{0,5} / [x + 0{,}4(1-x)]^{0,5}\right\}$ |
| Kedzierskiet al. [26] | $Nu = \frac{\alpha_e d_h}{\lambda_L} = 2{,}256 Re^{0,303} Ph_L^{-0,232x} Pr_L^{0,393} (p_R)^B (-\log 10 p_R)^C S_V^D$ |
| | $B = -0{,}578x^{"}\ \ C = -0{,}474x^2\ \ D = 2{,}531x$ |

*Continued on next page*

Table 2.3 – *Continued from previous page*

| Author | Correlation |
|---|---|
| | $Re = Gd_h/\mu_L \;\; p_R = p/p_{cr} \;\; S_V = [(\rho_L/\rho_G) - 1]/[x(\rho_L/\rho_G) + 1 - x]$ |
| Cavallini et al. [5] | $Nu = \frac{\alpha D}{\lambda_L} = 0{,}05 Re_{eq}^{0,8} Pr_L^{1/3} Rx^S (Bo * Fr)^t$ |
| | $Re_{eq} = 4M \left[(1-x) + x(\rho_L/\rho_G)^{1/2}\right] / (\phi d \mu_L) Pr_L = \mu_L c_{pL}/\lambda_L$ |
| | $Rx = \{[2hn_g(1 - \sin(\gamma/2))] / [\phi d \cos(\gamma/2)] + 1\} / \cos(\beta)$ |
| | $Fr = u_{GO}^2/(gd) \;\; Bo = g\rho_L h \phi d/(8\sigma n_g)$ |
| | $Low - fins \; (h/d \geq 0{,}04) \;\; s = 1{,}4 \;\; t = -0{,}08$ |
| | $Micro - fins \; (h/d < 0{,}04) \;\; s = 2{,}0 \;\; t = -0{,}26$ |
| | $Cross - frooved \;\; s = 2{,}1 \;\; t = -0{,}26$ |
| | $Re_{eq} < 15000 \;\; 3 < Pr_L < 6{,}5 \;\; 0{,}3 < Bo * Fr < 508 \;\; 7° < \beta < 30°$ |
| Shikazono et al. [40] | $\alpha = \frac{\lambda_L}{d_i} \left[(f * Nu_B)^2 + Nu_F^2\right]^{1/2}$ |
| | $Nu_B = 0{,}725 * H(\xi) * \left(\frac{Ga * Pr_L}{H_L}\right)^{1/4}$ |
| | $Nu_F = 0{,}0152(1 + 0{,}6 Pr_L^{0,8}) \frac{\Theta_V}{X_{tt}} Re_L^{0,77}$ |
| | $H(\xi) = \xi + \left\{10(1-\xi)^{0,1} - 8{,}9\right\} \sqrt{\xi}(1 - \sqrt{\xi})$ |
| | $\Theta_V = 1 + 0{,}5 \left[\frac{G}{\sqrt{g d_i \rho_G (\rho_L - \rho_G))}}\right]$ |
| | $X_{tt} = \left(\frac{1-x}{x}\right)^{0,9} \left(\frac{\rho_G}{\rho_L}\right)^{0,5} \left(\frac{\mu_L}{\mu_G}\right)^{0,1}$ |
| | $Ga = \frac{g\rho_L^2 d_i^3}{\mu_L^2} \;\; H_L = \frac{c_{p_L}(T_i - T - w)}{L}$ |
| | $Re_L = \frac{G(1-x)d_i}{\mu_L}$ |

## 2.4 Pressure drop

In designing condensation heat transfer equipment, the prediction of pressure drop is as important as the prediction of heat transfer coefficient for having an accurate design and optimization of refrigeration systems. In a reverse cycle, the pressure drops influence the temperature profile of both the condenser and evaporator. Indeed, due to pressure losses, the saturation pressure inside the heat exchangers decreases and therefore the saturation temperature decrease too. In the condenser, this drop of temperature negatively influence the logarithmic temperature difference and consequently the performance of the condenser.

### 2.4.1 Single-Phase pressure drop

When a single-phase fluid flows in a hydraulic system the fluid pressure changes both as a result of the conversion of the kinetic energy to potential one and vice versa and also due to an irreversible conversion of part of the mechanical energy of the fluid to heat due to viscous friction forces in the flow. In a tube, there are three types of fluid regimes depending on the flow conditions. They are laminar, transient and turbulent flows regimes. In laminar flow, fluid particles have all the same direction and the velocity of the fluid is small, but flow turns turbulent when the velocity is increased. The transition from laminar to turbulent flows does not happen sharply, it can be defined as a mixture of laminar and turbulent flows. Turbulent flow can be seen with high flow rates and the flow particles behave randomly. Contrary to laminar flow, the boundary layer is thin in a turbulent flow. The flow regime in most engineering applications is assumed as turbulent. In real applications, is difficult to define precise values of Reynolds number, calculated as in eq. 2.17 for laminar, transitional and turbulent flows because the transition between different flows depends on many variables. Under most practical conditions, flow in a tube is laminar for $Re < 2300$, turbulent for $Re > 10{,}000$ and transitional between this numbers. In industrial applications, for all types of internal flows such as laminar or turbulent flows, circular or non circular tubes, and smooth or rough surfaces, an equation can be used to calculate pressure drop and it is given below:

$$\Delta P = f * \frac{L}{D} * \frac{\rho * u^2}{2} \tag{2.24}$$

where $L$ is the tube length, $D$ is the tube diameter, $\rho$ is the fluid density, $w$ is the fluid velocity and the dimensionless quantity $f$ is the friction factor. The friction factor for fully developed laminar flow in a circular tube is [12]:

$$f = \frac{64 * \mu}{\rho * D * u} = \frac{64}{Re} \tag{2.25}$$

This equation shows that in laminar flow, the friction factor is a function of the Reynolds number only and is independent of the roughness of the tube surface. For turbulent flow, the determination of the frictional factor depends also on the geometry of the tube and its surface roughness. The use of structured tubes causes an increase in the heat transfer coefficient but at the same time, the pressure drop increases too. Several studies have been carried out for analyzing the relations between the increase of heat transfer coefficient and pressure drop for single-phase process and to determine various equation able to calculate the pressure drop for structured tubes. Coppetti et al. [14] compared experimentally heat transfer performances of smooth and micro-fin tubes at different flow rates. They compared measured friction factor data with Blasius [6] and Petukhov [35] equations and heat transfer coefficient data with Dittus–Boelter [16] and Gnielinski [21] equations. The experimental study showed that the heat transfer coefficient of the micro-fin tube was 2.9 times higher than the smooth tube in a turbulent flow. Although the pressure drop of the micro-fin tube was 1.7 times higher than a smooth tube, the heat transfer increase was approximately 80%. Wei at al. [29] carried out an experimental study in order to determine the single-phase heat transfer and pressure drop in micro-fin tubes. In the study, experiments were conducted for Reynolds number ranging between 2500 and 90,000. Friction factors of smooth and micro-fin tubes were just about equal for Reynolds number less than 10,000 but friction factor of the micro-fin tube was 40–50% higher when it was compared with a smooth tube for Reynolds number higher than 30,000. Jensen and Vlakancic [24] proposed new correlations for the prediction of Nusselt number and friction factor of both high and micro-fin tubes. They investigated the effect of fin geometry on the performance of finned tubes using of these correlations and compared friction factor and Nusselt number results with Filonenko [6] and Gnielinski [21] correlations for the smooth tube. The correlations were applied to a smooth tube and 15 finned tubes having a different outside diameter, inside diameter fin height, fin thickness and fin helix angle. Their study showed that the friction factor and Nusselt number increased with increasing numbers of fins. As another result of their study, friction factor and Nusselt number increased with increasing fin height under the same conditions. Celen et al. [12] proposed a new correlation for the calculation of friction factor for micro-fin tubes and compared the experimental results with the equations in the literature. As results of their studies, it was found out that the friction factor decreased gradually as the Reynolds number increased for both smooth and micro-fin tubes. Also, the pressure drop increased gradually as the Reynolds number increased for both smooth and micro-fin tubes. Other results are that the friction factor and pressure drop values for the micro-fin tubes were higher than those for smooth tubes. This implies that the micro-fin tube produced more

flow disturbance by the occurrence of the swirl flow and flow recirculation produced by the fins, which led to a higher frictional pressure drop. Here are reported some of the equation for the calculation of the frictional factor for smooth tubes and micro-fin tubes in case of turbulent flows.

| | Author | Correlation |
|---|---|---|
| Smooth Tubes | Blasius | $f = 0{,}316 * Re^{-1/4}$ |
| | Colebrook | $f = \left(1{,}8 * log\frac{Re}{6{,}9}\right)^{-2}$ |
| | Konakov | $f = (1{,}8 * logRe - 1{,}5)^{-2}$ |
| Micro-fin Tubes | Zdaniuk et al. | $f = 0{,}128 * Re^{-0{,}305} n^{0{,}235} (\frac{e}{D})^{0{,}319} \alpha^{0{,}397}$ |
| | Al Fahed et al. | $f = 0{,}9978 Re^{-0{,}2943}$ |
| | Haaland | $f = \frac{0{,}3086}{\left\{log\left[\frac{6{,}9}{Re} + (\frac{e}{3{,}7D})^{1{,}11}\right]\right\}^2}$ |

Table 2.4: Equations for the calculation of frictional factor

### 2.4.2 Two-Phase pressure drop

Due to the occurrence of different flow regimes and the consequent discontinuity, multi-phase flows, in contrast, to single-phase flows, are highly complex. The calculation of pressure losses therefore presupposes simplified modeling of the discontinuous flow conditions by averaging the flow variables. The averaging can be based on different model approaches which treat the discontinuous flow as a continuous flow. Two elementary model approaches, that are most frequently mentioned in the literature, are the homogeneous model and the heterogeneous model. Both models assume constant average flow velocities over the entire pipe cross-section. The homogeneous model is based on the assumption that gas and liquid have the same velocities. This means that the two-phase mixture can be treated as a single-phase fluid and calculated using the relations for single-phase flows. For this purpose, the fluid characteristics and velocities of the homogeneous mixture resulting from the mean values of both phases are used. The heterogeneous model is much more realistic than the homogeneous model. It is based on the assumption that both phases flow separately from each other at different velocities in the pipe. Constant fluid characteristics are assumed for both phases. The two-phase pressure drops for flows

inside tubes is the sum of three contributions: the static pressure drop $\Delta p_{static}$, the momentum pressure drop $\Delta p_{mom}$ and the frictional pressure drop $\Delta p_{frict}$ as:

$$\Delta p_{total} = \Delta p_{static} + \Delta p_{mom} + \Delta p_{frict} \tag{2.26}$$

For horizontal tube, there is no change in static head so $\Delta p_{static} = 0$. The momentum pressure drop reflects the change in kinetic energy of the flow and can be

- **Homogeneous model**
  As already explained before, this model considers the two-phase fluid as homogeneous mixture in which both phases flow at the same average speed

$$u_l = u_g \tag{2.27}$$

  that is equal to define the slip factor is equal to 1 where this factor is defined as:

$$S = \frac{u_g}{u_l} \tag{2.28}$$

  From this hypothesis is possible to calculate the expression of the homogeneous void fraction

$$u_g = \frac{Gx}{\xi \rho_g} = u_l = \frac{G(1-x)}{(1-\xi)\rho_l} \tag{2.29}$$

$$\xi_{HO} = \frac{\frac{x}{\rho_g}}{\frac{x}{\rho_g} + \frac{(1-x)}{\rho_l}} = \frac{1}{1 + \frac{(1-x)\rho_g}{x\rho_l}} \tag{2.30}$$

  As already defined in equation 2.2 the void fraction is a parameter defined as the cross-sectional area occupied by the vapour in relation to the area of the flow channel. This factor is always used to determine the flow pattern transition, heat transfer coefficient and two-phase pressure drop. Because of its importance, numerous studies have been conducted on the modeling of void fractions and are based on different models and correlations, however, there is a lack of void fraction correlations on the condensation inside micro-fin tubes in the literature. Determination of void fraction in a micro-fin tube is an important design and operating parameter for the heat exchanger, and it is necessary to calculate the amount of refrigerant charge in the evaporator and the condenser. The homogeneous model for the calculation of the void fraction remains the simplest one because it assumed a homogeneous mixture providing uniform velocities for both phases. Other methods of calculation are: slip ratio void fraction models; Lockhart and Martinelli parameter based

| Void Fraction model | Correlation |
|---|---|
| Homogeneous model | $\xi_H = \frac{1}{1+\left(\frac{1-x}{x}\right)\left(\frac{\rho_g}{\rho_l}\right)S} \quad S = 1$ |
| Chen | $\xi = (1 + 0{,}18(\frac{1-x}{x})^{0{,}6}(\frac{\rho_g}{\rho_l})^{0{,}33}(\frac{\mu_l}{\mu_g})^{0{,}007})^{-1}$ |
| Lockhart and Martinelli | $\frac{1-\xi}{\xi} = 0{,}28(\frac{1-x}{x})^{0{,}64}(\frac{\rho_g}{\rho_l})^{0{,}36}(\frac{\mu_l}{\mu_g})^{0{,}07}$ |
| Rohuani | $\xi = \frac{(x\rho_L)}{\left\{C_O[x\rho_L+(1-x)\rho_G]+\frac{(\rho_L\rho_G u_{gj})}{G}\right\}}$ |
| Hammersma and Hart | $\xi = (1 + 0{,}26(\frac{1-x}{x})^{0{,}67}(\frac{\rho_g}{\rho_l})^{0{,}33})^{-1}$ |
| Chisholm and Laird | $\xi = 1 + \left[\frac{0{,}8}{\left(1+\frac{21}{X}+\frac{1}{X^2}\right)}\right]^{1{,}75}$ |

Table 2.5: Model for calculation of void fraction

void fraction models; flow regimes based void fraction models; and general void fraction models. [15] In the table 2.5 are reported the most common models for the calculation of the void fraction based on the different models.

Regarding the homogeneous methods for the pressure drop, after the initial assumption is possible to define the density of the two-phase mixture as:

$$\rho_M = \rho_{HO} = \xi\rho_g + (1-\xi)\rho_l = \left[\frac{x}{\rho_g} + \frac{(1-x)}{\rho_l}\right]^{-1} \tag{2.31}$$

So in the homogeneous model, the two-phase mixture is managed as an equivalent single-phase compressible fluid with average velocity of $u = u_l = u_g$ and density $\rho_{HO}$. With the hypothesis of homogeneous motion, the expression for total pressure gradient is equal to the sum of three component: the gravity pressure drop component; the acceleration pressure gradient and the frictional pressure gradient. [6]

$$\left(-\frac{dp}{dz}\right) = \left(-\frac{dp}{dz}\right)_{gr} + \left(-\frac{dp}{dz}\right)_{a} + \left(-\frac{dp}{dz}\right)_{f}. \tag{2.32}$$

The gravity pressure drop component can be calculated as

$$\left(-\frac{dp}{dz}\right)_{gr} = g\xi_{HO}sin\beta \tag{2.33}$$

and $\beta$ represent the inclination of the tube. The acceleration gradient can be

expressed with

$$\left(-\frac{dp}{dz}\right)_a = G^2 \frac{d}{dz}\left(\frac{x^2}{\xi\rho_g} + \frac{(1-x)^2}{(1-\xi)\rho_l}\right) = G^2 \frac{d}{dz}\left(\frac{1}{\rho_{HO}}\right). \tag{2.34}$$

The frictional component can be calculated as

$$\left(-\frac{dp}{dz}\right)_f = \frac{2 f_{HO} G^2}{D_h \rho_{HO}} \tag{2.35}$$

and $f_{HO}$ is the friction factor that can be calculated with the equations of a single phase flow

$$Re_{HO} = \frac{GD}{\mu_{HO}} \qquad \begin{array}{ll} f_{HO} = \frac{16}{Re_{HO}} & Re_{HO} < 2000 \\ f_{HO} = 0{,}079 Re_{HO}^{-0{,}25} & Re_{HO} > 2000 \end{array}$$

In the literature, it is possible to find a lot of expressions for the calculation of the viscosity of the homogeneous two-phase mixture $\mu_{HO}$. The homogeneous model can be applied with sufficient accuracy in the system where one of the two phases is finely dispersed in the other one so that the average speeds of the two phases result in almost the same. This model is not realistic when there is the presence of rapid variations of the motion parameters or when there is a separation of the phases. This model can give good results if the two-phase flow can be represented as a single-phase one. That can be assumed as true when velocity and pressure are high so that the inertial forces are bigger than the gravitational ones.

- **Heterogeneous model**
  With this model each phase flow in a different region of the pipe with its own mean velocity. The total pressure gradient is calculated in the same way as the case of the homogeneous model as it showed in equation 2.32. The determination of the gradient of gravity and momentum change can be carried out in the same way as the homogeneous model, through the use of the void fraction. The calculation of the void fraction is done using one of the equation described in the previous section and resumed in the table 2.5. Otherwise, the frictional gradient can be calculated through the use of an empirical equation based on experimental measurement. However, if this data are calculated using measurements of the total pressure gradient and then subtracting the component of gravity and momentum change, also the frictional component can be related to the void fraction. In adiabatic two-phase flow, the frictional

pressure gradient can be related to single-phase frictional pressure gradients by considering the vapour or the liquid phase flowing alone in the channel with their actual flow rates or with the total mass flow rate. For this reason, it is possible to define the frictional multipliers. This parameters are defined as the ratio between the two-phase frictional pressure gradient and the liquid or gas phase pressure gradient when they flow alone in the tube with their own flow.

$$\Phi_G^2 = \frac{-\left(\frac{dp}{dz}\right)_f}{-\left(\frac{dp}{dz}\right)_{f,G}} \quad (2.36) \qquad \Phi_L^2 = \frac{-\left(\frac{dp}{dz}\right)_f}{-\left(\frac{dp}{dz}\right)_{f,L}} \quad (2.37)$$

$$\Phi_{GO}^2 = \frac{-\left(\frac{dp}{dz}\right)_f}{-\left(\frac{dp}{dz}\right)_{f,GO}} \quad (2.38) \qquad \Phi_{LO}^2 = \frac{-\left(\frac{dp}{dz}\right)_f}{-\left(\frac{dp}{dz}\right)_{f,LO}} \quad (2.39)$$

where the different index have the following meaning.

| | |
|---|---|
| G | vapour flow with its own mass flux |
| L | liquid flow with its own mass flux |
| GO | vapour flow with total mass flux |
| LO | liquid flow with total mass flux |

The single-phase frictional pressure gradient can be evaluated by using the correlations which make use of the friction factor $f$ as showed below

$$\left(-\frac{dp}{dz}\right)_{f,L} = \frac{2f_L G^2(1-x)^2}{D_h \rho_L} \quad (2.40) \qquad \left(-\frac{dp}{dz}\right)_{f,G} = \frac{2f_G G^2(1-x)^2}{D_h \rho_G} \quad (2.41)$$

$$\left(-\frac{dp}{dz}\right)_{f,LO} = \frac{2f_{LO} G^2}{D_h \rho_L} \quad (2.42) \qquad \left(-\frac{dp}{dz}\right)_{f,GO} = \frac{2f_{GO} G^2}{D_h \rho_L} \quad (2.43)$$

The frictional factor should be calculated through the equation for the single-phase flow as a function of the respective Reynolds number

$$Re_L = \frac{G(1-x)D}{\mu_L} \tag{2.44}$$

$$Re_G = \frac{GxD}{\mu_G} \tag{2.45}$$

$$Re_L = \frac{GD}{\mu_L} \tag{2.46}$$

$$Re_G = \frac{GD}{\mu_G} \tag{2.47}$$

In the literature is possible to find several correlations for the determination of the frictional multipliers. Lockhart and Martinelli [30] introduced in their study a calculation model based on the frictional multipliers that form the basis for many other correlations of frictional pressure losses. Some of the best-known models are listed in [33]. These include the Chisholm [13] correlation that adapted the Baroczy model, which introduced the mass flow as an influencing parameter, for the use in flows with evaporation process in smooth tubes. Fridel [20] also described a method developed based on the correlation of Lockhart and Martinelli [30] and still very used to determine the frictional pressure losses. This correlation was developed through the use of a database consisting of 25000 measured data of various refrigerants and mixtures. To determine the frictional multiplier $\Phi$ the density $\rho$ and the dynamic viscosity $\mu$ of the gas or liquid are required. Furthermore, the pipe friction coefficient $f$ of each phase is calculated as a function of the Reynolds number. The validity range of this model is for a viscosity ratio of $\mu_L/\mu_G < 1000$ and for a mass flow density $\dot{G} > 100 kg/m^2 s$. Another correlation is presented by Müller-Steinhagen and Heck [32]. Their model for the calculation of the frictional pressure loss of an adiabatic two-phase flow is based on an interpolation of the single-phase friction pressure losses of gas and liquid. This idea is based on the knowledge that the frictional pressure loss of a two-phase flow, increase with increasing steam content till it reaches a maximum at $x \cong 0{,}85$ and than decrease again till the value of the single-phase pressure loss of the gas flow. Another important factor is that the pressure loss for a pure gas flow ($x = 1$) almost always corresponds to the frictional pressure loss of a two-phase flow with a vapour content of $x = 0{,}5$. Based on this concept the model, developed through experimental investigations, defined a correlation in which the single-phase friction pressure losses of the two phases are described through the definition of two coefficient A and B. These parameters depend on mass flow, density of the phase, tube diameter and coefficient of friction. The range of validity of this model is for Reynolds number $Re_g < 100$ of the gas phase.

The correlation of Cavallini et al. [8], which is used to calculate the heat transfer during condensation, is based on the model of Friedel [20]. In their study, the shear stress forces that occur in an annular flow during condensation in the horizontal pipe, are to be determined with the help of the friction pressure loss. The model by Friedel [20] is modified by Cavallini et al. [8] so that dimensionless parameters are introduced, which are calculated depending on the material proprieties of the gas or the liquid. The two-phase friction pressure loss is calculated with the modified two-phase multiplier of the liquid phase $\Phi_{f,L}$. The two-phase multiplier is a function of the Weber number of the vapour, which describes the ratio of the inertial forces acting on the gas phase to the surface forces. The use of structured tubes like micro-fin tube is the most common passive enhancement device for the condensers in use nowadays due to their high heat transfer performance and a moderate increase in pressure drop. All the model described have been developed regarding pressure drop inside smooth tubes, so without considering the effect of the structure of the tube on the pressure loss. The determination of frictional pressure drop in the case of micro-fin tubes has to consider the effect on the flow of the structure. Numerous researches have been conducted on condensation in micro-fin tubes as for example the one on Kedzierski and Goncalves [26]. In their study, they investigated the fluids R32, R125, R134a and R410a in micro-fin tubes and modified a previous correlation developed by Pierre et al. [2] for flow boiling pressure drop in a horizontal tube, to compute a friction factor that takes account of the fin effect on the flow. In the model a new friction factor was developed to account for the fin effect on the flow and the influence of the fin height on the Reynolds number exponent was consistent with the Moody chart, suggesting that the surface behaves like a roughness in enhancing the heat transfer. As reported in Cavallini et al. [6] some of the studies developed for smooth tubes can be used for the determination of pressure drop also with structured tubes by using a suitable friction factor. As showed by Ito and Kimura [22], the single-phase friction factor for micro-finned tubes tends to the value for smooth tubes at low Reynolds numbers. At high Reynolds numbers, it depends on the ratio of fin height to tube diameter and the fins spiral angle. Cavallini et al. [6] suggest for the correlation of Cavallini et al. [8] that the single-phase friction factor to be used, should be taken as the higher value of the one obtained from the Blasius equation for smooth tubes. Also, the Friedel [20] equations used in the Cavallini et al. [8] have been developed for adiabatic two-phase flow so they need a correction when applied for condensation. A correction factor $\Theta$ is suggested for the effects of mass transfer on the interfacial shear stress- This factor is a function of the mass flow, the

condensation interface mass flux, the interfacial shear stress for adiabatic flow and the mean velocity.

Table 2.6: Models for calculation of pressure drop for smooth tubes

| **Author** | **Correlation** |
|---|---|
| Friedel [20] | $\Delta p_{frict} = \delta p_L \Phi_{LO}^2$ |
| | $\Delta p_L = 4 f_L (L/d_i) \dot{m}_{total}^2 (1-x)^2 (1/2\rho_L)$ |
| | $\Phi_{Lo}^2 = E + \frac{3{,}24FH}{Fr_h^{0,045} We_L^{0,035}}$ |
| | $Fr_h = \frac{\dot{m}_{total}^2}{g d_i \rho_h^2}$ |
| | $E = (1-x)^2 + x^2 \frac{\rho_L f_G}{\rho_G f_L}$ |
| | $F = x^{0,78} W (1-x)^{0,224}$ |
| | $H = \left(\frac{\rho_L}{\rho_G}\right)^{0,91} \left(\frac{\mu_G}{\mu_L}\right)^{0,19} \left(1 - \frac{\mu_G}{\mu_L}\right)^{0,7}$ |
| | $We_L = \frac{\dot{m}_{total}^2 d_i}{\sigma \rho_{OM}}$ |
| | $f_L = 64/Re$ |
| Chisholm [13] | $\left(\frac{dp}{dz}_{frict}\right) = \left(\frac{dp}{dz}_{LO}\right) \Phi_{LO}^2$ |
| | $f_{LO} = 16/Re \;\; for\ Re < 2000$ |
| | $f_{LO} = 0{,}09/Re^{0,25} \;\; for\ Re < 2000$ |
| | $\Phi_{LO}^2 = 1 + (Y^2 - 1)[B x^{(2-n)/2} (1-x)^{(2-n)/2} + x^{2-n}]$ |
| | $Y^2 = \frac{(dp/dz)_{GO}}{(dp/dz)_{LO}}; \;\; n = 0{,}25$ |
| if 0<Y<9,5 | $B = 55/\dot{m}_{total}^{1/2} \; for\ \dot{m}_{total} \geq 1900 kg/m^2 s$ |
| | $B = 2400/\dot{m}_{total} \; for\ 500 < \dot{m}_{total} < 1900 kg/m^2 s$ |
| | $B = 4{,}8 \; for\ \dot{m}_{total} \leq 500 kg/m^2 s$ |
| if 9,5<Y<28 | $B = 520/Y \dot{m}_{total}^{1/2} \; for\ \dot{m}_{total} \leq 600 kg/m^2 s$ |
| | $B = 21/Y \; for\ \dot{m}_{total} > 600 kg/m^2 s$ |
| if Y>28 | $B = 15000/Y^2 \dot{m}_{total}^{1/2}$ |

*Continued on next page*

Table 2.6 – *Continued from previous page*

| Author | Correlation |
|---|---|
| Müller-Steinhagen and Heck [32] | $\left(\frac{dp}{dz}\right)_{frict} = G(1-x)^{1/3} + Bx^{1/3}$ |
| | $G = A + 2(B-A)x$ |
| | $A = \left(\frac{dp}{dz}\right)_{f,L} = f_L \frac{\dot{m}^2}{\rho_l d}$ |
| | $B = \left(\frac{dp}{dz}\right)_{f,G} = f_G \frac{\dot{m}^2}{\rho_g d}$ |
| | $f_L = 64/Re_L;\ f_G = 64\Re_G \ \ for\ Re_G, Re_L \leq 1187$ |
| | $f_L = 0{,}3164/Re_L^{1/4};\ f_G = 0{,}3164\Re_G^{1/4} \ \ for\ Re_G, Re_L > 1187$ |
| Cavallini et al. [8] | $\left(\frac{dp}{dz}_{frict}\right) = \left(\frac{dp}{dz}_{LO}\right) \Phi_{LO}^2 = \Phi_{LO}^2 2 f_{LO} G^2/(D\rho_L)$ |
| | $\Phi_{LO}^2 = E + (1{,}262FH)/(We^{0{,}1458})$ |
| | $E = (1-x)^2 + x^2(\rho_L f_{GO})/(\rho_G f_{LO})$ |
| | $F = x^{0{,}6978} \ \ We = G^2 D/(\rho_G \sigma)$ |
| | $H = (\rho_L/\rho_G)^{0{,}3278}(\mu_G/\mu_L)^{-1{,}181}(1-\mu_G/\mu_L)^{3{,}477}$ |
| | $f_{LO} = 0{,}046[GD/\mu_L]^{-0{,}2} \ \ GD/\mu_L > 2000$ |
| | $f_{GO} = 0{,}046[GD/\mu_G]^{-0{,}2} \ \ GD/\mu_G > 2000$ |
| | $f_{LO} = 16/[GD/\mu_L] \ \ GD/\mu_L \leq 2000$ |
| | $f_{GO} = 16/[GD/\mu_G] \ \ GD/\mu_G \leq 2000$ |

Table 2.7: Models for calculation of pressure drop for two-phase flow in structured tubes

| Author | Correlation |
|---|---|
| Kedzierski and Goncalves [26] | $\Delta p = fG^2(1/\rho_{out} + 1/\rho_{in})L/d_h + G^2(1/\rho_{out} - 1/\rho_i n)$ |
| | $f = \{0{,}002275 + 0{,}00933 exp[h/(-0{,}003 d_r)]\} * \ldots$ |
| | $* Re^B [(x_{in} - x - out h_{LG}/(Lg))]^{0{,}211}$ |

*Continued on next page*

Table 2.7 – *Continued from previous page*

| Author | Correlation |
|---|---|
| | $Re = Gd_h/\mu_L \;\; B = -(4{,}16 - 532h/d_r)^{-1}$ |
| Cavallini et al. [8] | $\left(\frac{dp}{dz}_{frict}\right) = \left(\frac{dp}{dz}_{LO}\right) \Phi_{LO}^2 = \Phi_{LO}^2 2 f_{LO} G^2/(D\rho_L)$ |
| | $\Phi_{LO}^2 = E + (3{,}23FH)/(We^{0{,}035} Fr^{0{,}045})$ |
| | $E = (1-x)^2 + x^2(\rho_L f_{GO})/(\rho_G f_{LO})$ |
| | $F = x^{0{,}78}(1-x)0{,}224 \;\; We = G^2 D/(\rho_G \sigma)$ |
| | $H = (\rho_L/\rho_G)^{0{,}91}(\mu_G/\mu_L)^{0{,}19}(1-\mu_G/\mu_L)^{0{,}7} \;\; Fr = G^2/(gd\rho_{OM})$ |
| | $f_{LO} = max(f_{LO1}, f_{LO2}) \;\; f_{GO} = max(f_{GO1}, f_{GO2})$ |
| | $f_{LO1} = 0{,}079[GD/\mu_L]^{-0{,}25} \;\; GD/\mu_L > 2000$ |
| Cavallini et al. [8] | $f_{GO1} = 0{,}079[GD/\mu_G]^{-0{,}25} \;\; GD/\mu_G > 2000$ |
| | $f_{LO1} = 16/[GD/\mu_L] \;\; GD/\mu_L \leq 2000$ |
| | $f_{GO1} = 16/[GD/\mu_G] \;\; GD/\mu_G \leq 2000$ |
| | $(4f_{LO2})^{-0{,}5} = (4f_{GO2})^{-0{,}5} = 1{,}74 - 2\log 10[2e/d]$ |
| | $e/d = 0{,}18(h/d)/(0{,}1 + \cos\beta)$ |
| | $\Theta = \Phi_F[exp(\Phi_F) - 1] \;\; \Phi_F = -[G_c u_G/\tau_1]$ |
| | $G_c = M(dx/dz)/(\phi d) \;\; \tau_1 = (dp/dz)_{f,adiab} d/4u_g = Gx/(\rho_G \xi)$ |
| | $\xi = (x\rho_L)/\{C_o[x\rho_L + (1-x)\rho_G] + (\rho_l \rho_G u_g)/G\}$ |
| | $G_c = M(dx/dz)/(\phi d) \;\; \tau_1 = (dp/dz)_{f,adiab} d/4u_g = Gx/(\rho_G \xi)$ |
| | $u_g = 1{,}18(1 - x[\sigma g(\rho_L - \rho_G)/\rho_L^2]^{1/4})$ |
| | $C_o = 1 + 0{,}2(1-x)[(gd\rho_L^2)/G^2]^{1/4} \;\; for\ \xi > 0{,}1 \;\; C_o \rightarrow 0 \;\; for\ \xi \rightarrow 0$ |

# Chapter 3

# EXPERIMENTAL SETUP

In this chapter, the main component of the test rig will be described. Next to the experimental setup, the data reduction will be explained in detail.

## 3.1 Test facility

The KIIR test rig was built by the Thermodynamic department of Kassel University to measure the convective heat transfer coefficient, the pressure drop, the heat transfer and the momentum transport inside tubes during condensation. Due to the characteristics of the test rig, it is possible to investigate various parameters over a wide range. The working fluid may be changed as well, to analyse different test conditions. The facility, presented in figure 3.1, consists mainly of a primary cycle which includes the test section, a bypass cycle and three secondary cycles, one of them involved in the test section.

### 3.1.1 Primary Cycle

In the primary cycle, the test fluid gets conditioned to be investigated in the test section. The secondary cycles, consisting of 4 heat exchangers, are used for regulating the test fluids temperature and pressure. 3.2. A multi-phase pump (1) delivers a two-phase working fluid into a phase separator (2). The multi-phase pump is a specially developed prototype screw pump for low-viscosity liquids and to ensure that it works properly, three conditions must be checked:

- The gas content (mass-based) at suction has to be greater than 94% to avoid overheating due to compression.
- The suction pressure must be greater than 0.5 bar to avoid cavitation

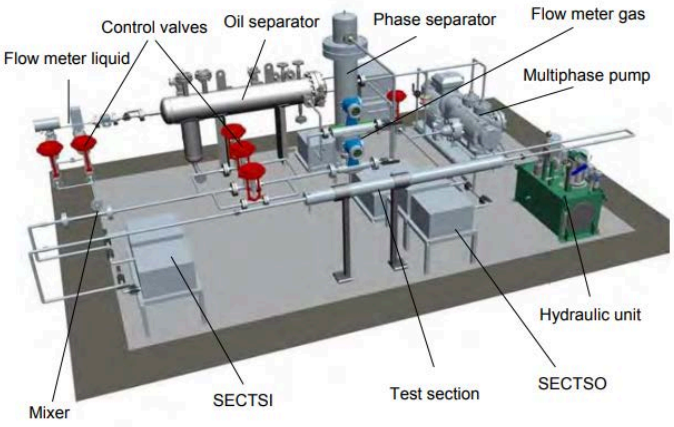


Figure 3.1: Representation of the main component of the test facility

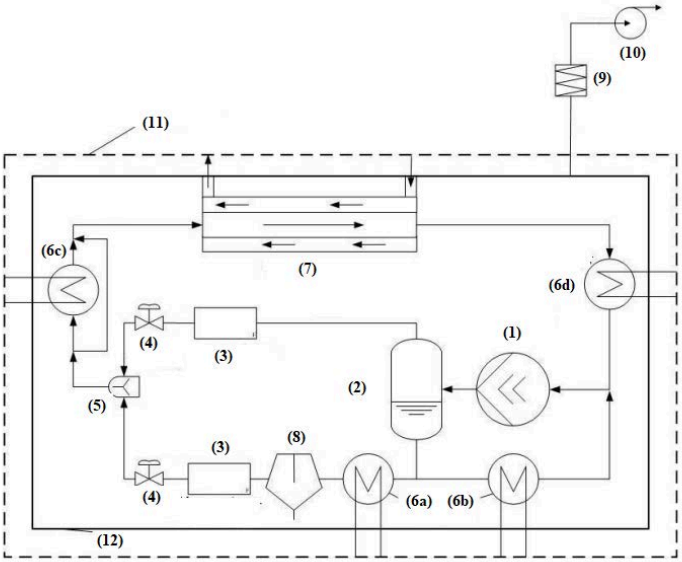


Figure 3.2: Design of the test facility

- The pressure difference between suction and discharge must be lower than 10 bar due to mechanical limitation.

The rotational speed range of the pump is between 400 rpm and 1500 rpm. In the phase separator the two phases, liquid and gas, are divided by gravitational effect and from here they will follow a different path. The liquid line, after the separator, splits in two. One side leads to the liquid by-pass section where is provided with a flow meter and a heat exchanger (6b) that dissipate the heat injected by the pump. The heat exchanger can control the pressure in the separator (and therefore at the

| Number | Description |
|---|---|
| 1 | Multi-phase pump |
| 2 | Phase separator |
| 3 | Mass flow meters |
| 4 | Control valve |
| 5 | Static mixer |
| 6 | Heat exchanger |
| 7 | Measuring section |
| 8 | Oil separator |
| 9 | Activated carbon filter |
| 10 | Ventilator |
| 11 | Secondary circuit |
| 12 | Plastic case |

Table 3.1: Description of the facility's components

inlet of the test suction) by controlling the temperature of the liquid because, as it is in saturation condition, every change in the liquid temperature correspond to a variation of its pressure. This by-pass line has also the purpose of both preserve the integrity of the multi-phase pump and give the possibility to adjust the liquid mass flux at the inlet of the pump with a valve. The other liquid line after the separator leads to the test section, conducting the liquid through a series of components. The first one is a heat exchanger (6a), which subcool the liquid to prevent it from evaporating, as it is in saturated conditions after passing through the phase separator. Afterwards, the liquid pass through an oil separator unit (8). This component extracts the oil from the liquid flow that is used as sealing and lubricant in the pump. This process takes place due to coalescence phenomena and is important since oil presence in the working fluid can affect the heat transfer measurements. After being purified, the liquid flows in two parallel pipes, connected with two Coriolis flow meters (3) able to measure mass flow in different but partially overlapped ranges. Next to this measurement section, there are two needle valves (4) that control the mass flow allowed in the static mixer (5). The gas line instead, start from the top of the phase separator and its path is composed of a measurement station (3) involved two Coriolis mass flux meters and three-needle valves (4) in parallel capable of setting the pressure loss like the previous one. The two lines converged in a static mixer (5) that is able to provide the desired fluid composition to the test section.

### 3.1.2 Secondary Cycles

The secondary cycles used in this test facility are auxiliary components placed to vary the temperature of the working fluid. They are mainly composed of a heating or cooling machine, a pump, a heat exchanger and a thermostat that controls the temperature of the secondary working fluid. In total three cycles are installed:

- **Test Section Inlet Cycle** (*SECTSI*), placed before the entrance of the test section, provides heat to the working fluid to raise the inlet temperature, especially to provide overheated gas for the test. In two-phase applications, it can be used to control the gas quality of the working fluid. It is equipped with five valves that allow the working fluid to bypass the heat exchanger or to flow in a smaller part of it to reduce the pressure drop for high mass flows.

- **Test Section Cycle** (*SECTS*), is the cycle connected to the test section and will be discussed in the next section.

- **Test Section Outlet Cycle** (*SECTSO*) is connected to a heat exchanger downstream the test section and is used for the validation of the test rig and to complete the condensation in phase transition tests. It is also connected to one of the two heat exchangers in the bypass. So its purpose is to cool the working fluid.

### 3.1.3 Test Section

The test section is the main component of the test facility and it is composed of the test pipe coupled with the Test Section Cycle (SECTS). The test section is a straight tube-shell heat exchanger and it is positioned between an inlet and outlet compensator sleeve that has the function to avoid stress on the test section due to pressure change. The test tube is connected to the test facility by screwed connections suitable for high pressure (up to 120 bar) so that the test tube can be changed quickly and easily if necessary. Outside the test tube, in the shell, flows a thermal oil (therminol D12) which is used for cooling the working fluid.

In every measurement typologies, the disposition of pressure and temperature sensors for measurements of secondary fluid (therminol D12) characteristics are the same. The temperature of the secondary fluid, along the test section, is measured in 20 positions through the use of resistance thermometers (PT100). In every measurement section, the position of the temperature sensor has an offset of 180° so that along the test tube all the PT100 are alternated in the upper and bottom side of the tube. The reason for this displacement is improving accuracy in the measurement of the oil temperature and to avoid errors that the turbulent flow

inside the annulus could create. The pressure of the secondary fluid is measured at the inlet and outlet section. Based on the typology of measurement needed, the configuration of the sensors in the test tube will be different. In this test facility, is possible to perform measurements of heat transfer with detection of the temperature in various sections along the test tube (local measurement) or measurements of heat transfer with the detection of the temperature only at the inlet and outlet section (integral measurements). Based on the needed typologies, the configuration and number of the sensor will be different. For both integral and local measurement, temperature and differential pressure across the test section are measured by two pressure and temperature sensors positioned at the inlet and outlet of the test tube. Figure 3.3 shows the configuration of the sensors common to both types of measurements.

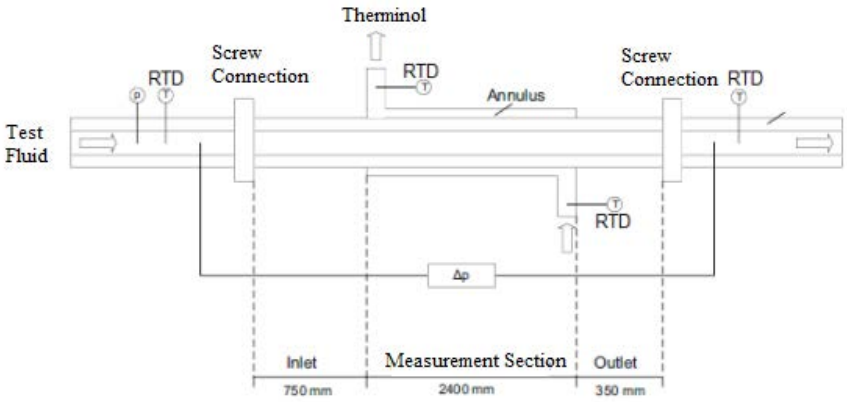


Figure 3.3: Configuration test section

- **Local measurement** To not disturb the in-pipe flow and consequently to have a better hydro thermodynamic behavior of the working fluid, inside the test pipe there are no sensors. To obtain temperature data along the test tube, shielded type K thermocouples are glued into grooves positioned around the test tube wall. Along the test tube there are 4 measurement positions and in every position are placed 6 thermocouples for a total of 24 temperature sensors positions on the test section. In every measurement sections are present 12 grooves for placing thermocouples but only 6 are glued in each section. The reason for this is to have a tidy disposition of the thermocouple wire along the test tube and to avoid the crossing of different thermocouples cables that can create turbulence which involves disturbances to the flow of the secondary fluid. The presence of turbulence in the thermal oil can be a source of errors because of its behaviour change and so the amount of heat that can exchange

with the working fluid can be affected. Also, the measurement of the temperature in the secondary fluid can be affected by the presence of this kind of turbulence. In every measurement position, the layout of the 6 temperature sensor is different to have the most homogeneous possible coverage of the tube surface and therefore the most realistic temperature data collection possible. In every section, 4 thermocouples are placed at 45° from each other in the same position along the tube, while the other 2 change position in a clockwise direction from a measurement position to the next one. Figure 3.4 shows the cross-section of the measuring section.

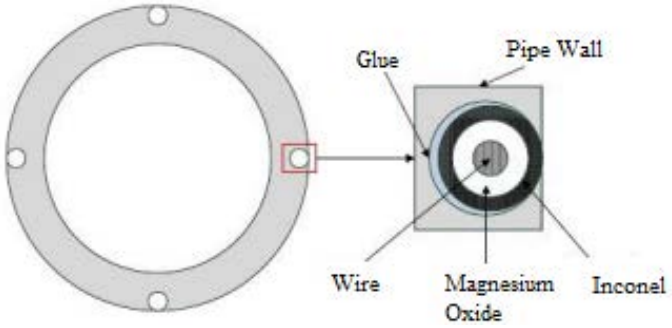


Figure 3.4: Cross section of the measuring section

- **Integral measurement** This kind of measurement is carried out with the purpose of analyzing the trend of the temperature and consequently of the heat transfer coefficient without having data regarding the actual temperature along the tube. This is very important because in the industrial application, is difficult and not very common to have a sensor along with the condenser but, in the real system, usually is possible to find temperature and pressure sensor at the inlet and outlet of every component. So in this kind of measurement the temperature and pressure of the working fluid are known only at the inlet and outlet of the test section while, regarding the secondary fluid, the measurement configuration is the same as the one used in the local measurement

As mentioned in the previous section, the Test Section Cycle (SECTS) is the secondary cycle connected to the test section. It is equipped with a cooling machine (Huber 65 W) which provides the set temperature to its working fluid and conveys it toward the test section.

## 3.2 Sensors

In the test facility, several types of sensor are used to analyze the process and measure the thermo-hydro characteristics of the fluids. Every sensor is connected to a multiplexer which allows the recording of every data recorded by the sensors and the connection to the computer. Using LabView software is possible to control every needed valve to perform the test but also to watch live the data recorded from every sensor. In the test facility there are 3 type of sensors:

- Temperature sensors
- Pressure sensors
- Mass flow sensors

### 3.2.1 Temperature sensors

As already described in the previous sections two types of temperature sensors are used in the test facility: Thermocouple ($TC$) and Resistance Temperature Detector $RTD$.

- **Thermocouple *TC***: The thermocouples installed are type K composed so by two-conductor alloys: Chromel and Alumel (Positive leg (Chromel): 90% Nickel, 10% Chromium; Negative leg (Alumel): 95% Nickel, 2% Manganese, 2% Aluminium, 1% Silicon ). The thermocouples are active sensor so they don't need electrical alimentation and their output is a voltage difference treated by the junctions for the Seebeck effect. The hot junction used for measuring is glued in the grooves of the test tube while the cold junction used as a reference for calculating the actual thermal output given by the sensor is placed in a metal plate where the temperature is measured with a resistance temperature detector. The type k thermocouple is adapted to work in an oxidant environment due to the characteristics of their conductor alloys. They have a quick response to temperature variations and usually have a longer life compared to other kinds of thermocouples, especially in a rugged environment. Since the hot junction used for the actual measurement of the temperature of the working fluid is glued in the groove, is necessary to use a thermocouple with the exposed junction. So the sensible part of the sensor is cover in concentric layers: the outer one is Inconel and the inner one is Magnesium oxide. Since the thermocouples are glued in the grooved, for the heat transfer coefficient calculation, a wall correction have to be done to take into account the fact that between the actual junction and the tube wall there is a layer of glue.

The thermal resistance of the used glue is considered in the calculation of the heat transfer coefficient.

- **Resistance Temperature Detector *RTD***: The RTD operating principle is based on the variation of the resistance of a conductor when its temperature change. The variation of the resistance is linear so is possible, knowing the trend of it, obtain the value of the temperature. The resistance temperature detector is built with materials that have to have, concerning the thermal resistivity coefficient, high value for having high sensitivity but also constant value at different temperature for having high linearity. The RTD's use in this test facility are PT100 which means that the material used is Platinum and the resistance of the sensor at 0°C is 100 $\omega$. The RTD are suitable for working in a rugged environment, have linear behavior, are usually small size and have high stability on the measurement. These kind of sensor are passive so a power supply circuit is needed and also, due to the protective sheath they have a longer response time.

### 3.2.2 Pressure sensors

Absolute and Differential Pressure transducers are used for the measurement of the pressure in the facility. Pressure measurements are used to calculate the fluid proprieties in the test section and to analyse the pressure drop while measuring the heat transfer coefficient. Furthermore, they are used to ensure the orderly functioning and integrity of the multiphase pump. Here installed are strain gauges pressure sensors, a diaphragm in contact with the fluid which is deformed by the pressure and the deformation can be measured by strain gauged element.

### 3.2.3 Mass flow sensors

There are two types of sensors in the test facility:

- **Coriolis flow meters**: The Coriolis flow meter, also known as inertial flow meter is a mass flow meter. Coriolis meters are primarily used to measure the mass flow rate of liquids. The flow meter consists either of a pair of parallel vibrating tubes or else as a single vibrating tube that is formed into a configuration that has two parallel sections. The two vibrating tubes deflect according to the mass flow rate of the measured fluid that is flowing inside. Tubes are made of various materials, of which stainless steel is the most common. The tubes are anchored at two points. An electromechanical drive unit, positioned midway between the two anchors, excites vibrations in each tube at

the tube resonant frequency. The vibration in the two tubes, are 180° out of phase. The vibratory motion of each tube causes forces on the particles in the flowing fluid. These forces induce motion of the fluid particles in a direction that is orthogonal to the direction of flow, and this produces a Coriolis force. This Coriolis force causes a deflection of the tubes that are superimposed on top of the vibratory motion. This deflection is measured by a suitable sensor. Coriolis meters give excellent accuracy, with measurement uncertainties of ±0.2% being typical. They also have low maintenance requirements. However, apart from being expensive, tubes are also subject to both corrosion caused by chemical interaction with the measured fluid and abrasion caused by particles within the fluid. Diversion of the flowing fluid around the flow meter causes it to suffer a significant pressure drop, though this is much less evident in straight tube designs.

- **Rota meter flow meter**: A Rota meter is a form of variable area flow meter which has a simplistic operation whereby a liquid or gas passes through a tapered tube. For this gas to pass through the tube it must first raise a float held within the tube. When a rotameter is used with a liquid the float rises because of a combination of the velocity head of the fluid and the buoyancy of the liquid. With gas the buoyancy is negligible and the float moves in the most part due to the velocity head of the gas. In both cases, the greater the flow the higher up the tube the float moves. The float moves up and down the tapered tube in proportion to the flow rate and the annular area between the float and the tapered tube wall. As the float moves up through the tube because of its tapered nature the annular opening increases. As this increases the differential pressure across the float decreases. The float stabilizes when the weight of the float is in equilibrium with the upward force being exerted by the fluid or gas. The float can then be compared to a calibrated scale either printed onto the tube itself or placed next to the tube on the outside of the flow meter. The calibrated scale will commonly give a volumetric flow reading, for example, liters per minute (LPM).

## 3.3 Fluids

In all facility, varieties of fluids are used. Every fluid used can be categorized into primary and secondary working fluids. Two types of secondary fluids are used in the secondary cycle:

- **Water**: Used directly only in the first heat exchanger of the bypass cycle and then as waste heat fluid in the cooling machine of the SECTSO and in

all the Huber thermostats. It is not directly involved in the heat transfer coefficient calculation but, if necessary, its proprieties are simply retrievable from REFPROP software.

- **therminol D12**:therminol D-12 is a synthetic, liquid phase heat transfer fluid with excellent heat transfer properties over a wide temperature range. therminol D-12 heat transfer fluid is a liquid phase heat transfer fluid specially developed for process cooling combined with moderate heating cycles using a single fluid in place of the traditional dual steam/brine or steam/glycol systems. Is based on halogen-free chemistry and has an operating temperature range from -85°C to 190°C.

- **propylene**: Also know as *Propene* is a hydrocarbon fluid and its chemical formula is $C_3H_6$. When it is used as a refrigerant is also known as R1270. Is suitable for use in low and medium temperature refrigeration applications. The advantages of R1270 are:

  - Zero ozone depletion potential (ODP=0)
  - Very low global warming potential (GWP=2)
  - Excellent thermodynamic proprieties leading to high efficiency
  - Good compatibility with system components
  - Low charges allowing smaller heat exchangers and piping dimensions

  The main disadvantage is represented by its high flammability. Is classified as A3 according to the ASHRAE safety Group, which means extremely flammable gas but with low toxicity. Its characteristics are summarized in the following table

## 3.4 Safety measures

Since the facility primarily investigates hydrocarbons, explosion protection must be taken into account. The first safety solution is regarding the multi phase pump. The hydrostatic mechanical seals of the multi phase pump are supported and cooled by a special sealing oil (Renolin PG 68) which is provided by a hydraulic power pack with an over pressure of 10 bar. As results, small quantities of sealing oil can dissolve in the test fluid, which is filtered out by the coalescence oil separator. Any droplets that may have formed in the gas phase are removed by a means of special demister in the upper part of the phase separator.

| **R1270** | | |
|---|---|---|
| Formula | 0 | $C_3H_6$ |
| Molecular Mass | $g/mol$ | 42,1 |
| Normal boiling point | $°C$ | -47,6 |
| Liquid density | $kg/dm^3(40°C)$ | 0,48 |
| Critical temperature | $°C$ | 96,1 |
| Critical pressure | $bar$ | 49,9 |
| Safety Group | 0 | A3 |
| Ozone Depletion Potential | $ODP$ | 0 |
| Global Warming Potential | $GWP$ | 3 |

Table 3.2: Proprieties of R1270

In addition to the seal, the entire primary circuit of the test facility is surrounded by an enclosure as showed in figure 3.5. A gas warning sensor detects the hydrocarbon content in the air and, if a certain limit value exceeded, a ventilation system is activated and the test substance is adsorbed by an activated carbon filter.

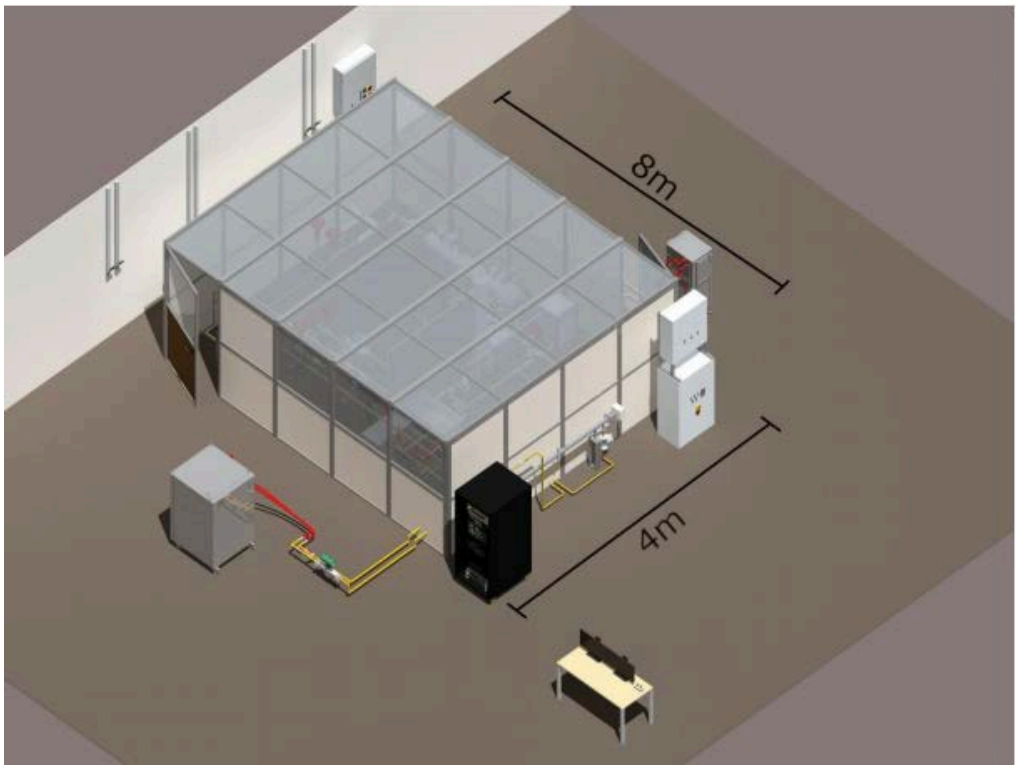


Figure 3.5: Facility enclosure

# Chapter 4

# DATA REDUCTION

In this chapter the method of evaluation of the data collected from the test section is described. With the recorded raw data, the single-phase and two-phase heat transfer and the pressure loss in the measuring section can be determined.

## 4.1 Heat Transfer Coefficient

The determination of the heat transfer coefficient from the raw data collected in the test facility is carried out in different ways depending on which typologies of measurement is implemented.

### 4.1.1 Local Measurements

As explained in chapter 4, with this kind of measurement, thermocouples sensors are installed in the external surface of the inner tube for the determination of the wall temperature profile and so indirectly, of the temperature trend of the primary fluid, propylene. The positions of the thermocouples along the test tube are showed in figure 4.2 and the characteristics of thermocouples, thermal glue and inner tube are known, so it is possible to calculate the total thermal resistance. In each measurement section, the sensors give the local temperature of the external wall but, for better accuracy, the wall temperature in each measurement section is assumed as the mean value of every thermocouple installed in that section

$$T_{wall,i} = \sum_{j=1}^{6} \frac{T_{wall,i,j}}{6}. \tag{4.1}$$

Several reasons like bad electric connection or actual malfunction could affect some sensors recorded data which could affect the final results. To avoid this problem is

possible to disconnect the sensors from the multiplexer or to ignore their records and substitute them with the mean value of the adjacent thermocouples. To determine the internal heat transfer coefficient, an energy balance between the secondary fluid (therminol) and the primary fluid (propylene) must be established and due to this balance, the heat flow is calculated. Considering the energy balance between the two fluids and neglecting the pressure drop, the heat flux from the propylene to the thermal oil in the $i-th$ section is expressed as

$$\dot{Q}_{p,i} = \dot{Q}_{oil,i} + \dot{Q}_{loss} \tag{4.2}$$

with the heat losses determined as

$$\dot{Q}_{loss} = \frac{\lambda_{ins}\, 2\pi z_i}{\ln\left(\frac{d_{in,out}}{d_{in,in}}\right)} \Delta T_{ins,i} \tag{4.3}$$

where $\lambda_{ins}$ is the thermal conductivity of the insulation material, $d_{int,out}$, $d_{int,in}$ are the internal and external diameters of the insulation cover and $\Delta T_{ins,i}$ is defined as:

$$\Delta T_{ins,i} = T_{ins,ext,i} - T_{ins,int,i}. \tag{4.4}$$

Since the temperatures inside and outside the insulation layer are not measured, the calculation of the heat losses is not possible. As a simplification assumption, the measuring section is assumed to be an adiabatic system due to the thermal insulation, so that the energy balances for the heat transfer oil and the test substance can neglect the pressure losses. This assumption creates an error that is considered acceptable since the insulation thermal conductivity is low ($\lambda_{ins} = 0{,}033 W/m\ K$) and, since the overall heat flux losses are controlled by this value, is possible to neglect the losses. With these assumptions the reduced one-dimensional energy balance of the not compressible heat transfer oil is

$$\dot{Q} = cp_{oil}\, \dot{m}_{oil}\ \left(T_{i+1,oil} - T_{i,oil}\right) \tag{4.5}$$

as $cp_{oil}$ is the specific heat capacity of the therminol, $\dot{m}_{oil}$ the mass flux and $T_{i,oil}$ the temperature of the oil-related to the measurement section. Depending on which kind of flow is present in the test tube, single or two-phase flow, the determination of the energy balance for the primary fluid is executed in different ways. In the case of single-phase flow, the heat flux is calculated employing a reduced energy balance while neglecting the pressure losses with:

$$\dot{Q} = cp_p\, \dot{m}_p\ \left(T_{i+1,p} - T_{i,p}\right). \tag{4.6}$$

The specific heat capacity is assumed to be constant between two measurement sections and the mean temperature of the propylene between the two sections is

used for its determination. Since due to the experimental setup is not possible to measure the temperature of the working fluid inside the test section but only the external wall temperature with the thermocouples, the temperature trend has to be determined indirectly. From the initial energy balance, is possible to determine the temperature of the propylene in each measurement section as

$$T_{p,1+i} = Tp, i + \frac{\dot{Q}_i}{cp_{p,i}\,\dot{m}_{p,i}}. \tag{4.7}$$

For the case of two-phase flow, the heat flux in the propylene is determined as:

$$\dot{Q} = \Delta h_{evap}\,\dot{m}_p\ (x_{i+1,p} - x_{i,p}) \tag{4.8}$$

where $\Delta h_{evap}$ represents the enthalpy of evaporation of propylene at the working pressure and $x_{i,p}$ the flow vapour content in the measurement section. Since the vapour content inside the inner pipe of the measuring section cannot be measured due to the experimental setup, the trend of the vapour content has to be determined indirectly as:

$$x_{i+1,p} = \frac{\dot{Q}_{i,i+1}}{\dot{m}_p\,cp_p} + x_{i,p} \tag{4.9}$$

The inlet vapour quality is calculated indirectly from the reduced energy balance of the test substance in the static mixer as

$$x = \frac{h_{inlet} - h_{l,sat}}{h_{g,sat} - h_{l,sat}} \tag{4.10}$$

The enthalpy of saturated liquid $h_{l,sat}$ and the saturated vapour $h_{g,sat}$ are specific for each substance and also they are a function of the pressure. Since the pressure in the static mixer and at the inlet of the test section is measured, it is possible to determine the value of the saturated enthalpies with the software REFPROP. The enthalpy of mixing

$$h_{inlet} = \frac{\dot{m}_g\,h_g + \dot{m}_l\,h_l}{\dot{m}_g + \dot{m}_l} \tag{4.11}$$

is determined as a function of the mass flow measured in the gas and liquid lines before entering the mixer. The specific enthalpies $h_g$ and $h_l$ are caloric equation of state and they are a function of

$$h = f\{\rho; T\} \tag{4.12}$$

of the test substance. The density is measured by the Coriolis sensor in the gas and liquid line and the temperature by platinum resistance thermometer PT 100.

Due to the determined flow vapour content, the real mass flow of the liquid and gaseous phase at the inlet can be compared with

$$\dot{m}_g = x\,\dot{m}_{tot} \tag{4.13}$$

$$\dot{m}_l = (1-x)\,\dot{m}_{tot} \tag{4.14}$$

On this basis, the volumetric flow vapour content is calculated via the ratio of the gas volume flow to total volume flow as:

$$\xi = \frac{V_g}{V} = \frac{\frac{\dot{m}_g}{\rho_G}}{\frac{\dot{m}_g}{\rho_G} + \frac{\dot{m}_l}{\rho_l}} \tag{4.15}$$

To determine the local heat transfer coefficient, the local heat flux density $\dot{q}$ is required. Due to non-measurable temperature and vapour quality, the local heat flux density $\dot{q}$ is calculated by differentiating the heat flux of the secondary fluid, according to equation 4.5 over the pipe length $z$

$$\frac{\delta \dot{Q}_{oil}}{\delta z} = cp_{oil}\,\dot{m}_{oil}\,\frac{\delta T_{oil}}{\delta z} \tag{4.16}$$

To determine the local therminol temperature not only at the measuring sections but also at any point of the pipe length ($z$) is possible to implement the method of least squares. The oil temperature is adopted as a second-degree polynomial

$$T_{oil}(z) = Az^2 + Bz + C \tag{4.17}$$

The derivation of equation 4.17 yields to

$$\delta T_{oil}(z) = 2Az + B \tag{4.18}$$

where A, B and C are the constants of the polynomial function. To determine the local therminol temperature of the temperature trend of the thermal oil within the measuring sections, it is assumed that an exponential function is more suitable to the reality than a second-degree polynomial. To better understand the heat exchange and the temperature trend in the heat exchanger, the picture 4.1 shows a scheme of the heat transfer in a countercurrent heat exchanger. First, the energy balance of the thermal oil is established considering the process of the heating process as isobaric. If the kinetic energy is neglected, the first law of thermodynamic states

$$d\dot{Q} = -dH_2 \tag{4.19}$$

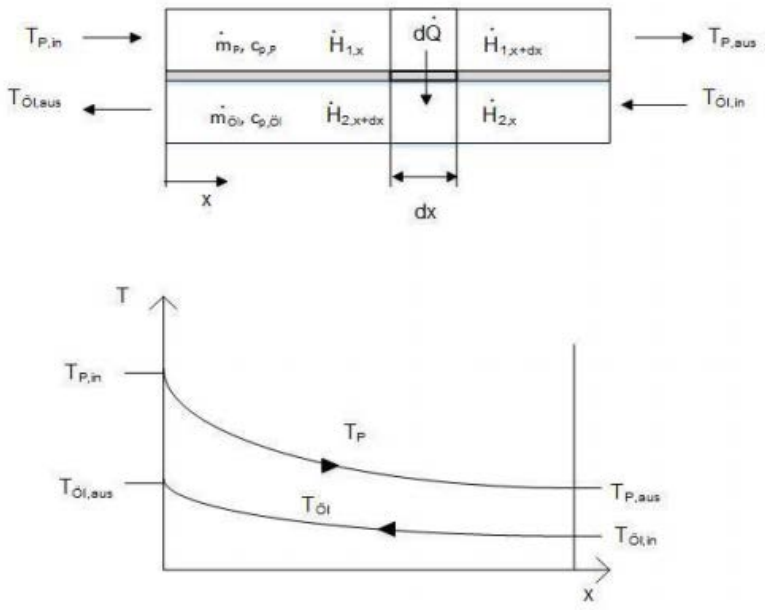


Figure 4.1: Heat transfer in a double-tube counter flow heat exchanger

The transmitted heat flow can also be expressed as

$$d\dot{Q} = k\ (T_p - T_{oil})\ dA \tag{4.20}$$

where $dA = 2\,\pi\,dl$. The enthalpy variation in the thermal oil is defined also as:

$$dH_2 = \dot{m}_{oil}\ cp_{oil}\ dT_{oil} \tag{4.21}$$

So it is possible to replace the individual terms in the first law of thermodynamic as

$$k\ (T_p - T_{oil})\ dA = \dot{m}_{oil}\ cp_{oil}\ dT_{oil} \tag{4.22}$$

and transforming the equation for express the temperature results is possible to obtain

$$\frac{dT_2}{(T_p - T_{oil})} = \frac{2\,\pi k}{\dot{m}_{oil}\ cp_{oil}}\ dl. \tag{4.23}$$

Assuming $(T - p - T_{oil}) = a$ and $dT_{oil}/da = -1$ the equation becomes

$$\frac{1}{a}\ da = -\frac{2\,\pi\,k}{\dot{m}_{oil}\ cp_{oil}}\ dl \tag{4.24}$$

and logarithmising the equation it possible to obtain

$$\ln(a) = -\frac{2\,\pi\,k}{\dot{m}_{oil}\ cp_{oil}}\ dl + C \tag{4.25}$$

with $C = \left(T_p - T_{oil,0}\right)$ and $a = (T_p - T_{oil})$. With this function is possible to determine the trend of the thermal oil temperature in every position along the test section

$$T_{oil,i} = T_p - e^{\left(-\frac{2\,\pi\,k}{\dot{m}_{oil}\,cp_{oil}}\right)}\,(T_p - T_{oil}) \tag{4.26}$$

To determine the mean internal heat transfer coefficient, the heat flow $\delta\dot{Q}_{oil}/\delta z$ is inserted into the heat transfer equation for cylindrical bodies.

$$\frac{\delta\dot{Q}_{oil}}{\delta z} = \frac{2\,\pi\,(T_p - T_{oil})}{\frac{1}{\alpha_{i,m}\,r_i} + \sum_i \frac{1}{\lambda_i} \ln\left(\frac{r_{i+1}}{r_i}\right)} \tag{4.27}$$

where $\sum_i \frac{1}{\lambda_i}$ corresponds to the sum of all thermal resistances of the tube wall and the glued thermocouples. Figure 4.2 shows the structure of the thermocouples in the tube wall. The average internal heat transfer coefficient is obtained by the

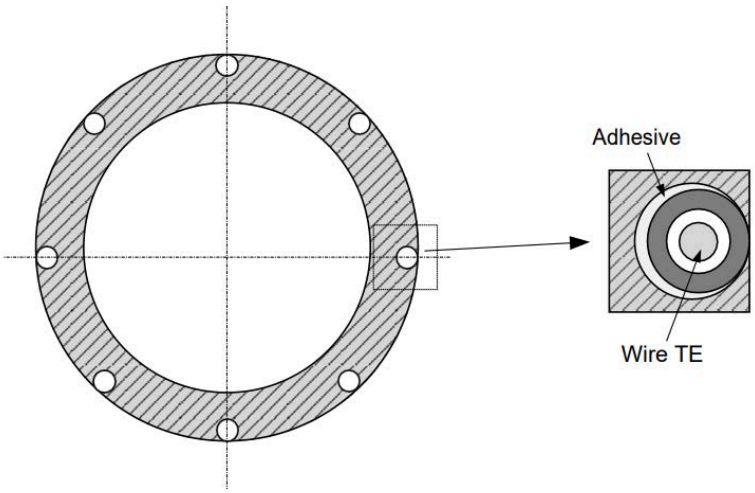


Figure 4.2: Structure and construction of the thermocouple in the tube wall

conversion of equation 4.27

$$\alpha_{i,m} = \frac{1}{r_i \left(\frac{2\,\pi\,(T_p - T_{wall,mean})}{\frac{\delta\dot{Q}_{oil}}{\delta z}} - \sum_i \frac{1}{\lambda_i} \ln\left(\frac{r_{i+1}}{r_i}\right)\right)} \tag{4.28}$$

For the determination of the average heat transfer coefficient, the heat flow differentiated over the length of the pipe is calculated using the thermal oil temperature. The mean outside wall temperature $T_{wall,mean}$ is determined from the sum of local wall temperatures via the thermocouples wall as defined in equation 4.1. To calculate the local heat transfer coefficient, the local heat flow density must be determined. To calculate this parameter, the equation for the mean heat flux density

| Material | $d_i$ $[mm]$ | $\lambda_i$ $[W/mK]$ |
|---|---|---|
| Pipe wall (structural steel) | 20,8 | 57 |
| Glue | 24,8 | 1 |
| TE-Inconel | 24,9 | 15 |
| TE-Magnesium Oxide | 25,1 | 50 |
| TE-Wire | 25,2 | - |
| TE-Magnesium Oxide | 25,3 | 50 |
| TE-Inconel | 25,4 | 15 |

Table 4.1: Description of materials, diameters and thermal conductivity of thermocouples and inner tube

as well as for local heat flux density is established

$$\dot{q}_{mean} = \alpha_A \left(T_{wall,mean} - T_{oil}\right) \tag{4.29}$$

$$\dot{q}_{local} = \alpha_A \left(T_{wall,local} - T_{oil}\right) \tag{4.30}$$

Here $\alpha_a$ gives the heat transfer coefficient of the puter wall pipe, $T_{oil}$ the therminol temperature in corresponding the measuring section, $T_{wall,mean}$ the average outer wall temperature and $T_{wall,local}$ the local outside wall temperature. The two equations 4.29 and 4.30 are converted according to the external heat transfer coefficient and equated

$$\frac{\dot{q}_{local}}{\dot{q}_{mean}} = \frac{\left(T_{wall,local} - T_{oil}\right)}{\left(T_{wall,mean} - T_{oil}\right)} \tag{4.31}$$

So the local heat flux density can be measured via

$$\dot{q}_{local} = \dot{q}_{mean} \frac{\left(T_{wall,local} - T_{oil}\right)}{\left(T_{wall,mean} - T_{oil}\right)} \tag{4.32}$$

The local heat transfer coefficient is so defined as:

$$\alpha_{int,local} = \frac{1}{\frac{(T_p - T_{wall,local})}{\dot{q}_{local}} - \sum_i \frac{1}{\lambda_i} \ln\left(\frac{r_{i+1}}{r_i}\right) r_i} \tag{4.33}$$

### 4.1.2 Integral Measurements

For the determination of the internal heat transfer coefficient in the case of integral measurement, the information's regarding the trend of the external temperature of the inner tube in the test section are not available due to the missing thermocouple sensors. This kind of measurement aims to determine the heat transfer coefficient and the pressure drop without the use of the thermocouples located on the external surface of the inner tube. This could be an advantage in economics terms due to the reduced number of sensors used and also in technical terms because the use of a reduced number of sensors simplify the set up of the test section and also reduced the possibility of failing sensors. As explained before, due to the experimental setup, only the mean heat transfer coefficient over all length of the test section is determined in this kind of measurement. An energy balance between the two fluids in the heat exchanger is necessary for the determination of the internal heat transfer coefficient. As in the case of the local measurement, the assumption of considering the test section as an adiabatic system is valid and is possible to neglect the heat losses and consider the process isobaric. In this case, the energy balance can be expressed as

$$\dot{Q}_{oil} = \dot{Q}_p \tag{4.34}$$

and the energy balance regarding the thermal oil is calculated as

$$\dot{Q} = \dot{m}_{oil}\, cp_{oil}\, \left(T_{outlet,oil} - T_{inlet,oil}\right) \tag{4.35}$$

assuming that the specific heat capacity is determined at the mean value of temperature between the inlet and outlet. The heat flux exchanged by the two fluids can be determined also in the following way

$$\dot{Q} = U_{int}\, A_{int}\, \Delta T_{lm} \tag{4.36}$$

where $U_{int}$ represents the overall heat transfer coefficient referred to the internal area of the inner tube , $A_{int}$ is the internal exchange area and $\Delta T_{lm}$ is the log-mean temperature difference that is defined as

$$\Delta T_{lm} = \frac{\Delta 1 - \Delta 2}{\ln\left(\frac{\Delta 1}{\Delta 2}\right)} = \frac{\left(T_{oil,out} - T_{p,in}\right) - \left(T_{oil,in} - T_{p,out}\right)}{\ln\left(\frac{(T_{oil,out} - T_{p,in})}{(T_{oil,in} - T_{p,out})}\right)}. \tag{4.37}$$

The overall heat transfer coefficient is defined as

$$\frac{1}{U_{int}} = \frac{1}{\alpha_{ext}}\, \frac{A_i nt}{A_e xt} + \frac{\ln\left(d_{int,out}/d_{int,in}\right)}{2\,\lambda_t} d_{int,in} + \frac{1}{\alpha_{int}} \tag{4.38}$$

where $\alpha_{ext}$ represent the convective heat transfer coefficient between the thermal oil and the external wall of the inner tube, $\frac{\ln(d_{int,out}/d_{int,in})}{2\,\lambda_t}$ the thermal resistance of the tube and $\alpha_{int}$ the internal convective heat transfer coefficient. Regarding the calculation of the external heat transfer coefficient, since the thermal oil flow as a single-phase fluid, it is possible to determine the heat transfer coefficient through the theory of convective heat transfer. It is necessary to determine the fluid characteristics of the thermal oil. First of all, the mean temperature of the therminol

$$T_{m,oil} = \frac{T_{inlet,oil} + T_{outlet,oil}}{2} \tag{4.39}$$

between the inlet and the outlet temperature is defined. The thermal oil producer had determined a correlation for the calculation of the oil characteristics as a function of temperature, so using the mean temperature of therminol is possible to calculate density, viscosity, thermal conductivity and specific heat capacity of the secondary fluid. At this point it is necessary to calculate the Reynolds number of the therminol to determine which flow condition is present in the annular section. The Reynolds number for the thermal oil is defined as

$$Re_{oil} = \frac{u_{oil}\ (d_{int,out} - d_{ext,in})}{\mu_{oil}} \tag{4.40}$$

and the annular section, represented in the figure 4.3, is expressed by the expression

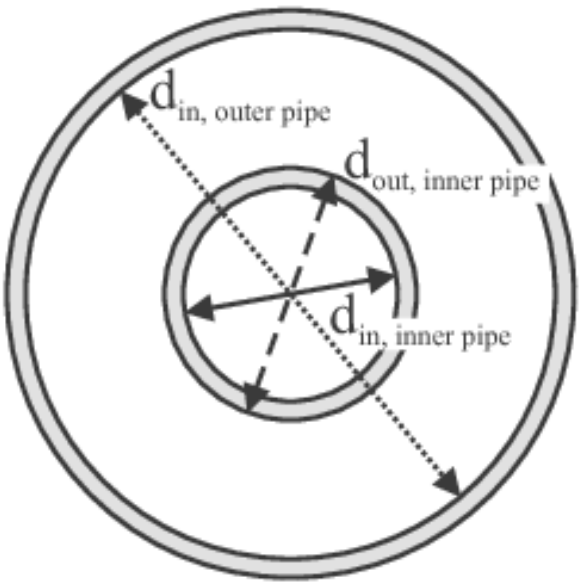


Figure 4.3: Rappresentation of the annulus section and relative diameters

$(d_{int,out} - d_{ext,in})$. The oil velocity in this section is defined as

$$u_{oil} = \frac{\dot{m}_{oil}}{\rho_{oil}\,\pi\,\left(d_{int,out}^2 - d_{ext,in}^2\right)\,0{,}25}. \tag{4.41}$$

. Knowing the Reynolds number is possible to define the flow condition occurring inside the test section that could be laminar flow if $Re < 2000$ or turbulent flow if $Re > 3500$. Once the flow condition has been defined, the choice between free convection correlation or forced convection correlation it is made. The operating conditions used in the tests carried out for the compilation of this work were such as to ensure that the fluid flowed only under turbulent conditions so that the forced convection correlation could be employed. These correlations, as already defined in equation 2.20, allow us to define the Nusselt number knowing the characteristic of the fluid and the coefficient $C$ and $n$ specific for each geometry and configuration. The constructor of the inner tube has calculated the parameters after performing several tests and have defined a correlation for the determination of the Nusselt number in case of turbulent flow. The correlation is expressed as

$$Nu_{oil} = 0{,}122\,Re_{oil}^{0{,}706}\,Pr_{oil}^{0{,}445} \tag{4.42}$$

and the Prandtl number for the oil is calculated in the following way

$$Pr_{oil} = \frac{\mu_{oil}\,\rho_{oil}\,cp_{oil}}{\lambda_{oil}}. \tag{4.43}$$

From the definition of the Nusselt number is possible to define the external convective heat transfer coefficient as

$$\alpha_{ext} = \frac{Nu_{oil}\,\lambda_{oil}}{(d_{int,out} - d_{ext,in})}. \tag{4.44}$$

At this point is possible to obtained the internal heat transfer coefficient from the formula 4.38 as:

$$\alpha_{int} = \left(\frac{1}{U_{int}} - \frac{1}{\alpha_{ext}}\frac{d_{int,in}}{d_{int,out}} - d_{int,in}\frac{\ln\left(d_{int,out}/d_{int,in}\right)}{2\,\lambda_t}\right)^{-1} \tag{4.45}$$

and using the overall heat transfer coefficient determined from the formula 4.36 it is possible to derive the final formula for the internal heat transfer coefficient

$$\alpha_{int} = \frac{d_{int,out}}{d_{int,in}\left(\frac{\pi\,d_{int,out}\,L\,\Delta T_{lm}}{\dot{Q}} - \frac{1}{\alpha_{ext}} - d_{int,out}\frac{\ln(d_{int,out}/d_{int,in})}{2\,\lambda_t}\right)} \tag{4.46}$$

where $L$ is the length of the test tube. Only in the case of gas cooling test, since the working fluid flow as a single-phase fluid, is possible to calculate directly the energy balanced regarding the propylene as

$$\dot{Q} = \dot{m}_p \, cp_p \, (T_{p,in} - T_{p,out}) \tag{4.47}$$

This value can be used in this kind of measurement directly inside the equation for the determination of the internal heat transfer coefficient 4.46. In this typology of measurement, due to the characteristics of the test facility is also possible to calculate directly the vapour quality at the outlet of the test section. First of all is necessary to determine the vapour quality at the inlet of the test tube. This is executed in the same way as the case of local measurement so is possible to use the equation 4.10 for the calculation of the vapour quality and the equation 4.11 to calculate the enthalpy of the propylene at the inlet of the test section. Knowing the total heat flux exchanged between the working fluid and the thermal oil since we consider the system adiabatic, is possible to calculate the enthalpy of the propylene at the outlet condition with the equation

$$h_{p,out} = h_{p,in} - \frac{\dot{Q}}{\dot{m}_p}. \tag{4.48}$$

At this point is possible to obtain the value of the vapour quality at the outlet of the test section as

$$x_{out} = \frac{h_{p,out} - h_{l,sat}}{h_{g,sat} - h_{l,sat}}. \tag{4.49}$$

## 4.2 Analysis of uncertainty

A physical quantity, measured indirectly, is a function of $n$ independent parameters

$$y = f(x_1, x_2, \ldots, x_n) \tag{4.50}$$

in which every independent parameter have its own uncertainty $i_i$. So the overall uncertainty of the physical quantity $y$ can be expressed as

$$y \pm i_y = f(x_1 \pm i_1, x_2 \pm i_2, \ldots, x_n \pm i_n) \tag{4.51}$$

and developing the Taylor series of first order

$$f(x_1 \pm i_1, x_2 \pm i_2, \ldots, x_n \pm i_n) \approx f(x_1, x_2, \ldots, x_n) \pm \left( \frac{\delta f}{\delta x_1} i_1 + \frac{\delta f}{\delta x_2} i_2 + \cdots + \frac{\delta f}{\delta x_n} i_n \right) \tag{4.52}$$

so the uncertainty of the physical quantity $y$ is defined as

$$i_y \approx \pm\frac{\delta f}{\delta x_1} i_1 \pm \frac{\delta f}{\delta x_2} i_2 \pm \cdots \pm \frac{\delta f}{\delta x_n} i_n = \pm\theta_1 i_1 \pm \theta_2 i_2 \pm \cdots \pm \theta_n i_n \tag{4.53}$$

where $\theta_i = \delta f / \delta x_i$ are the sensibility index evaluated in the point $x_i$ and describe how the physical quantity $y$ change when the estimation of input values $x_i$ change. The uncertainty can so be calculated by the formula proposed by Kline and McClintok [41]

$$i_y = \pm\sqrt{\sum_{i=1}^{n} \left(\frac{\delta f}{\delta x_i}\right)^2 i_i^2} \tag{4.54}$$

where $i_i$ is the uncertainty of the i-measurement. The measurement uncertainties are divided into two categories: type A and type B. The first is the one derived from more experimental measurement, obtained in a controlled ambient and conditions, maintaining constant all influencing and controllable parameters. Type B uncertainty is the one derived from previous measurement data, experience with relevant measuring instruments and materials, calibration certificate and manufacturer's specifications. The measurement uncertainties of the individual measuring instrument are showed in Table 4.2. As explained in the previous chapter of this

| **Measured variable** | **Measurement uncertainty** |
|---|---|
| $T_{oil}$, $T_p$ | $\pm 0{,}05\,°C$ |
| $T_{wall}$ | $\pm 0{,}1\,°C$ |
| $\dot{m}_{oil}$ | $\pm 0{,}004\,\%$ |
| $\dot{m}_p$ | $\pm 0{,}1\,\%$ |
| $\Delta p$ | $\pm 0{,}4\,mbar$ |
| $p_{abs}$ | $\pm 0{,}08\,bar$ |
| $L$ | $\pm 0{,}01\,m$ |
| $\phi$ | $\pm 5\,°C$ |

Table 4.2: Uncertainty of measurement of individual measuring instrument

work, two kinds of measurement are carried out in the test facility. Depending on the typology of measurement, the data reduction for the determination of the thermodynamics characteristics change. In the next section, the uncertainty of the different parameters used in both methods is analyzed.

### 4.2.1 Local measurement uncertainty

#### Vapour quality uncertainty

The inlet vapour quality of the propylene is calculated with the relation 4.10 and is a function of:

- Inlet enthalpy $h_{inlet}$ calculated with the equation 4.11, itself a function of
  - Liquid and vapour mass flow $\dot{m}_l$, $\dot{m}_g$
  - liquid and vapour enthalpy at inlet conditions $h_l$, $h_g$
- Saturated liquid enthalpy $h_{l,sat}$
- Saturated vapour enthalpy $h_{g,sat}$

Deriving the equation 4.10 give the sensibility index

$$\frac{\delta x}{\delta h_{inlet}} = \frac{1}{h_{g,sat} - h_{l,sat}} \tag{4.55}$$

$$\frac{\delta x}{\delta h_{g,sat}} = \frac{h_s - h_{g,sat}}{\left(h_{g,sat} - h_{l,sat}\right)^2} \tag{4.56}$$

$$\frac{\delta x}{\delta h_{l,sat}} = \frac{h_{l,sat} - h_s}{\left(h_{g,sat} - h_{l,sat}\right)^2} \tag{4.57}$$

Consequently, the combined uncertainty of the inlet vapour quality is

$$u(x) = \sqrt{\left(\frac{\delta x}{\delta h_{inlet}}\right)^2 i_{h_{inlet}}^2 + \left(\frac{\delta x}{\delta h_{g,sat}}\right)^2 i_{h_{g,sat}}^2 + \left(\frac{\delta x}{\delta h_{l,sat}}\right)^2 i_{h_{l,sat}}^2}. \tag{4.58}$$

The uncertainty of the inlet enthalpy $h_{inlet}$ is defined considering the equation 4.11 and deriving it, to obtain the sensibility index related to the inlet enthalpy.

$$\frac{\delta h_{inlet}}{\delta \dot{m}_g} = \frac{\dot{m}_l}{\left(\dot{m}_g + \dot{m}_l\right)^2} \tag{4.59}$$

$$\frac{\delta h_{inlet}}{\delta \dot{m}_l} = -\frac{\dot{m}_g}{\left(\dot{m}_g + \dot{m}_l\right)^2} \tag{4.60}$$

$$i_{h_{inlet}} = \sqrt{\left(\frac{\delta x}{\delta \dot{m}_g}\right)^2 i_{\dot{m}_g}^2 + \left(\frac{\delta x}{\delta \dot{m}_l}\right)^2 i_{\dot{m}_l}^2} \tag{4.61}$$

**Local flow vapour quality uncertainty**

The local flow vapour content, calculated with the equation 4.9, is a function of:

- Heat flow of therminol $\dot{Q}_{oil}$
- propylene mass flow $\dot{m}_p$
- Local flow vapour content at point z of measuring section $\delta x_{i,p}$

Deriving the equation 4.9, is possible to obtain the sensibility index

$$\frac{\delta x_{i+1,p}}{\delta x_{i,p}} = 1 \tag{4.62}$$

$$\frac{\delta x_{i+1,p}}{\delta \dot{m}_p} = -\frac{\dot{Q}_{oil}}{\dot{m}_p^2\,\Delta h} \tag{4.63}$$

$$\frac{\delta x_{i+1,p}}{\delta \dot{Q}_{oil}} = -\frac{1}{\dot{m}_p\,\Delta h} \tag{4.64}$$

Consequently the uncertainty of the local flow vapour quality can be expressed as follows

$$u(x_{i+1,p}) = \sqrt{\left(\frac{\delta x_{i+1,p}}{\delta \dot{x}_{i,p}}\right)^2 i^2_{\dot{x}_{i,p}} + \left(\frac{\delta x_{i+1,p}}{\delta \dot{m}_p}\right)^2 i^2_{\dot{m}_p} + \left(\frac{\delta x_{i+1,p}}{\delta \dot{Q}_{oil}}\right)^2 i^2_{(\dot{Q}_{oil})}} \tag{4.65}$$

**Length-related heat flow of the oil uncertainty**

The length-related heat flow of the therminol can be represented, according to the equation 4.16, as a function of

- Thermal oil mass flow $\dot{m}_{oil}$
- Trend of thermal oil temperature along the test section $\frac{\delta T_{oil}}{\delta z}$
- Thermal oil specific heat capacity $cp_{oil}$

Deriving the equation 4.16, is possible to obtain the sensibility index

$$\frac{\delta \frac{\delta \dot{Q}}{\delta z}}{\delta \dot{m}_{oil}} = cp_{oil}\,\frac{\delta T_{oil}}{\delta z} \tag{4.66}$$

$$\frac{\delta \frac{\delta \dot{Q}}{\delta z}}{\delta \frac{\delta T_{oil}}{\delta z}} = cp_{oil}\,\dot{m}_{oil} \tag{4.67}$$

$$\frac{\delta \frac{\delta \dot{Q}}{\delta z}}{\delta cp_{oil}} = \dot{m}_{oil} \frac{\delta T_{oil}}{\delta z} \tag{4.68}$$

The uncertainty of the length related heat flow can be calculated as follows

$$u\left(\frac{\delta \dot{Q}}{\delta z}\right) = \sqrt{\left(\frac{\delta \frac{\delta \dot{Q}}{\delta z}}{\delta \dot{m}_{oil}}\right)^2 i^2_{\dot{m}_{oil}} + \left(\frac{\delta \frac{\delta \dot{Q}}{\delta z}}{\delta cp_{oil}}\right)^2 i^2_{cp_{oil}} + \left(\frac{\delta \frac{\delta \dot{Q}}{\delta z}}{\delta \frac{\delta T_{oil}}{\delta z}}\right)^2 i^2_{\left(\frac{\delta T_{oil}}{\delta z}\right)}} \tag{4.69}$$

**Local heat flux density uncertainty**

The local heat flux density, expressed by the function 4.32, can be represented as a function of

- The mean heat flux density $\dot{q}_m$
- The thermal oil temperature $T_{oil}$
- The local outside wall temperature $T_{wall,loc}$
- The mean outside wall temperature $T_{wall,m}$

Deriving the equation 4.32, is possible to obtain the sensibility index

$$\frac{\delta \dot{q}_{loc}}{\delta \dot{q}_m} = \frac{(T_{wall,loc-T_{oil}})}{(T_{wal,m} - T_{oil})} \tag{4.70}$$

$$\frac{\delta \dot{q}_{loc}}{\delta T_{wall,loc}} = \frac{\dot{q}_m}{(T_{wal,m} - T_{oil})} \tag{4.71}$$

$$\frac{\delta \dot{q}_{loc}}{\delta T_{wall,m}} = \frac{\dot{q}_m \left(T_{oil} - T_{wall,loc}\right)}{(T_{wal,m} - T_{oil})^2} \tag{4.72}$$

$$\frac{\delta \dot{q}_{loc}}{\delta T_{oil}} = \frac{\dot{q}_m \left(T_{wall,loc-T_{oil}}\right)}{(T_{wal,m} - T_{oil})^2} \tag{4.73}$$

The uncertainty of the local flux density is determined as follows

$$u(\dot{q}_{loc}) = \sqrt{\left(\frac{\delta \dot{q}_{loc}}{\delta \dot{q}_m}\right)^2 i^2_{\dot{q}_m} + \left(\frac{\delta \dot{q}_{loc}}{\delta T_{wall,loc}}\right)^2 i^2_{T_{wall,loc}} + \left(\frac{\delta \dot{q}_{loc}}{\delta T_{wall,m}}\right)^2 i^2_{T_{wall,m}} + \left(\frac{\delta \dot{q}_{loc}}{\delta T_{oil}}\right)^2 i^2_{T_{oil}}} \tag{4.74}$$

### Mean internal heat transfer coefficient uncertainty

The mean internal heat transfer coefficient, expressed with the formula 4.28, can be represented as a function of

- The heat flow related to the length $\frac{\delta\dot{Q}}{\delta z}$
- The propylene temperature $T_p$
- The mean outside wall temperature $T_{wall,m}$

Deriving the equation 4.28, is possible to obtain the sensibility index

$$\frac{\delta\alpha_{int,m}}{\delta\frac{\delta\dot{Q}}{\delta z}} = \frac{2\,\pi\,(T_p - T_{wall,m})}{r_i\left(2\,\pi\,(T_{wall_m} - T_p) + \frac{\delta\dot{Q}}{\delta z}\,\sum_i \frac{1}{\lambda_i}\ln(\frac{r_{i+1}}{r_i})\right)^2} \tag{4.75}$$

$$\frac{\delta\alpha_{int,m}}{\delta T_p} = -\frac{2\,\pi\,\delta\frac{\delta\dot{Q}}{\delta z}}{r_i\left(2\,\pi\,(T_{wall_m} - T_p) + \frac{\delta\dot{Q}}{\delta z}\,\sum_i \frac{1}{\lambda_i}\ln(\frac{r_{i+1}}{r_i})\right)^2} \tag{4.76}$$

$$\frac{\delta\alpha_{int,m}}{\delta T_{wall,m}} = \frac{2\,\pi\,\delta\frac{\delta\dot{Q}}{\delta z}}{r_i\left(2\,\pi\,(T_{wall_m} - T_p) + \frac{\delta\dot{Q}}{\delta z}\,\sum_i \frac{1}{\lambda_i}\ln(\frac{r_{i+1}}{r_i})\right)^2} \tag{4.77}$$

The uncertainty of the mean internal heat transfer coefficient can be determined as follows

$$u(\alpha_{int,m}) = \sqrt{\left(\frac{\delta\alpha_{int,m}}{\delta\frac{\delta\dot{Q}}{\delta z}}\right)^2 i^2_{\left(\frac{\delta\dot{Q}}{\delta z}\right)} + \left(\frac{\delta\alpha_{int,m}}{\delta T_p}\right)^2 i^2_{T_p} + \overline{\left(\frac{\delta\alpha_{int,m}}{\delta T_{wall,loc}}\right)^2 i^2_{T_{wall,m}}}} \tag{4.78}$$

### Local internal heat transfer coefficient uncertainty

The local internal heat transfer coefficient, expressed with the equation 4.33, can be represented as a function of

- The local heat flux density $\dot{q}_{loc}$
- The propylene temperature $T_p$
- The local outside wall temperature $T_{wall,local}$

Deriving the equation 4.33, is possible to obtain the sensibility index

$$\frac{\delta\alpha_{int,local}}{\delta\dot{q}_{local}} = \frac{(T_p - T_{wall,local})}{\left(-T_p + T_{wall_m} + \dot{q}_{local} \sum_i \frac{1}{\lambda_i} \ln(\frac{r_{i+1}}{r_i})\, r_i\right)^2} \tag{4.79}$$

$$\frac{\delta\alpha_{int,local}}{\delta T_p} = -\frac{\dot{q}_{local}}{\left(-T_p + T_{wall_m} + \dot{q}_{local} \sum_i \frac{1}{\lambda_i} \ln(\frac{r_{i+1}}{r_i})\, r_i\right)^2} \tag{4.80}$$

$$\frac{\delta\alpha_{int,local}}{\delta T_{wall,local}} = \frac{\dot{q}_{local}}{\left(-T_p + T_{wall_m} + \dot{q}_{local} \sum_i \frac{1}{\lambda_i} \ln(\frac{r_{i+1}}{r_i})\, r_i\right)^2} \tag{4.81}$$

The uncertainty of the local internal heat transfer coefficient can be determined as follows

$$u(\alpha_{int,local}) = \sqrt{\left(\frac{\delta\alpha_{int,local}}{\delta\dot{q}_{local}}\right)^2 i^2_{\dot{q}_{local}} + \left(\frac{\delta\alpha_{int,local}}{\delta T_p}\right)^2 i^2_{T_p} + \left(\frac{\delta\alpha_{int,local}}{\delta T_{wall,loc}}\right)^2 i^2_{T_{wall,local}}} \tag{4.82}$$

### 4.2.2 Integral measurement uncertainty

In this section, the uncertainty of the parameters analyzed in the integral measurement typology. Some of the uncertainty present in this kind of measurement has already been analyzed in the local measurement section, so only the parameters uncertainty that hasn't been described will be reported in this section.

#### Logarithmic mean temperature difference uncertainty

The logarithmic mean temperature difference uncertainty, expressed with the equation 4.37, can be represented as a function of

- Outlet temperature of the oil $T_{oil,out}$
- Inlet temperature of the oil $T_{oil,in}$
- Outlet temperature of the propylene $T_{p,out}$
- Inlet temperature of the propylene $T_{p,in}$

To express the sensibility index is appropriate to make the following simplification

$$\Delta T_1 = T_{oil,out} - T_{p,in} \tag{4.83}$$

$$\Delta T_2 = T_{oil,in} - T_{p,out} \tag{4.84}$$

Deriving the equation 4.37, is possible to obtain the sensibility index

$$\frac{\delta \Delta_{lm}}{\delta T_{oil,out}} = \ln\left(\frac{\Delta T_1}{\Delta T_2} - \frac{\Delta T_1 - \Delta T_2}{\Delta T_1 \left(\ln\left(\frac{\Delta T_1}{\Delta T_2}\right)\right)^2}\right) \tag{4.85}$$

$$\frac{\delta \Delta_{lm}}{\delta T_{p,in}} = -\ln\left(\frac{\Delta T_1}{\Delta T_2} - \frac{\Delta T_1 - \Delta T_2}{\Delta T_1 \left(\ln\left(\frac{\Delta T_1}{\Delta T_2}\right)\right)^2}\right) \tag{4.86}$$

$$\frac{\delta \Delta_{lm}}{\delta T_{oil,in}} = -\ln\left(\frac{\Delta T_1}{\Delta T_2} - \frac{\Delta T_1 - \Delta T_2}{\Delta T_2 \left(\ln\left(\frac{\Delta T_1}{\Delta T_2}\right)\right)^2}\right) \tag{4.87}$$

$$\frac{\delta \Delta_{lm}}{\delta T_{p,out}} = \ln\left(\frac{\Delta T_1}{\Delta T_2} - \frac{\Delta T_1 - \Delta T_2}{\Delta T_2 \left(\ln\left(\frac{\Delta T_1}{\Delta T_2}\right)\right)^2}\right) \tag{4.88}$$

The uncertainty of the logarithmic mean temperature difference can be determined as follows

$$u(\Delta_{lm}) = \sqrt{\left(\frac{\delta \Delta_{lm}}{\delta T_{oil,out}}\right)^2 i^2_{T_{oil,out}} + \left(\frac{\delta \Delta_{lm}}{\delta T_{p,in}}\right)^2 i^2_{T_{p,in}} + \left(\frac{\delta \Delta_{lm}}{\delta T_{oil,in}}\right)^2 i^2_{T_{oil,in}} + \left(\frac{\delta \Delta_{lm}}{\delta T_{p,out}}\right)^2 i^2_{T_{p,out}}} \tag{4.89}$$

**Integral internal heat transfer coefficient uncertainty**

The internal heat transfer coefficient uncertainty in the case of integral measurement is calculated based on the equation 4.46 and can be represented as a function of

- Logarithmic mean temperature difference $\Delta T_{lm}$
- Heat flux from the thermal oil side $\dot{Q}_{oil}$

- External heat transfer coefficient $\alpha_{ext}$

Deriving the equation 4.46, is possible to obtain the sensibility index

$$\frac{\delta\alpha_{int}}{\delta\Delta_{lm}} = \frac{(4\,\pi\,L)}{d_{int,in}\,\dot{Q}_{oil}\left(\frac{2\,\pi\,L\,\Delta_{lm}}{\dot{Q}_{oil}} - \frac{1}{\lambda\,\ln\left(\frac{d_{in,ext}}{d_{int,in}}\right)} - \frac{2}{\alpha_{ext}\,d_{int,out}}\right)^2} \tag{4.90}$$

$$\frac{\delta\alpha_{int}}{\delta\dot{Q}_{oil}} = \frac{(4\,\pi\,L\,\Delta_{lm})}{d_{in,in}\,\dot{Q}_{oil}^2\left(\frac{2\,\pi\,L\,\Delta_{lm}}{\dot{Q}_{oil}} - \frac{1}{\lambda\,\ln\left(\frac{d_{int,ext}}{d_{int,in}}\right)} - \frac{2}{\alpha_{ext}\,d_{int,out}}\right)^2} \tag{4.91}$$

$$\frac{\delta\alpha_{int}}{\delta\alpha_{ext}} = \frac{4}{d_{int,out}\,\alpha_{ext}\,d_{int,in}\left(\frac{2\,\pi\,L\,\Delta_{lm}}{\dot{Q}_{oil}} - \frac{1}{\lambda\,\ln\left(\frac{d_{int,ext}}{d_{int,in}}\right)} - \frac{2}{\alpha_{ext}\,d_{int,out}}\right)^2} \tag{4.92}$$

The uncertainty of the logarithmic mean temperature difference can be determined as follows

$$u(\alpha_{int}) = \sqrt{\left(\frac{\delta\alpha_{int}}{\delta\Delta_{lm}}\right)^2 i^2_{\Delta_{lm}} + \left(\frac{\delta\alpha_{int}}{\delta\dot{Q}_{oil}}\right)^2 i^2_{\dot{Q}_{oil}} + \left(\frac{\delta\alpha_{int}}{\delta\alpha_{ext}}\right)^2 i^2_{\alpha_{ext}}} \tag{4.93}$$

where the uncertainty in the formula has been described previously. Since the definition of the external heat transfer coefficient is defined by the test tube manufacturer, also the uncertainty is given by a relation defined by the manufacturer. In this case the uncertainty relative to the external heat transfer coefficient is evaluated as $i_{\alpha_{ext}} = 0{,}05 * \alpha_{ext}$.

### Single phase propylene heat flux uncertainty

Only, in the case of gas cooling test, due to the condition of the single phase of the working fluid, is possible to directly calculate the heat flux of the propylene with the data collected. In this case, the heat flux, expressed with the equation 4.47, can be represented as a function of

- Outlet temperature of the propylene $T_{p,out}$
- Inlet temperature of the propylene $T_{p,in}$
- Mass flow of propylene $\dot{m}_p$

- Specific heat of propylene $cp_p$

Deriving the equation 4.47, is possible to obtain the sensibility index

$$\frac{\delta \dot{Q}}{\delta \dot{m}_p} = cp_p \left(T_{p,in} - T_{p,out}\right) \tag{4.94}$$

$$\frac{\delta \dot{Q}}{\delta T_{p,in}} = cp_p \, \dot{m}_p \tag{4.95}$$

$$\frac{\delta \dot{Q}}{\delta T_{p,out}} = -cp_p \, \dot{m}_p \tag{4.96}$$

$$\frac{\delta \dot{Q}}{\delta cp_p} = \dot{m}_p \left(T_{p,in} - T_{p,out}\right) \tag{4.97}$$

The uncertainty of the single phase propylene heat flux can be determined as follows

$$u(\dot{Q}) = \sqrt{\left(\frac{\delta \dot{Q}}{\delta \dot{m}_p}\right)^2 i^2_{\dot{m}_p} + \left(\frac{\delta \dot{Q}}{\delta T_{p,in}}\right)^2 i^2_{T_{p,in}} + \left(\frac{\delta \dot{Q}}{\delta T_{p,out}}\right)^2 i^2_{T_{p,out}} + \left(\frac{\delta \dot{Q}}{\delta cp_p}\right)^2 i^2_{cp_p}} \tag{4.98}$$

**Outlet vapour quality uncertainty**

The outlet vapour quality of the propylene is calculated with the relation 4.49 and is a function of:

- Outlet enthalpy $h_{p,out}$ calculated with the equation 4.48, itself a function of
  - Inlet propylene enthalpy $h_{inlet}$
  - propylene heat flux $\dot{Q}_p$
  - Mass flow propylene $\dot{m}_p$
- Saturated liquid enthalpy $h_{l,sat}$
- Saturated vapour enthalpy $h_{g,sat}$

Deriving the equation 4.49 give the sensibility index

$$\frac{\delta x}{\delta h_{p,out}} = \frac{1}{h_{g,sat} - h_{l,sat}} \tag{4.99}$$

$$\frac{\delta x}{\delta h_{g,sat}} = \frac{h_{p,out} - h_{g,sat}}{\left(h_{g,sat} - h_{l,sat}\right)^2} \tag{4.100}$$

$$\frac{\delta x}{\delta h_{l,sat}} = \frac{h_{l,sat} - h_{p,out}}{\left(h_{g,sat} - h_{l,sat}\right)^2} \tag{4.101}$$

Consequently, the combined uncertainty of the inlet vapour quality is

$$u(x) = \sqrt{\left(\frac{\delta x}{\delta h_{p,out}}\right)^2 i^2_{h_{p,out}} + \left(\frac{\delta x}{\delta h_{g,sat}}\right)^2 i^2_{h_{g,sat}} + \left(\frac{\delta x}{\delta h_{l,sat}}\right)^2 i^2_{h_{l,sat}}}. \tag{4.102}$$

The uncertainty of the inlet enthalpy $h_{p,out}$ is defined considering the equation 4.48 and deriving it, to obtain the sensibility index related to the inlet enthalpy.

$$\frac{\delta h_{p,out}}{\delta \dot{m}_p} = \frac{\dot{Q}_p}{\left(\dot{m}_p\right)^2} \tag{4.103}$$

$$\frac{\delta h_{p,out}}{\delta \dot{Q}_p} = -\frac{1}{\left(\dot{m}_p\right)} \tag{4.104}$$

$$\frac{\delta h_{p,out}}{\delta h_{inlet}} = 1 \tag{4.105}$$

$$i_{h_{p,out}} = \sqrt{\left(\frac{\delta h_{p,out}}{\delta \dot{m}_p}\right)^2 i^2_{\dot{m}_p} + \left(\frac{\delta h_{p,out}}{\delta \dot{Q}_p}\right)^2 i^2_{\dot{Q}_p} + \left(\frac{\delta h_{p,out}}{\delta h_{inlet}}\right)^2 i^2_{h_{inlet}}} \tag{4.106}$$

# Chapter 5

# EXPERIMENTAL RESULTS

In this chapter, the results of the data acquisition are showed and analyzed for having a better understanding of the phenomena occurring in the test section.

## 5.1 Gas cooling

In the test facility, measurements are carried out with propylene as a pure vapour. For this purpose, the experimentally measured pressure losses, friction coefficients as well as heat transfer are presented, analyzed and compared with correlations from the literature. For measurements regarding single phase process, a integral typology of measurement was used, composed by pressure and temperature sensors positioned at the inlet and outlet of the test tube and described in the chapter on the experimental setup. This type of measurement was used because the single-phase measurement information regarding the temperature trend along the tube is not necessary since there is no phase change and the temperature trend is linear.

### 5.1.1 Pressure drop

Figure 5.1 shows the single-phase pressure losses occurring inside a micro-fin tube for propylene as gas phase in superheated condition at inlet pressure $p = 11{,}4\,bar$ with an inlet temperature of $70°C$ over the flow velocity. According to Figure 5.1, it is possible to observe the pressure loss increase as the flow velocity $u$ raises. Thus, a pressure loss of just under $600\,mbar$ at slightly less than $30\,m/s$ is measured. The increment of flow velocity implies an increase of the wall friction of the fluid with the tube wall which leads to higher pressure losses. The presence of the fins within the tube produces greater flow perturbation as velocity increases due to the increased vortical flow and recirculation of flow produced by the fins themselves,

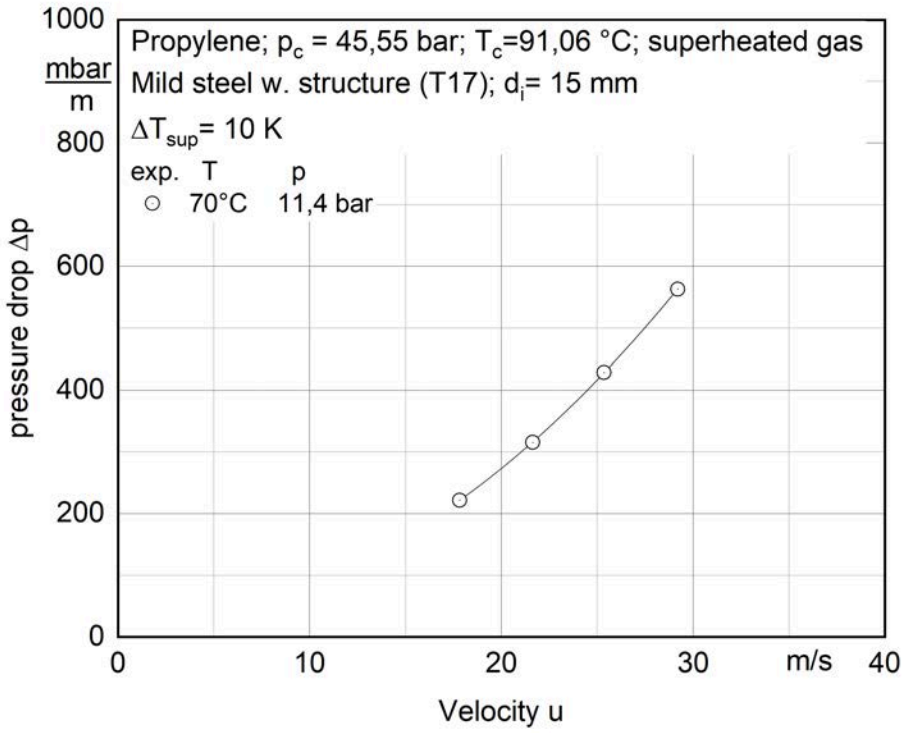


Figure 5.1: Single-phase pressure drop $\Delta p$ as a function of the flow velocity $w$ for gas propylene for $p_r = 45{,}55\,bar$ with a inlet temperature of $70\,°C$

leading to a greater frictional pressure drop. In their study, Celen et al. [12], reported the same trend of increasing pressure drop as the velocity increase and their experimental results confirmed the behaviour explained.

Figure 5.2 shows the single phase pressure drop $\Delta p$ for different inlet pressure and temperature, inside a micro-fin tube with propylene as gas phase in superheated condition as a function of the flow velocity $u$. In Figure 5.2 it is noticeable, as described previously, the increasing trend of pressure drop curves, for each inlet pressure, as the flow velocity increases. It is also possible to observe that, as the inlet pressure increases, the flow velocity decreases and both the absolute value and amplitude of the pressure drop curves decrease. Each tests were conducted changing the test facility parameters for the measurements with a different inlet pressure but with the same Reynolds number range. The decrease of the flow velocity for increasing inlet pressures can be explained considering the constant Reynolds number for each test. Indeed, considering the definition of the Reynolds number as

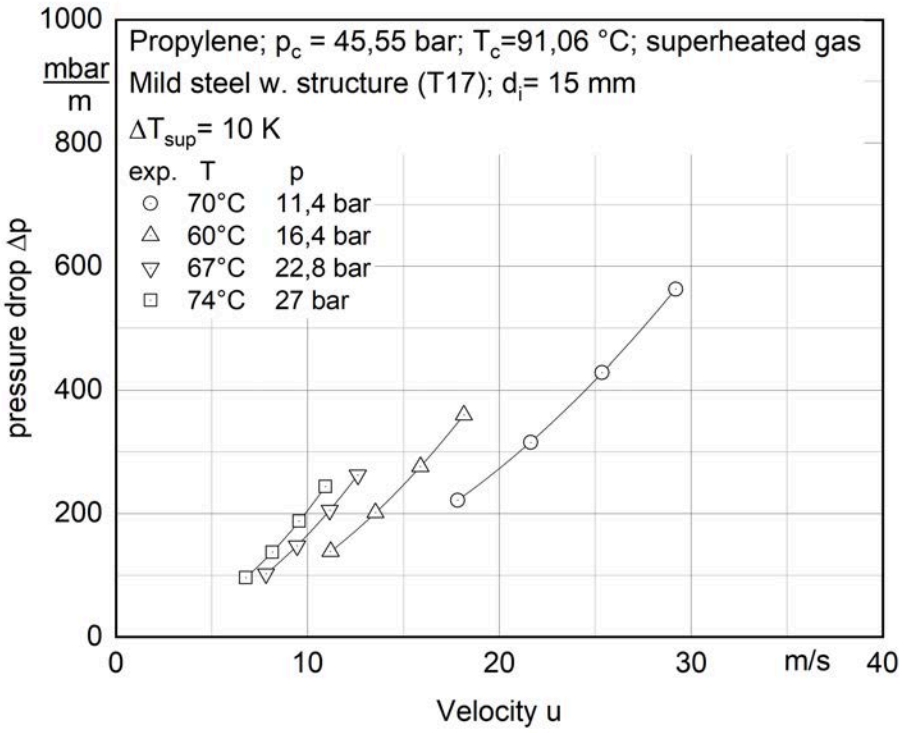


Figure 5.2: Single-phase pressure drop $\Delta p$, for different inlet pressure, as a function of the flow velocity $w$ for gas propylene for $p_r = 45{,}55\,bar$ with a inlet temperature of $70\,°C$

showed in equation 2.17, and deducing the velocity from the formula, it is observable that as the pressure of the fluid increases the density increases considerably causing the decrease of the fluid velocity. Considering all fluid properties, as the pressure increases, the viscosity also increases, but the increase in density relative to that of viscosity is considerably higher, so the increase in density has a greater influence on the velocity trend. Because of the velocity decrease at high pressure, the pressure drop decrease due to the reduced friction between the fluid and the tube wall.

Figure 5.3 shows the evolution of the single-phase friction factor $\xi$ inside a micro-fin tube with propylene as gas phase in superheated condition at inlet pressure $p = 11{,}4\,bar$ with a inlet temperature of $70\,°C$ over the Reynolds number $Re$. In the same graph is also represented the friction factor trend calculated with the Konakov [27] correlation for a smooth tube. According to Figure 5.3, the friction

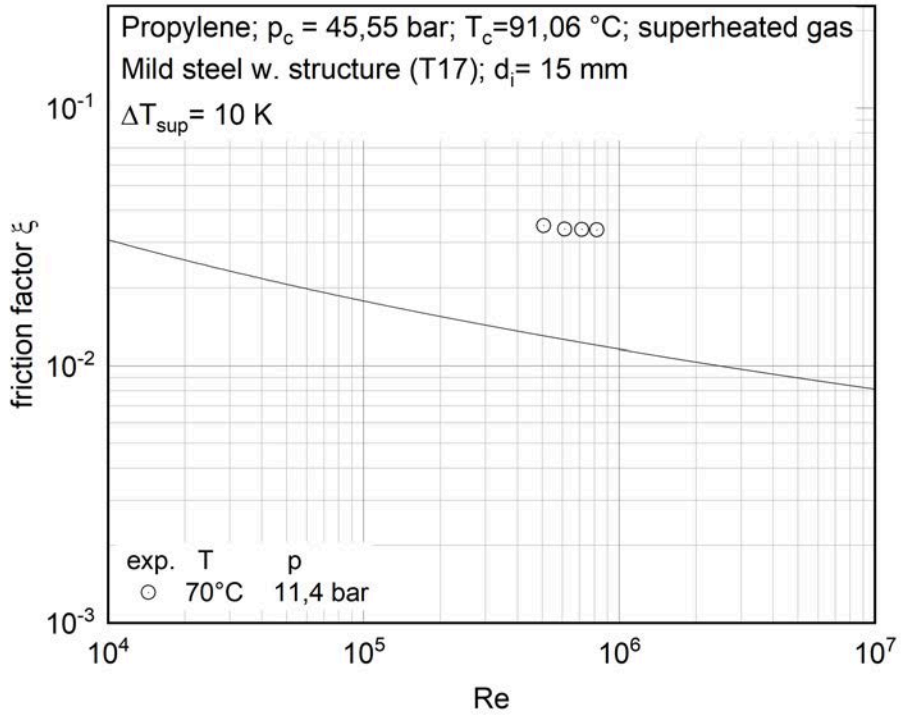


Figure 5.3: Coefficient of friction $\xi$ over Reynolds number $Re$ for propylene as gas phase and confrontation with the friction factor calculated with Konakov correlation [27]

factor is not strongly influenced by the evolution of the Reynolds number but is noticeable a limited decrease of $\xi$ as the Reynolds number increases. This trend, however, is considerably moderate so that is difficult to define an actual evolution of the friction factor as a function of the Reynolds number. Otherwise, a noticeable offset is observable between the experimental data and the Konakov friction factor calculated with the equation presented in table 2.4 using the same parameters used for determining the experimental point. Konakov et al. [27] developed a correlation for the calculation of the friction factor for turbulent flow inside a smooth tube. This correlation has been used by Gnielinski et al. [21] for the determination of the Nusselt number for fully developed turbulent flow. As reported before, the evolution of the friction factor over the Reynolds number does not present a strong influence but it is possible to notice a slight decrease in friction factor for increasing Reynolds number. This behaviour could be explained considering that the friction factor points reported in the graph are not directly measured on the test facility but

are calculated trough the equation 2.24. In this formula, it is possible to observe the direct proportionality of the friction factor with the pressure drop but also the inverse proportionality over the square of the flow velocity. As observed in figure 5.1 the pressure drop increase as the flow velocity raises so, considering that the Reynolds number increases when the fluid velocity increases, since the fluid proprieties stay constant due to constant pressure test characteristics, the friction factor should increase as the Reynolds number raises. But because the inverse proportionality with the square of the flow velocity has a higher impact on the equation of the friction factor, the decreasing trend of the latter can be explained. The combination of the opposed influence that pressure drop and fluid velocity have, leads to an attenuation of the friction factor curve downturn and so can be explained the limited reduction of the friction factor along with the Reynolds number. The evolution of the friction factor can also be analysed considering the flow behaviour inside the tube. At higher Reynolds numbers, the thickness of the viscous sub-layer decreases due to the increased velocity and inertial forces near the wall, so the dominance of the viscous force in the fluid flow is decreased [12]. For micro-fin tubes, as the Reynolds number increases, the viscous sub-layer decreases and becomes lower than the fins height, so the fins generate a large amount of additional turbulence that increases turbulent viscosity and the turbulence diffusivity near the wall, leading to an increase in flow resistance [29]. Regarding the confrontation with the Konakov friction factor, the offset of the experimental points can be explained considering that the Konakov friction factor is developed for a smooth tube and the presence of the internal structure creates a large amount of additional resistance to the fluid flow leading to a bigger friction factor.

Figure 5.4 shows the evolution of the single-phase friction factor $\xi$ with different inlet pressures and temperatures inside a micro-fin tube with propylene as gas phase in superheated condition as a function of the Reynolds number $Re$. In the same graph is also represented the friction factor trend calculated with the Konakov correlation [27] for smooth tubes. In Figure 5.4 it is can be observed that the friction factor presents the same trend with respect to Reynolds number as the inlet pressure increases. This phenomenon can be explained considering once again the definition of the friction factor reported in equation 2.24, where it is possible to notice that, as the inlet pressure rises, the flow velocity decreases while the density and viscosity of the fluid increase. The very limited influences of the pressure increment on the friction factor is explained considering that the decrease of the flow velocity is compensated by the increase of both density and viscosity, creating a situation where the pressure influence is kept very limited.

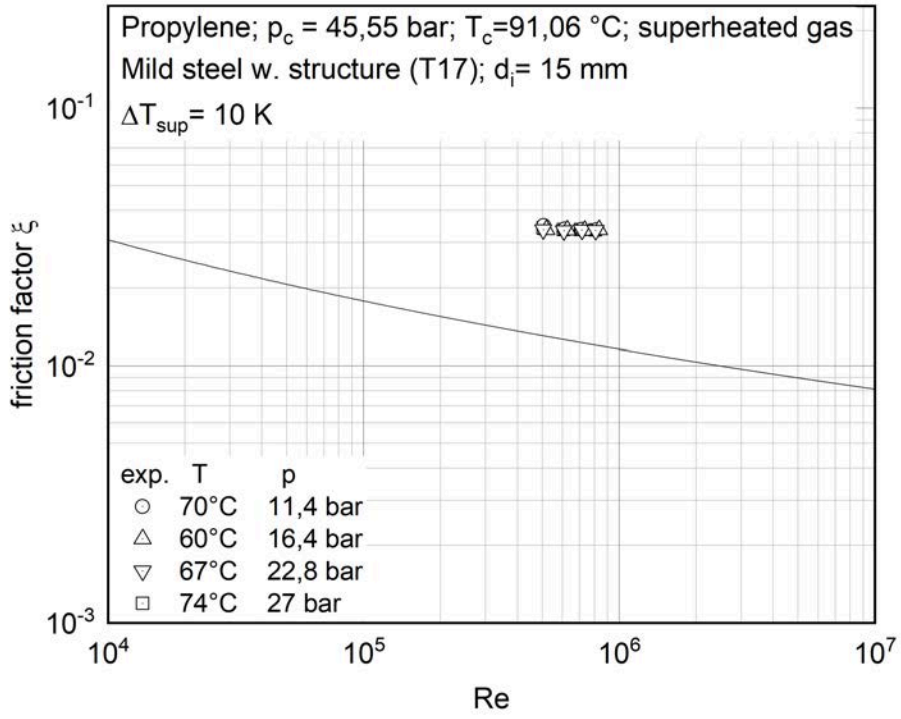


Figure 5.4: Friction factor $\xi$, for different inlet pressures, over the Reynolds number $Re$ for propylene as gas phase and confrontation with the friction factor calculated with Konakov correlation [27]

Figure 5.5 shows the pressure drop penalty factor occurring inside a micro-fin tube for propylene as gas phase in superheated condition at inlet pressure $p = 11{,}4\,bar$ with an inlet temperature of $70\,°C$ as a function of the Reynolds number $Re$. According to Figure 5.5, the penalty factor increases as the Reynolds number raises and the increment is linear except for the first measured point. The penalty factor is a parameter defined for having a direct confrontation with the increase of pressure drop caused by the presence of the micro-fin structure inside the tube. This parameter can be defined as

$$PF = \frac{f_{structured} - f_{smooth}}{f_{smooth}} \tag{5.1}$$

where $f_{structured}$ represents the friction factor calculated based on the experimental data as explained before while $f_{smooth}$ is the Konakov friction factor [27]. Considering the formula for the calculation of the penalty factor $PF$, it is noticeable that the

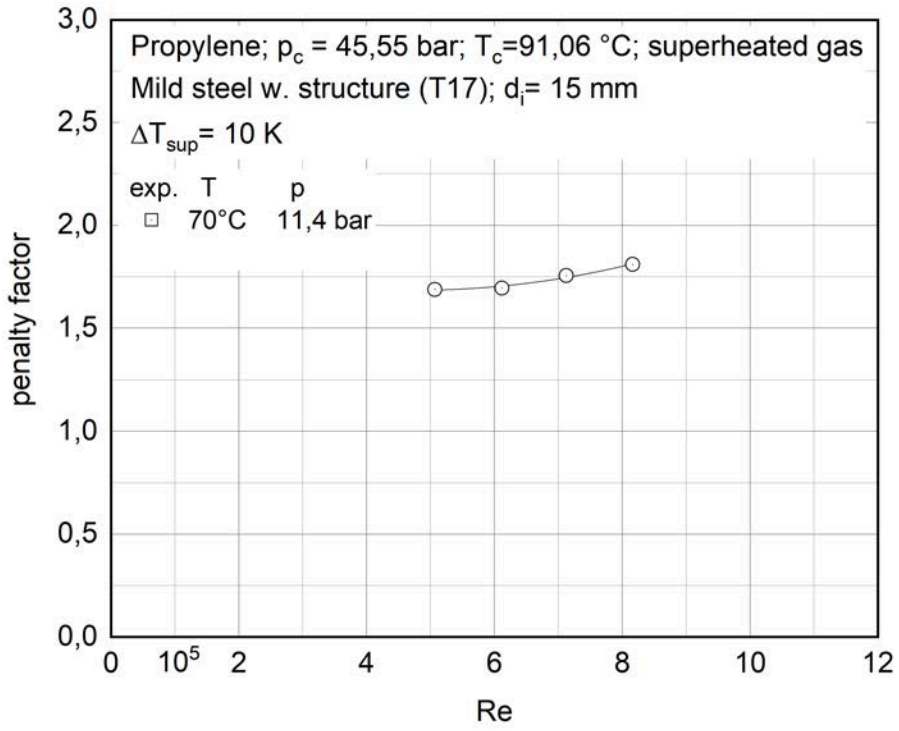


Figure 5.5: Pressure drop penalty factor as a function of Reynolds number $Re$ for gas propylene for $p_r = 45{,}55\,bar$ with a inlet temperature of $70\,°C$

increasing trend is due to the increment of the difference between the experimental friction factor values and the Konakov ones. This increase is explainable considering that the structured friction factor has a low dependency on the increases of the Reynolds number and its curve stay almost constant as the latter increases, as it can be seen in Figure5.3. Otherwise, the friction factor for smooth tubes, defined with Konakov correlation [27], has a strong dependency on the increase of Reynolds number so that the difference between the two factor increases as the Reynolds number increases. The increment of Reynolds number is determined by an increment of the flow velocity so the friction factor and pressure drop increases in both smooth and structured tubes. However, the presence of the fins creates a greater pressure drop due to increased friction with the pipe wall. As it is possible to observe in the graph, with a Reynolds number of 700000, the friction factor is approximately 150% greater than the friction factor for a smooth tube with the same diameter.

### 5.1.2 Heat transfer coefficient

Figure 5.6 shows the heat transfer coefficient calculated for a micro-fin tube with propylene as a gas phase in superheated condition at inlet pressure $p = 11{,}4\,bar$ with an inlet temperature of $70\,°C$ as a function of the flow velocity $u$.

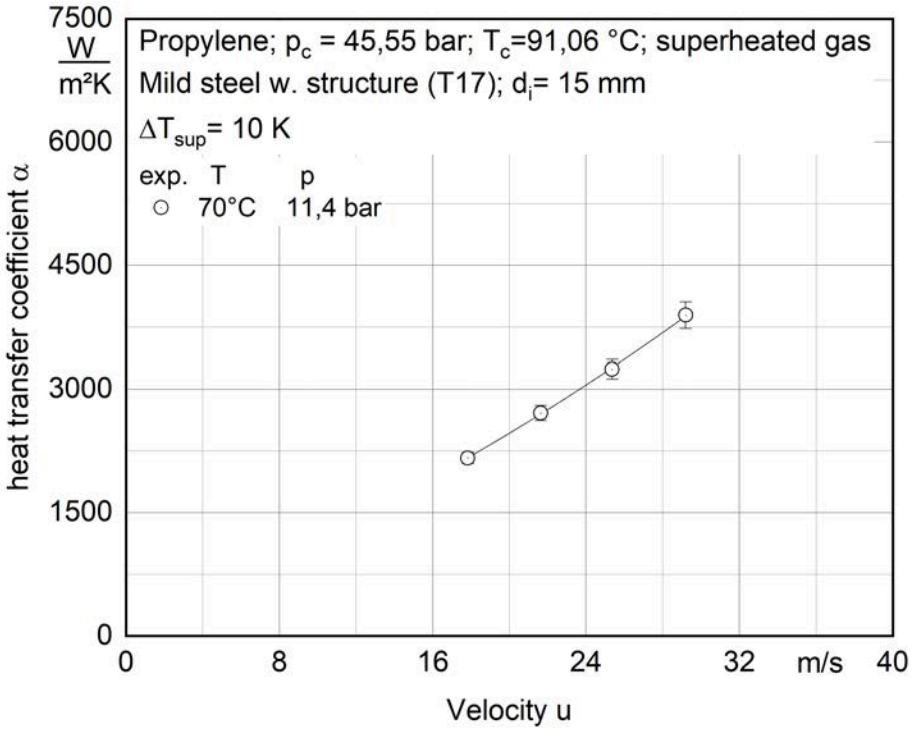


Figure 5.6: Single-phase heat transfer coefficient $\alpha$ as a function of the flow velocity $w$ for gas propylene with $p = 11{,}4\,bar$ and inlet temperature of $70\,°C$

In Figure 5.6 it is possible to observe that the heat transfer coefficient increases as the flow velocity inside the tube increases. It is also possible to note that the increment of $\alpha$ is linear and proportional to the fluid velocity $u$. From the graph, it is noticeable that a heat transfer coefficient of approximately $4000\frac{W}{m^2\,K}$ is calculated for a velocity of $29\,m/s$. The heat transfer coefficient is not a parameter that is directly measured in the test facility but its value is calculated using the formula 4.45, based on the measured data. Analyzing the formula of the heat transfer coefficient and considering its definition, reported in equation 2.14, it is possible to notice that the trend of $\alpha$ is influenced mainly by two changing parameters, the mean logarithmic temperature difference $\Delta T_{ml}$ and the heat flux $\dot{Q}$. The heat flux

,defined as

$$\dot{Q} = \dot{m}\,\Delta h \tag{5.2}$$

is greatly influenced by the increase of the flow velocity, since the velocity increment is a consequence of the increase of mass flux. As the mass flux increases, the enthalpy difference increases too but the increment of the latter is limited compared to the one of the mass flux so the mass flux increase is the controlling parameter. The mean logarithmic temperature difference is only marginally affected by the increase of the flow velocity since an increment of the latter determine an increase of the heat exchanged and so of the temperature difference between inlet and outlet, but this increment is limited. Li et al . [29] explained that the increment of the heat transfer as the flow velocity raises is due to the thinning of the viscous sub-layer that is caused by the increased velocity and inertial forces near the wall as the Reynolds number increases. This effect creates additional turbulence in the fluid flow which increase the turbulent viscosity and the turbulent diffusivity near the wall and so the heat transfer is increased. Another effect of the flow velocity increase inside a micro-fin tube is the increment of the turbulence in the flow which in return promotes a better cross-mixing of the flow, so the convective heat transfer is improved. A more even distribution of the temperature inside the tube itself is facilitated.

Figure 5.7 shows the heat transfer coefficient, for different inlet pressures, as a function of the mass flow rate for a micro-fin tube with propylene as a gas phase in superheated condition. As observed in the graph of figure 5.7, the heat transfer coefficient presents an increasing trend as the mass flow rate increases for every inlet pressure measured. From the graph, it is also possible to notice a tendency to measure higher heat transfer coefficient $\alpha$ for the measurement series with higher reduced pressure $p^*$. The heat transfer for forced convection is dependent on the Prandtl number, as it is possible to observe in equation 2.20, which defines the ratio between the velocity boundary layer thickness and the temperature boundary layer thickness. For higher reduced pressures $p^*$ the increment of the fluid proprieties, such as kinematic viscosity, thermal conductivity, specific heat capacity and the Prandtl number $Pr$, defined in equation 2.16, increase too so that the heat transfer improves.

Figure 5.8 shows the Nusselt number $Nu$ calculated for a micro-fin tube with propylene as a gas phase in superheated condition at inlet pressure $p = 11{,}4\,bar$ with an inlet temperature of $70\,°C$ as function of the Reynolds number $Re$. In Figure 5.8 is possible to observe the increasing trend of the Nusselt number as the Reynolds number raises. From the measured data is possible to determine a Nusselt number

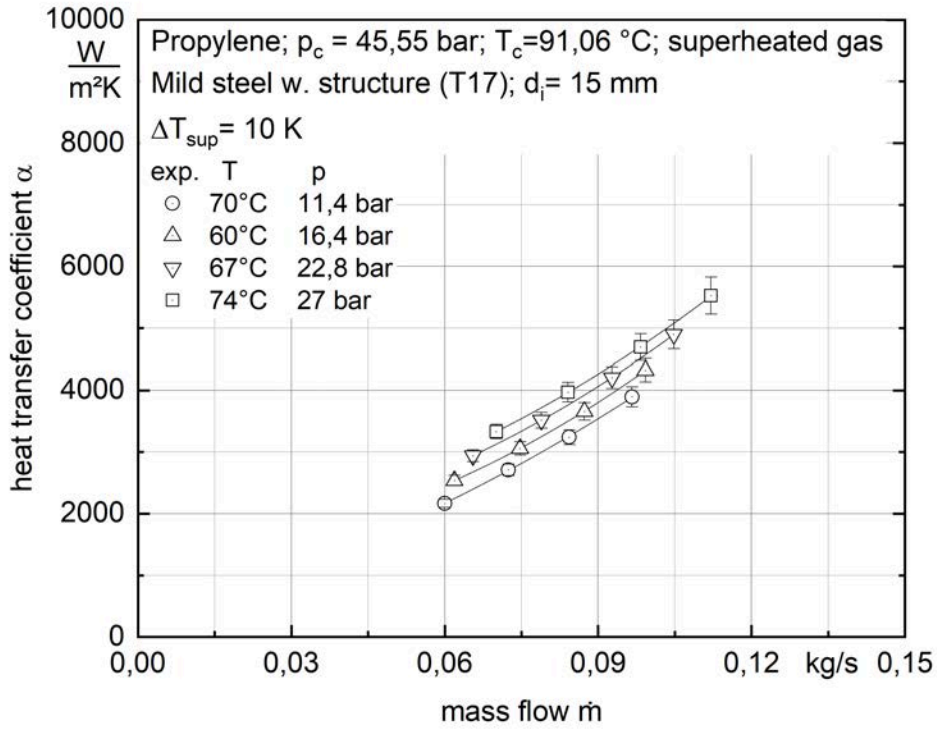


Figure 5.7: Single-phase heat transfer coefficient $\alpha$, for different inlet pressure, as a function of the mass flow rate $\dot{m}$ for gas propylene for $p_r = 45{,}55\,bar$ with a inlet temperature of $70\,°C$

of 2700 for a Reynolds number of approximately 800000. The increment of the Nusselt number can be explained considering the correlation for the determination of the adimensional number in the case of forced convection as reported in equation 2.20. As the Nusselt number is proportional to the Reynolds number if the latter increases the Nusselt number increases as consequence. The Prandtl number is not a function of the velocity of the flow since it depends only on fluid characteristics that stay constant during the test. The increment of the Nusselt number can be analysed also considering the definition of the adimensional number itself as reported in equation 2.15 where is possible to notice that the only factor that increases as the flow velocity and so Reynolds number increase is the heat transfer coefficient $\alpha$ as explained before.

Figure 5.9 shows the Nusselt number $Nu$ calculated for a micro-fin tube with propylene as a gas phase in superheated condition for different Reynolds number $Re$ as

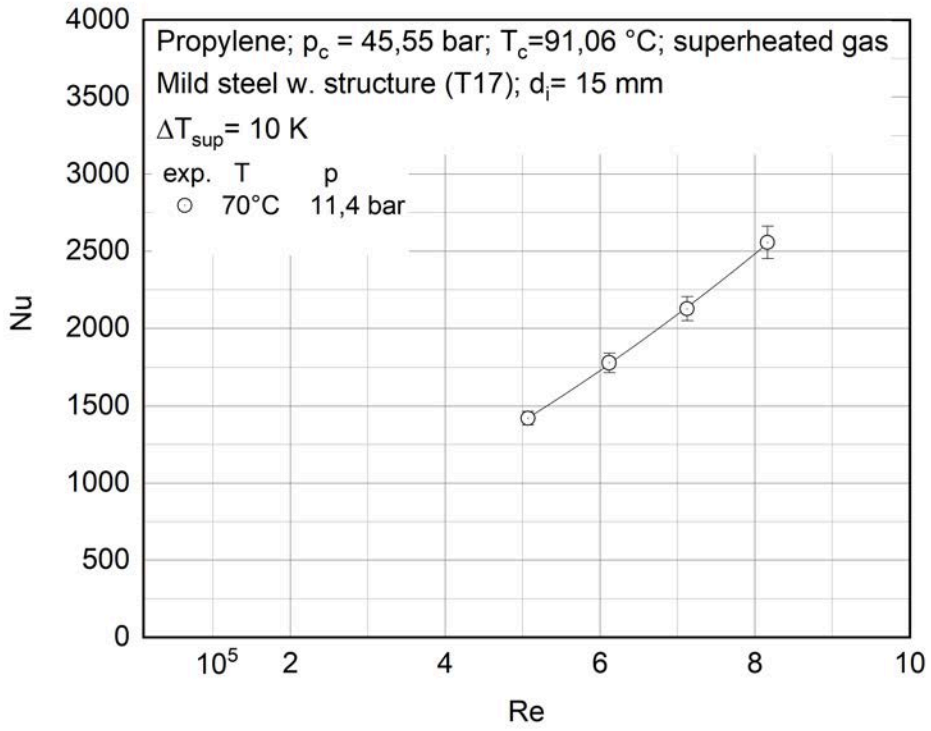


Figure 5.8: Single-phase Nusselt number $Nu$ as a function of the Reynolds number $Re$ for gas propylene for $p = 11{,}4\,bar$ with an inlet temperature of $70\,°C$

a function of the reduced pressure $p^*$. For a fixed Reynolds number, it can be seen that the number of Nusselt initially increases as the reduced pressure increases, and then plateaus at higher reduced pressures. The curves of the Nusselt number as the reduced pressure increases, for different Reynolds numbers, present all the same trend. It is also possible to observe that higher Nusselt numbers are calculated with higher Reynolds number, regardless of the reduced pressure. The plateau of the curves can be explained considering that from a value of reduced pressure around 0,4 the gradient of increment of the thermal conductivity becomes larger than the gradient of increase of the heat transfer coefficient resulting in an equilibrium between the two factors and in an overall plateau in the Nusselt number curves. Since the Nusselt number represents the ratio between the convection heat transfer over the conductive heat transfer, under a defined reduced pressure, the convective heat transfer, represented by the increasing heat transfer coefficient, has a bigger impact on the overall heat transfer phenomena. As the reduced pressure increases, the physical properties of the fluid, such as the thermal conductivity, raise as a

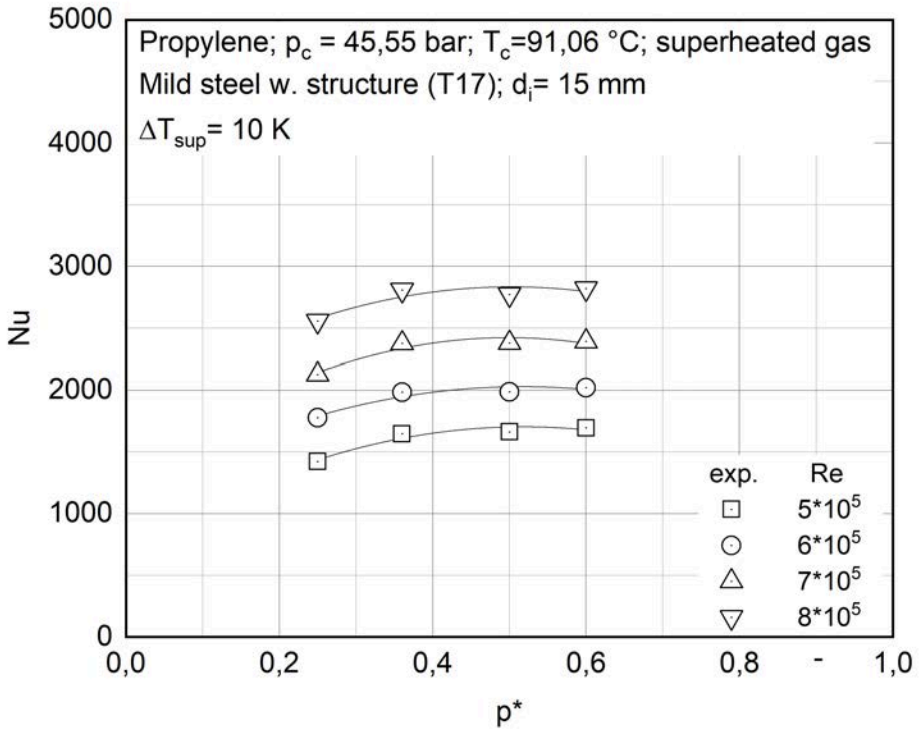


Figure 5.9: Single-phase Nusselt number $Nu$, for different Reynolds number $Re$ , as a function of the reduced pressure for gas propylene

consequence of the higher pressure, resulting in an increasingly higher influence of the conductive heat transfer phenomena and so on an equilibrium between the two different heat transfer methods.

In the figure 5.10 is showed the improvement factor calculated for a micro-fin tube with propylene as a gas phase in superheated condition at inlet pressure $p = 11{,}4bar$ with an inlet temperature of 70 $°C$ as a function of the Reynolds number $Re$. In Figure 5.10 is possible to notice the increment of the improvement factor as the Reynolds number increases. For the measured data, it is noticeable an improvement factor of 140% for a Reynolds number of approximately 800000. The improvement factor is a parameter defined to have a direct visualization of the heat transfer coefficient increase created by the presence of the micro-fin structure inside the tube. This parameter can be defined as

$$IF = \frac{\alpha_{structured} - \alpha_{smooth}}{\alpha_{smooth}} \tag{5.3}$$

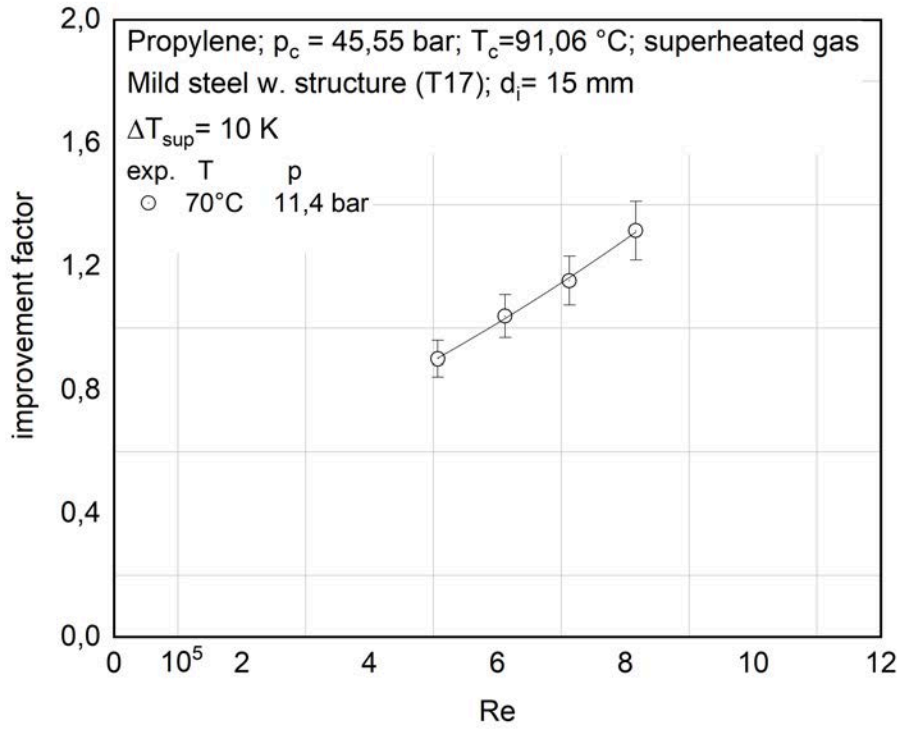


Figure 5.10: Single-phase improvement factor as a function of the Reynolds number $Re$ for gas propylene with $p = 11{,}4\,bar$ and inlet temperature of $70\,°C$

where $\alpha_{structured}$ represent the heat transfer coefficient calculated based on the experimental data as explained before while $\alpha_{smooth}$ is the heat transfer coefficient for smooth tube calculated with the correlation of Gnielinski [21] presented in table 2.1. The trend of the curve can be explained considering the difference of increment between the heat transfer coefficient for a micro-fin tube and the one for a smooth tube as the flow velocity increase. As showed in figure 5.6, for a structured tube, as the flow velocity increases the internal heat transfer increases proportionally due to the increased turbulence in the flow while for a smooth tube the increasing trend is not that pronounced for high flow velocity compared to the structured ones. It is possible, at this point, to make a consideration examining the penalty factor and the improvement factor for the same conditions and same tube. Considering the graph 5.10 and 5.5, it is possible to observe that for a Reynolds number of 500000 the penalty factor $PF$ is approximately 150% and the improvement factor $IF$ is approximately 90% while increasing the flow velocity and so the Reynolds number

to around 800000, the two factor becomes $PF = 180\%$ and $IF = 130\%$. So analyzing the two trends it is possible to notice that for the same increase of Reynolds number and so flow velocity, the improvement factor and the advantage in term of heat transfer coefficient for the micro-fin tube is bigger compared to the increase of penalty factor and pressure drop. Also, even if the absolute increase of friction factor, represented by the value of penalty factor, is high (around 180 % increase of friction factor) for a micro-fin tube, the overall pressure drop is contained under 600 *mbar* with, at the same time, an advantage in terms of heat transfer coefficient improve compared with a smooth tube of approximately 150 %.

Figure 5.11 shows the improvement factor calculated, for different inlet pressure,in a micro-fin tube with propylene as a gas phase in superheated condition at reduced pressure $p_r = 45{,}55\ bar$ with a inlet temperature of 70 $°C$ as a function of the Reynolds number *Re*. In the graph is noticeable the increasing trend of the improvement factor for the increasing Reynolds number, as showed also in the previous

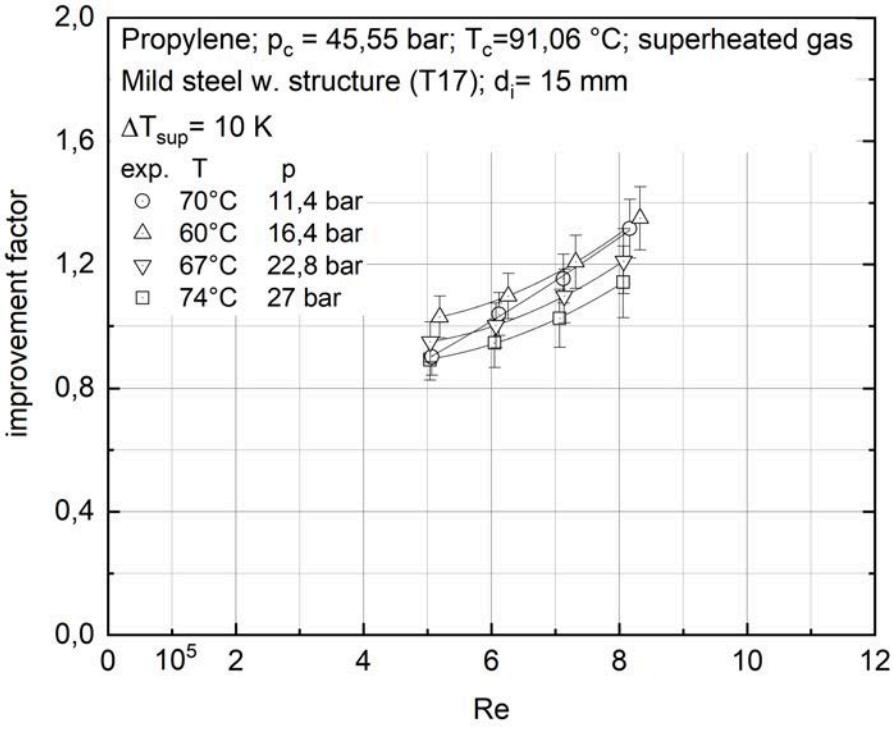


Figure 5.11: Single-phase improvement factor, for different inlet pressure, as a function of the Reynolds number *Re* for gas propylene

figure. It is possible to observe that a lower improvement factors are calculated for higher inlet pressure with the same Reynolds number. The measuring series with lower pressure present a different trend compared to the other measuring series and this could be due to uncertainties or error in the measuring process. As the pressure increases, as shown in figure 5.9, the Nusselt number for micro-fin tube reaches a plateau while this does not happen for the Nusselt number calculated with the Gnielinski correlation, the one used for determining of the heat transfer coefficient for a smooth tube. This difference of trend between the smooth and the structured tube can be explained considering that, as the pressure increases, since the density, thermal conductivity and viscosity increase, there is an enhancement of heat transfer also for smooth tube and so the advantage created by the structured tube is reduced only to the enhanced exchanged surface and so the improvement factor is less pronounced.

## 5.2 Condensation

In this chapter, the data acquired for condensation tests are showed and the results relative to the heat transfer coefficient and the pressure drop are displayed. Confrontation with correlations from the open literature are also showed. The tests were conducted on a micro-fin tube produced by Weiland with propylene as gas in two-phase condition. For the measurements regarding the condensation tests a local measurement setup was used, adding to the inlet and outlet pressure and temperature sensors a series of thermocouples glued in micro-grove on the outside wall of the inner tube in four different measurement sections along the test tube. This kind of measurement setup was used for having a better understanding of the condensation process along the test tube thanks to the information of temperature acquired by the thermocouples and more precise data regarding flow pattern inside the tube and the influence of the micro-fin internal structure on the fluid flow.

### 5.2.1 Flow pattern

In the following section, the data regarding the flow pattern inside the micro-fin tube are presented and the results discussed. Since the manufacturer did not provide data regarding the geometric characteristics of the internal structure of the micro-fin pipe analyzed, no model or flow pattern map related to flow regimes could be applied to determine the type of flow within the pipe. Only the data regarding the trend of the local temperature differences in the four measuring sections can be used to analyze the different flow type presents inside the test tube in

the different test conditions.

Figure 5.12 shows the local temperature difference measurements for propylene with vapour quality $x = 0{,}3$ and $x = 0{,}9$ for a specific mass flux of $\dot{G} = 600kg/(m^2s)$, reduced pressure $p_r = 0{,}25$ and saturation temperature of $24{,}5C$ measured at each measurement section as a function of the radial position $\phi$.

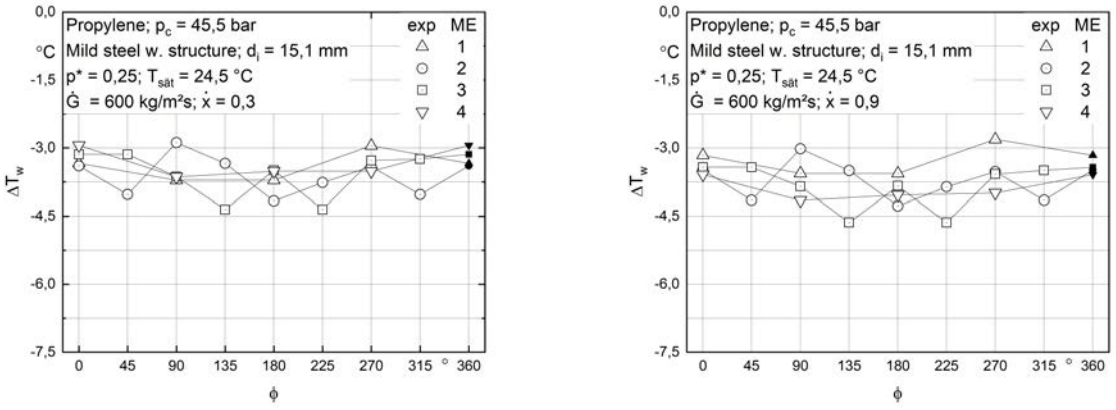


Figure 5.12: Local temperature difference measurements for propylene with vapour quality $x = 0{,}3$ and $x = 0{,}9$ measured at each measurement section as a function of the radial position $\phi$

In Figure 5.12 is noticeable the different values of temperature difference in every measurement section for vapour quality of $x = 0{,}3$ and $x = 0{,}9$. Analyzing the trend of both temperature differences trend it is observable an increment of the values of temperature difference moving from one measurement section to the following one. This trend can be explained considering the decrement of vapour content in the two-phase fluid as the fluid move along the tube because of the condensation process. As the vapour quality decrease, an increment in the temperature difference is noticeable due to the increased thickness of the liquid film and consequently an increase in the thermal resistance. The variation of vapour quality between the inlet and outlet of the tube is limited because the test conditions require a small variation of steam content for having more reliable data on the mean values. Analyzing the different graphs is also noticeable that the middle measuring sections (ME 2 and ME 3) present a more variable profile compared to the first and last measuring sections.

In Figure 5.13 are represented the single graphs of the temperature difference trend at each measurement section for propylene with specific mass flux $\dot{G} =$

$600kg/(m^2s)$, reduced pressure $p_r = 0{,}25$, saturation temperature of $24{,}5C$ and vapour quality $x = 0{,}3$ as a function of the radial position $\phi$.

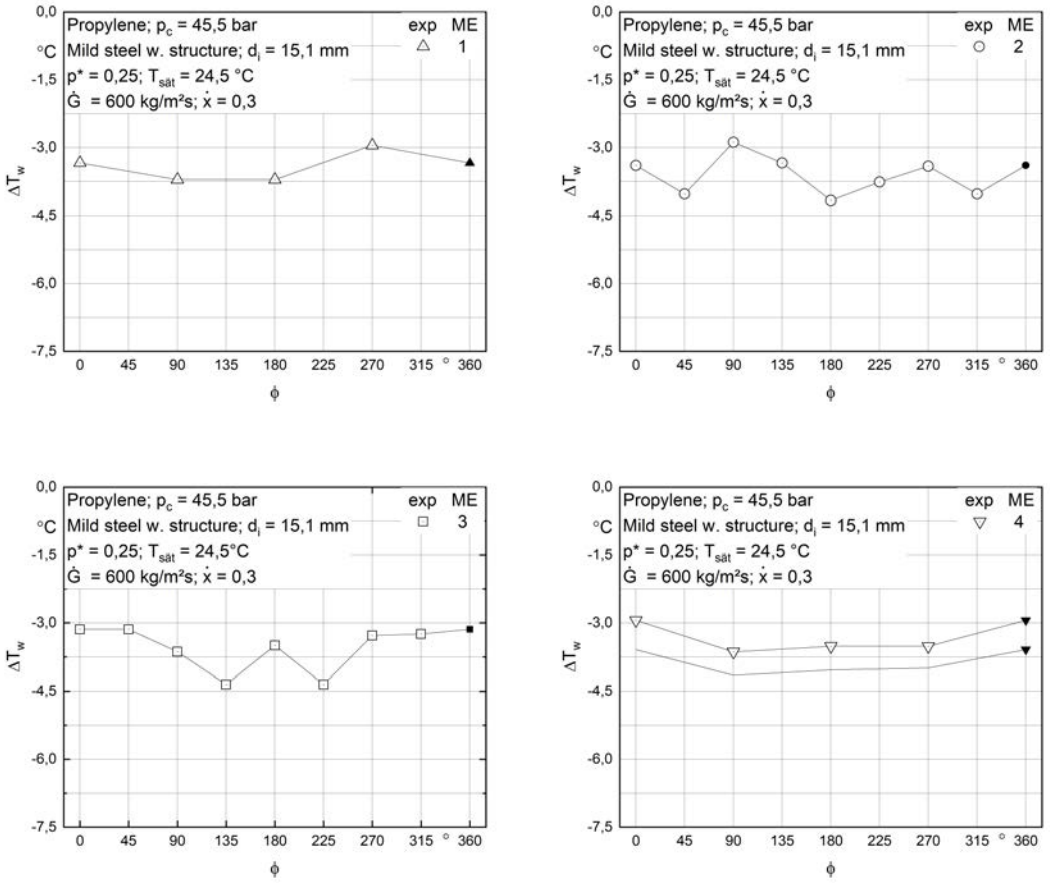


Figure 5.13: Local temperature difference measurements for propylene with vapour quality $x = 0{,}3$ measured in every measuring section as a function of the radial position $\phi$

In Figure 5.13 is possible to observe, more clearly, the trend of the local temperature difference at each measuring section. As described before is possible to observe the more variable profile of the temperature differences in the middle sections compared to the first and last ones. Considering the test conditions such as the high specific flow, the vapour quality of $x = 0{,}3$, the temperature and pressure values an annular flow is assumed as a flow regime. From the graphs, is also noticeable that in the first and last measurement sections, the temperature difference at the bottom of the tube presents higher values compared to the sensors located in the upper part of the tube. This could indicate an accumulation of liquid in the lower section due to the effect of gravity, given also the large specific flow rate. In the middle sections,

the trend is more variable so is difficult to observe the same phenomena. Without a visual verification of the flow inside the tube or a theoretical confirmation of the flow regime is not possible to confirm the hypothesis described.

In Figure 5.14 are represented the single graphs of the temperature difference trend in every measurement section for propylene with specific mass flux $\dot{G} = 600kg/(m^2s)$, reduced pressure $p_r = 0{,}25$, saturation temperature of $24{,}5C$ and vapour quality $x = 0{,}9$ as a function of the radial position $\phi$. In Figure 5.14 is

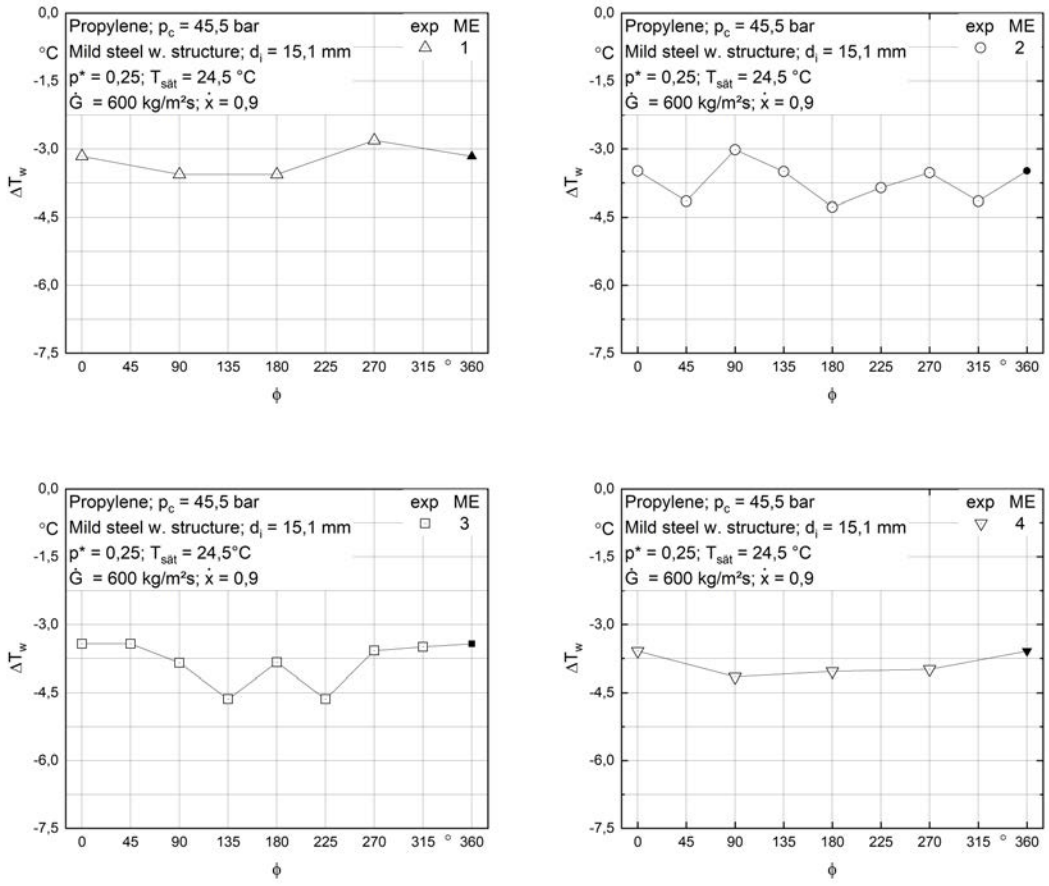


Figure 5.14: Local temperature difference measurements for propylene with vapour quality $x = 0{,}9$ measured in every measuring section as a function of the radial position $\phi$

possible to observe similar trends of the local temperature differences as those described in Figure 5.13. The same considerations made for the precedent figures are still valid for this one. Considering the vapour quality of $x = 0{,}9$, a fog flow could be assumed inside the tube. Regarding the temperature profile, with this typology

of flow, there should be almost no variations of temperature difference along with the different radial position because of the high quantity of gas component and consequently, only the gas phase is in touch with the tube wall. But, because of the high value of specific mass flux ($\dot{G} = 600kg/(m^2s)$), the conditions for a flog flow could be not respected and so an annular flow could be assumed inside the tube. This hypothesis can be verified considering the trend of the temperature difference in the different measuring sections. The profile is similar to the ones present for a vapour quality of $x = 0{,}3$, indicating a probable annular flow. As described before, without verification through visual prove or the applications of flow pattern maps is not possible to confirm the hypothesis.

In Figure 5.15 is represented a comparison between the local temperature difference measurements with vapour quality $x = 0{,}3$ and $x = 0{,}9$ for propylene with specific mass flux $\dot{G} = 600kg/(m^2s)$, reduced pressure $p_r = 0{,}25$ and saturation temperature of $24{,}5C$ measured in 2 different measuring sections as a function of the radial position $\phi$. In Figure 5.15 is possible to observe that the temperature difference

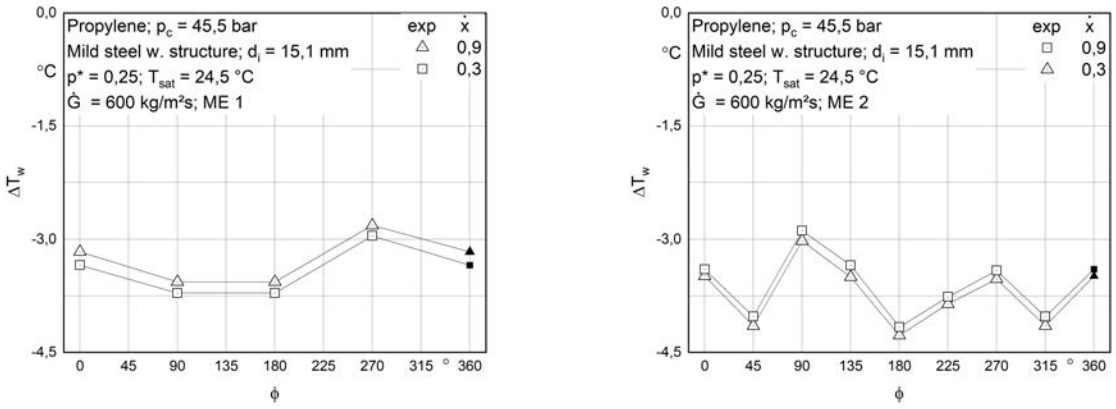


Figure 5.15: Comparison between local temperature difference measurements for propylene with vapour quality $x = 0{,}3$ and $x = 0{,}9$ measured in 2 different measuring section as a function of the radial position $\phi$

profile for different vapour quality in two different measuring sections, present a similar trend. An almost constant offset between the two curves is observable in the two graphs. This indicates that the disturbances in the temperature differences profiles, noticeable in the two middle measuring sections, are not caused by the flow conditions but are characteristics of the tube internal structure. From Figure 5.15 is also possible to notice that as the vapour quality increases, the temperature difference between the wall temperature and the saturation temperature of the propylene

decreases. This phenomena, as described before is due to the reduction of the liquid film thickness and consequently the reduction of the thermal resistance. Comparing the two temperature difference profiles is also possible to observe that there are no differences in terms of flow regime since there is no variation of profile moving from one vapour quality to the other.

### 5.2.2 Pressure drop

In the following section, the results regarding the pressure drop are presented. Figure 5.16 shows the pressure drop, for different specific mass flux, for propylene at reduced pressure $p_r = 0{,}25$ inside a micro-fin tube with inner diameter of $d_i = 15{,}1\,mm$ as a function of the vapour quality $x$. From figure 5.16 is possible to

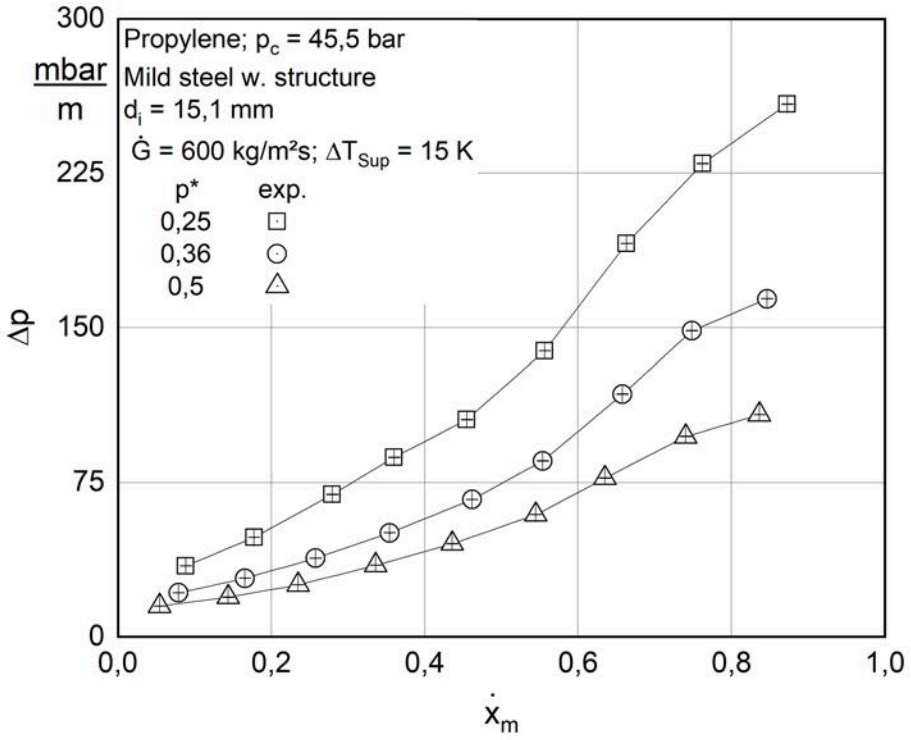


Figure 5.16: Pressure drop, for different specific mass flux, for propylene at reduced pressure $p_r = 0{,}25$ as a function of the vapour quality $x$

observe the increased pressure drop $\Delta p$ as the vapour quality $x$ increases for every specific mass flux $\dot{G}$ measurement series. Is also noticeable that for fixed vapour

quality, the increment of specific mass flux implies a higher pressure drop. Analyzing the trend of the curves in the graph is observable that for vapour quality under 0,5 the increment is linear for every specific mass flux with an increasing slope of the curves for higher mass flow. From vapour quality of approximately 0,5, the inclination of all the curves increases until it reaches a high value of vapour quality, over 0,8 where the gradient of the pressure losses decreases. As the vapour quality $x$ increases, the mean density of the two-phase fluid $\rho_m$ decreases so the overall velocity of the two-phase fluid increases. As a consequence of the fluid velocity increment, the friction between the fluid and the tube wall increases resulting in a higher pressure drop. These phenomena happens until the vapour quality reaches high values (approximately 0,9), after which there is a slight decrease of the pressure losses, so the pressure drop curve, therefore, presents a maximum corresponding to the vapour quality turning point. This behavior is explained by Cavallini et al. [7]: with a high value of vapour quality, the flow pattern tends to be annular and therefore dominates by the tangential force between vapour and liquid film. The shear stress deployed by the vapour phase on the liquid film causes a separation of liquid drops from the liquid phase and the consequent mixing of these drops in the vapour phase. This phenomena cause an increase of the gas-phase density and as consequence a reduction of the vapour velocity that leads to a reduction of pressure drops. In Figure 5.16 is not noticeable the reduction of the pressure drop values since the measured values of vapour quality is lower than 0,9 but is possible to notice the change of gradient in the final section of the pressure drop curves. Consideration should also be given to the fact that as the vapour quality increase, the liquid film thickness decrease resulting in a reduction of the interface liquid roughness [13] from which depends a further reduction of the pressure drop gradient. The increase of pressure drop, for the increasing mass flux considering a fix vapour quality can be explained taking into account the increase of mass flux and the consequent increment of flow velocity that results in higher shear stress on the pipe wall and higher pressure drop.

Figure 5.17 shows the pressure drop, for different reduced pressure, for propylene with specific mass flux $\dot{G} = 600 kg/(m^2 s)$ inside a micro-fin tube with an inner diameter of $d_i = 15{,}1\ mm$ as a function of the vapour quality $x$. Form Figure 5.17 is possible to notice the increasing trend of the pressure drop as the vapour quality raises. It is also observable the higher values of pressure drop, for fixed vapour quality, as the reduced pressure decreases. Comparing Figure 5.16 with 5.17 is noticeable a similarity of the curves trend, with a more accentuated increment of pressure losses for higher reduced pressure compared to the curves with lower specific mass flux. With higher reduced pressure and thus higher inlet pressure, the

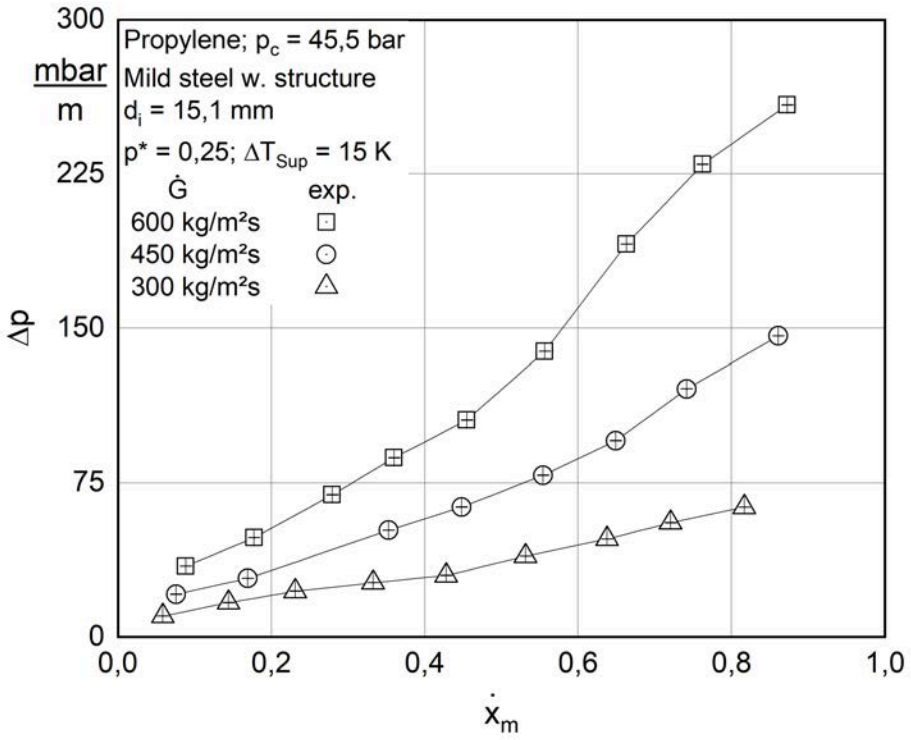


Figure 5.17: Pressure drop, for different reduced pressure, for propylene with specific mass flux $\dot{G} = 600kg/(m^2s)$ as a function of the vapour quality $x$

differences between the liquid and gas phase properties decreases leading to fewer interactions at the phase boundary thus influencing the reduction in pressure drop. The proprieties that influence the two-phase pressure drop are a function of the two-phase fluid pressure. As the pressure of the two-phase mixture increases, at constant temperature, the mean density of the fluid increases leading to a decrease of the flow velocity and so to a lower pressure drop. At the same time, as the pressure and so the temperature increases, lower values of liquid viscosity are measured resulting to further reduction of pressure drop. Furthermore, the density difference between liquid and vapour decreases with higher pressure so the shear stress and frictional pressure drop at phase boundary decrease. From the curve at reduced pressure $p_r = 0{,}5$, is visible the reduction of the increasing gradient in the curve trend leading to a maximum, explainable, as explained before, with the increases of gas-phase density due to liquid drops detached by the gas flow and mix in it.

### Comparison with the correlations for smooth tubes

As reported in the section related to the flow pattern maps, the manufacturer did not provide data on the geometric characteristics of the internal structure of the tubes such as fin height or winding angle. This makes it not possible to apply the correlations and the models for the calculation of pressure losses for structured tubes and consequently it is not possible to make a comparison between the experimental data and the models obtained from the studies found in the literature. For the reasons just presented, an analysis of the increase in pressure drop for the tested structured pipe compared to an equivalent smooth pipe is then performed. To do this, the pressure losses relative to the smooth tube are calculated through the application of correlations developed for smooth tubes obtainable from the literature related to this topic.

Figure 5.18 presents the ratio between the experimental pressure losses and those calculated for the equivalent smooth pipe using Friedel et al. correlation [20] with propylene at the reduced pressure of $p_r = 0{,}25$ for different specific mass flux $\dot{G}$ values. In Figure 5.18 is possible to observe that the ratio of the experimental and smooth tube's pressure losses has a similar trend for all the curves with different reduced pressure. It can be observed that, after an initial phase of instability where there is a small decrease in the ratio values, the curves grow as the experimental pressure drop value increases. Higher values of the ratio can be observed with lower values of reduced pressure.

Figure 5.19 presents the ratio between the experimental pressure losses and those calculated for the equivalent smooth pipe using Müller-Steinhagen et al. correlation [32] with propylene at the reduced pressure of $p_r = 0{,}25$ for different specific mass flux $\dot{G}$ values In Figure 5.19 is observable the increasing trend of the ratio between the experimental pressure drop and the pressure losses calculated for an equivalent smooth tube using the Müller-Steinhagen et al. correlation [32]. As in the Figure 5.18, all the curves present an initial decrease followed by the increment of the ratio values. Comparing Figures 5.18 and 5.19, it can be seen that in the latter, higher values of the ratio of experimental pressure drops to pressure drops for an equivalent smooth pipe can be detected than in the case where the values for the smooth pipe were calculated using the model of Friedel et al. [20]. In the case of reduced pressure $p_r = 0{,}36$, for an experimental pressure drop of $\Delta p_{st,exp} = 28{,}44\ mbar/m$ the ratio, in the case of the application of the Friedel et al. correlation [20], is $\Delta p_{st,exp}/\Delta p_{smooth,calc} = 1{,}48$ while in the case of application of the Müller-Steinhagen et al. correlation [32] the ratio is

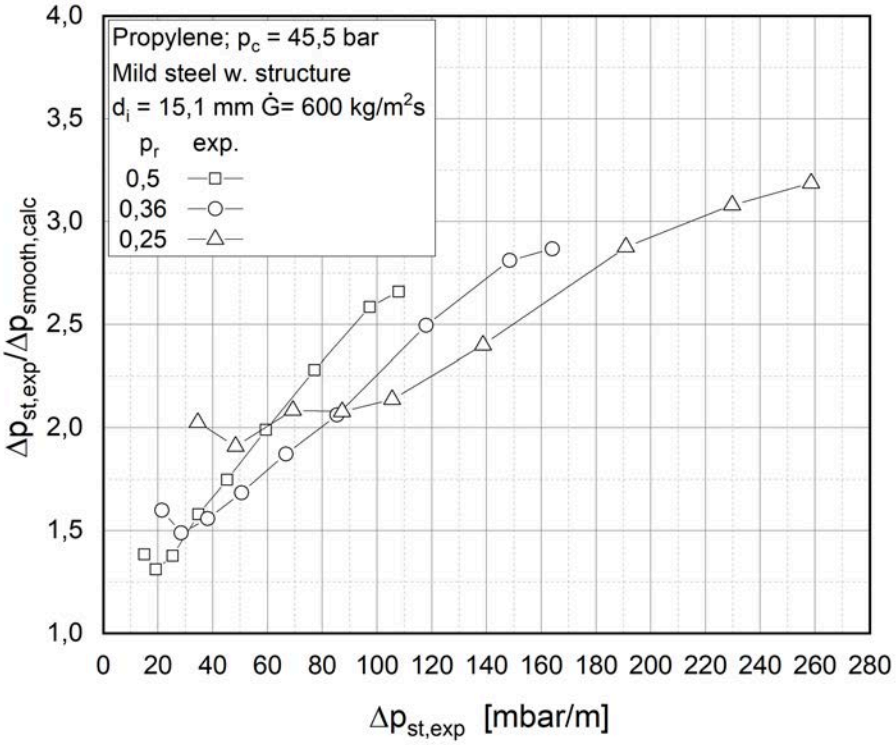


Figure 5.18: Ratio between experimental pressure losses and smooth tube's pressure drop calculated with Friedel et al. correlation [20] for different reduced pressure $p_r$

$\Delta p_{st,exp}/\Delta p_{smooth,calc} = 1{,}85$.

Figure 5.20 shows the trend in the ratio of experimental pressure drop to pressure drop for an equivalent smooth pipe, calculated using the Friedel et al. [20] correlation, as a function of vapor quality for for different values of reduced pressure $p_r$. In Figure 5.20 it is possible to observe how the curves present an initial unstable trend for low vapour quality values while subsequently all the curves present an increasing trend of the ratio between the experimental pressure drops and the pressure drops for an equivalent smooth pipe, calculated through Friedel's correlation [20]. It is also possible to notice that the curves with lower values of reduced pressure presents higher values of the ratio between the experimental and the smooth tubes values. As the pressure increase, the mean density of the two-phase fluid increase and, as explained before, the velocity decreases accordingly resulting in lower pressure loss in both micro-fin and smooth tubes. From the figure it is possible to observe a plateau present in all curves for high values of the vapor content, above 0.8. This

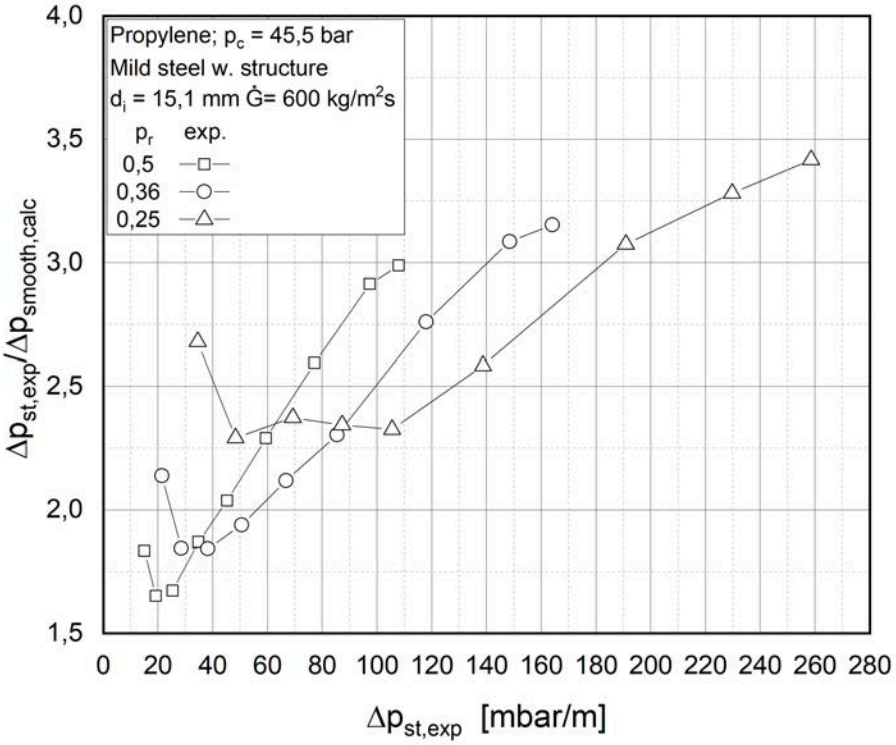


Figure 5.19: Ratio between experimental pressure losses and smooth tube's pressure drop calculated with Müller-Steinhagen et al.'s correlation [32] for different reduced pressure $p_r$

is due to the fact that, as already presented in figure 5.16, pressure drops increase until they reach a maximum after which a decrease in pressure drops is observed due to the detachment of liquid drops from the liquid phase that, mixing with the gas phase, cause an increase in the density of the latter reducing its velocity and consequently the pressure drops. Since this phenomenon occurs for both structured and smooth pipes, the curve will see a flattening.

Figure 5.21 shows the trend in the ratio of experimental pressure drop to pressure drop for an equivalent smooth pipe, calculated using the Friedel et al. [20] correlation, as a function of vapor quality for for different values of mass flux $\dot{G}$. In Figure 5.21 is observable that the curves present a similar trend to the ones presented in figure 5.20. As the vapour quality increase, after an initially unstable trend, an increment of the ratio values is noticeable. After a vapour quality of 0,4,

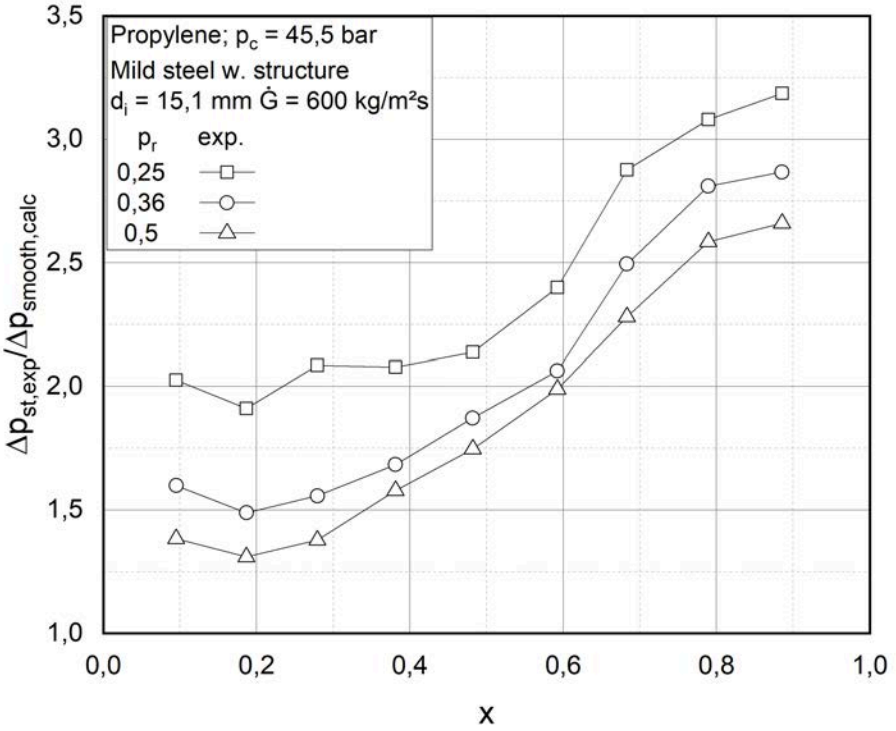


Figure 5.20: Ratio between experimental pressure losses and smooth tube's pressure drop calculated with Friedel's correlation [20] for different reduced pressure $p_r$ as a function of vapour quality

the grow of the curves is undisturbed. This trend could be explained by considering that as the vapor content increases, the velocity of the two-phase mixture increases as a result of the decrease in average density. The increase in velocity within the pipe causes an increase in pressure drop in both the case of a structured and smooth pipe. The increase in the ratio values are due to the fact that in the case of a structured pipe the increase in pressure losses is not linear, as can be seen in figures 5.16, while in the case of a smooth pipe, calculating the values for pressure losses for an equivalent smooth pipe, i.e. with an internal diameter equal to the diameter relative to the tip of the internal fins, a linear increase in pressure losses is observed. It is also observable that higher values of specific mass flux $\dot{G}$ result in higher values of the ratio between the experimental pressure losses and the pressure drop calcualted for an equivalent smooth tube using the correlation of Friedel et al. [20].

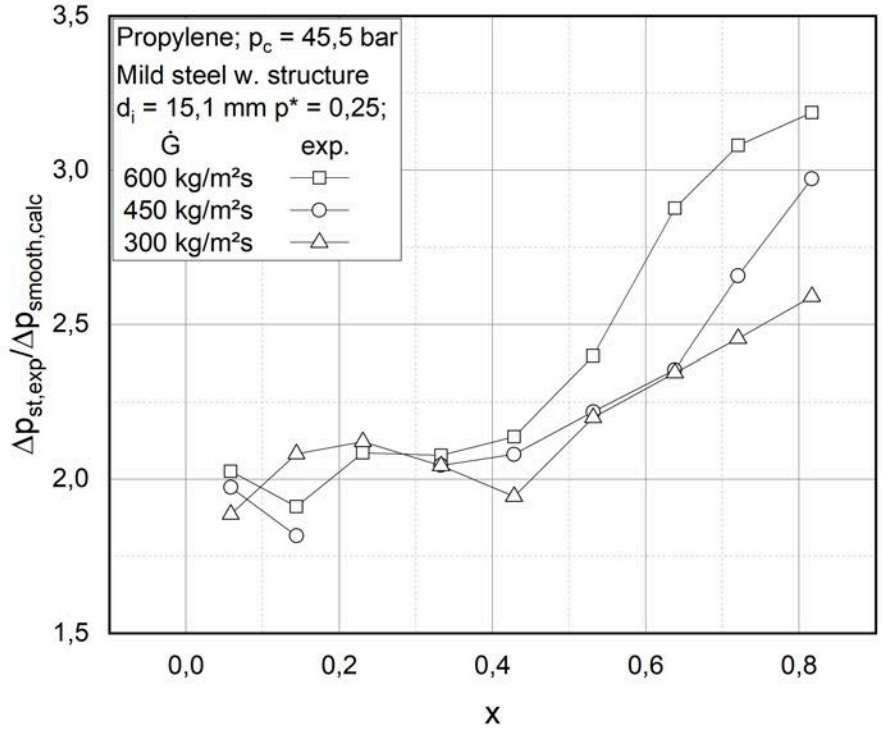


Figure 5.21: Ratio between experimental pressure losses and smooth tube's pressure drop calculated with Friedel et al.'s correlation [20] for different specific mass flux $\dot{G}$ as a function of vapour quality

### 5.2.3 Heat transfer coefficient

In the following section, the results regarding the heat transfer coefficient are presented. Figure 5.22 shows the heat transfer coefficient, for different specific mass flux, for propylene at reduced pressure $p_r = 0{,}25$ inside a micro-fin tube with inner diameter of $d_i = 15{,}1\ mm$ as a function of the vapour quality $x$. In Figure 5.22 is noticeable the increasing trend of the heat transfer coefficient $\alpha$ as the vapour quality $x$ increase. For a defined steam content, higher values of heat transfer coefficient are measured with higher specific mass flux $\dot{G}$. It is also observable that the curves, for higher values of specific mass flux such as $\dot{G} = 450\ kg/(m^2 s)$ and $\dot{G} = 600\ kg/(m^2 s)$, are similar in absolute value and trend while the curve with lower specific mass flux ($\dot{G} = 300 kg/(m^2 s)$) has a noticeable offset. Regarding the curves with higher mass flux values, is observable that the measured points are similar for vapour quality under 0,6, after which is noticeable a separation between

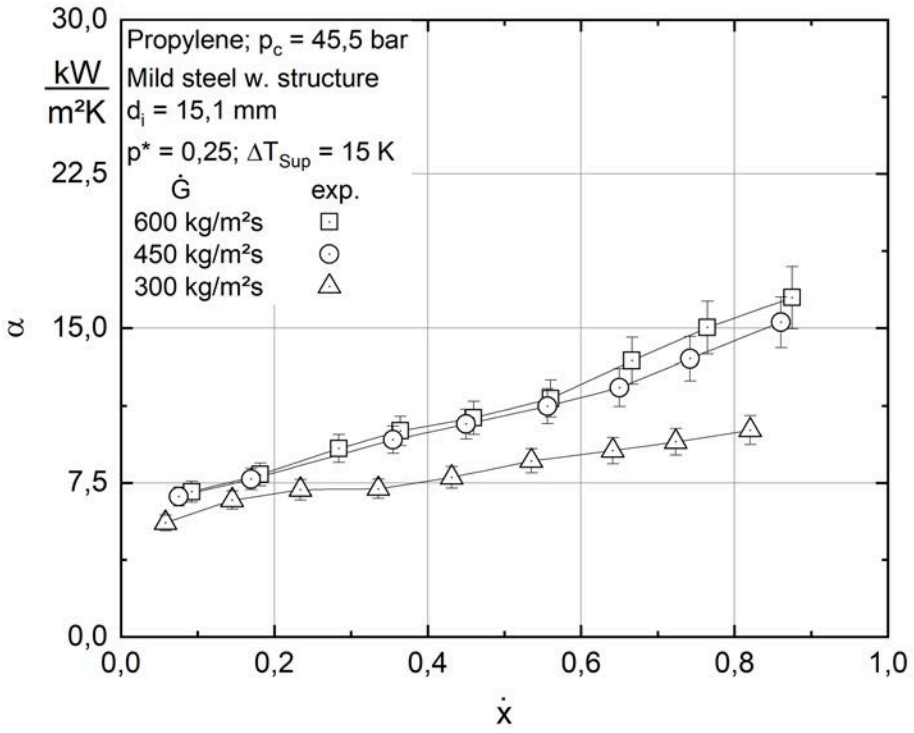


Figure 5.22: Heat transfer coefficient, for different specific mass flux, for propylene at reduced pressure $p_r = 0{,}25$ as a function of the vapour quality $x$

the two curves trend. The increasing trend of the heat transfer coefficient when the vapour quality increment can be explained considering that as the steam content raise, the flow velocity increase and so consequently the Reynolds number of the vapour flow. As a consequence of this increment, the convective heat transfer between the liquid and the gas phase is improved resulting in a higher heat transfer coefficient [39]. In their study, Kedzierski and Goncalves [26] explained how low Reynolds number flows may be enhanced more than high Reynolds number flows due to a reduction in the size of the turbulent eddies at the wall by the interaction of the flow with the fins. Smaller eddies transfer momentum more efficiently than larger eddies. Another reason for the increasing trend of the heat transfer coefficient with increasing vapour quality is the change of flow pattern. As the vapour content increase and the velocity of the gas phase raise, annular flow is established so the thermal resistance of the liquid film is reduced due to its reduced thickness and the condensation at the phase boundary improve [39]. Considering the curves in Figure 5.22, the higher values of heat transfer coefficient with higher specific

mass flux are due to an increment of the velocity of both phases resulting so in an increased level of turbulence and in an increase of heat transfer during condensation. With low values of vapour quality, the increase of specific mass flux results in an improvement of the convective heat transfer due to the cross-mixing with the core flow. Considering the graph, for low vapour quality, the curves with different specific mass flux present a similar value of heat transfer coefficient. This can be explained considering that for low values of vapour quality the fins are flooded by the condensate so there is a limited exchange surface is exposed to the gas phase on which the surface tension drainage can acts. In this situation, the heat transfer mechanism is the same as the one acting on a plain tube [48]. For higher values of vapour quality, the surface tension induces pressure gradients that acts to drain the condensate into the concave channel between the fins. Surface drainage force provides an additional condensing enhancement which adds to the effects provided by the vapour shear at high values of vapour quality.

Figure 5.23 shows the heat transfer coefficient, for different reduced pressure, for propylene with specific mass flux $\dot{G} = 600 kg/(m^2 s)$ inside a micro-fin tube with inner diameter of $d_i = 15{,}1\ mm$ as a function of the vapour quality $x$. In Figure 5.23 is noticeable the increasing trend of the heat transfer coefficient as the vapour quality increase. Is also possible to observe that for vapour quality under 0,6 there is no noticeable difference between heat transfer coefficient values with different reduced pressure while for higher values, is possible to notice that lower reduced pressure corresponds to slightly superior values of heat transfer coefficient compared to the curve with higher reduced pressure. The increasing values of the heat transfer coefficient as the reduced pressure decrease is because the fluid proprieties such as density, viscosity and enthalpy of vaporization are a function of the reduced pressure and have an influence on the flow pattern and heat transfer in the flow. At low reduced pressure, higher gas phase velocity is observable resulting in an increased heat transfer coefficient because of the increased turbulence in the flow and increased wettability of the liquid phase on the pipe wall. According to the Nusselt theory, lower reduced pressure leads to higher heat transfer coefficient values during condensation since larger heat flow $\dot{Q}$ can be supplied to the liquid due to higher enthalpy of vaporization. A similar trend of the curves, besides for small deviation with a high value of vapour quality, is explainable considering that the change of reduced pressure influences the fluid proprieties. But since the diameter of the micro-fin tube tested is modest and the curves presented are measured with a high specific mass flux ($\dot{G} = 600\ kg/(m^2 s)$) and so the overall flux has a high velocity, the change of proprieties has a limited influence on the heat transfer. The only noticeable difference is observable with high vapour quality values because the

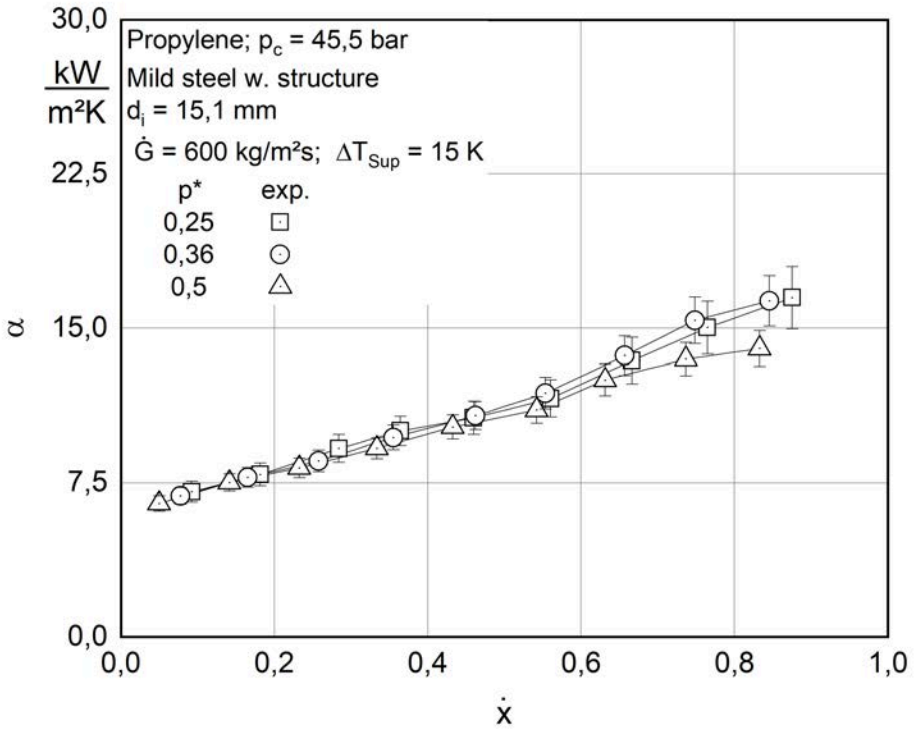


Figure 5.23: Heat transfer coefficient, for different reduced pressure, for propylene with specific mass flux $\dot{G} = 600kg/(m^2s)$ as a function of the vapour quality $x$

change of gas-phase proprieties is bigger compared to the change of liquid phase proprieties with increasing reduced pressure. Comparing the graphs presented in Figure 5.22 and Figure 5.23, is observable that the change of specific mass flux has a bigger impact on the heat transfer coefficient compared to the change of reduced pressure.

In the following figures the local measurement of temperature and heat transfer coefficient are presented. These data are measured through the usage of thermocouples sensors glued in specific groves located on the external wall of the inner tube of the test section as explained in the chapter related to the experimental setup. The local measurements is a key feature of the test plant since allow to have an improved control on the condensation parameters and characteristics along the test tube, allowing to have higher precision of the measured data and resulting in an increased reliability of the calculation for the tested tube thermal performances. The availability of local data allow also to observe the influence of the micro-fin

structure, analyzing the trend of the temperature difference and the heat transfer coefficient in the different radial positions for every measurement section.
Figure 5.24 presents the measured values of the local heat transfer coefficient calculated in all 4 measuring sections situated on the test tube, for propylene with a reduced pressure of $p_r = 0{,}25$ and specific mass flux of $\dot{G} = 600kg/(m^2s)$ as a function of the radial position. In Figure 5.25 is shown the local temperature difference between the saturation temperature of the propylene at the conditions of reduced pressure $p_r = 0{,}25$ and the temperature measured by the thermocouples inserted in the test tube for all 4 of the measuring sections situated on the test section with a specific mass flux of $\dot{G} = 600kg/(m^2s)$ as a function of the radial positions.

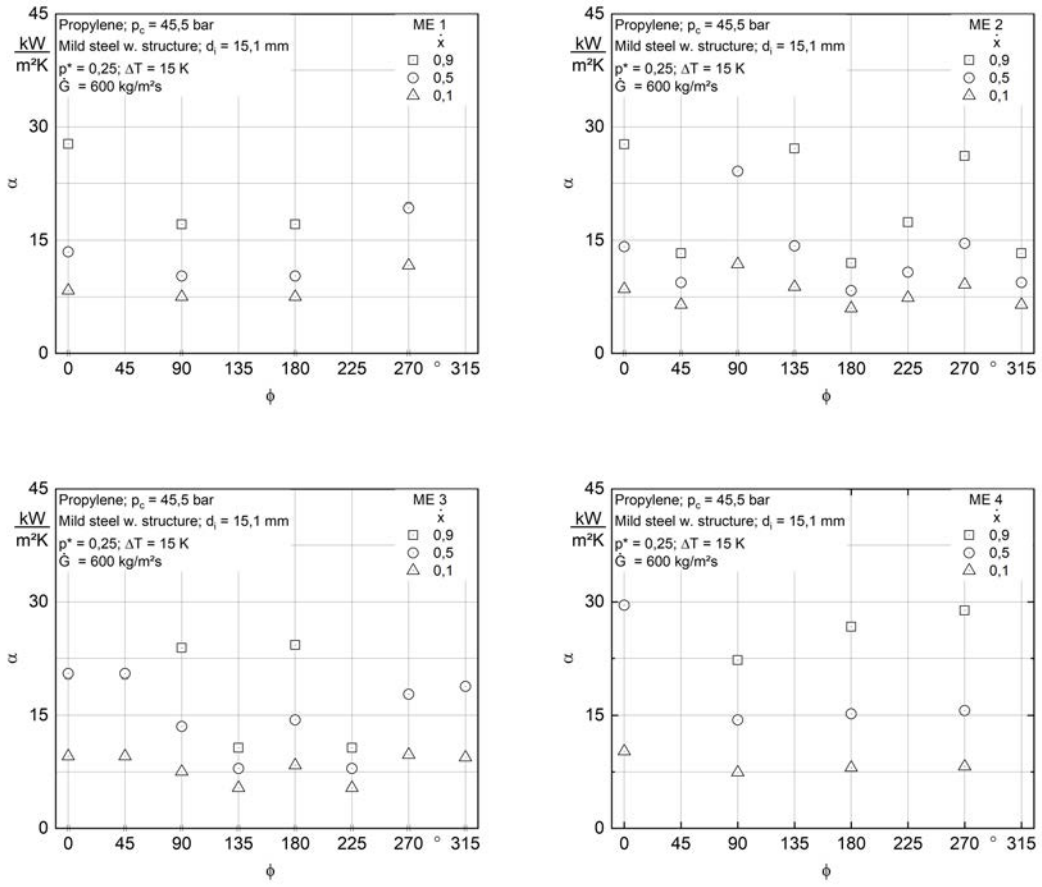


Figure 5.24: Local heat transfer coefficient for propylene with specific mass flux $\dot{G} = 600kg/(m^2s)$ for 3 different vapour quality measured in every measuring section as a function of the radial positions $\phi$

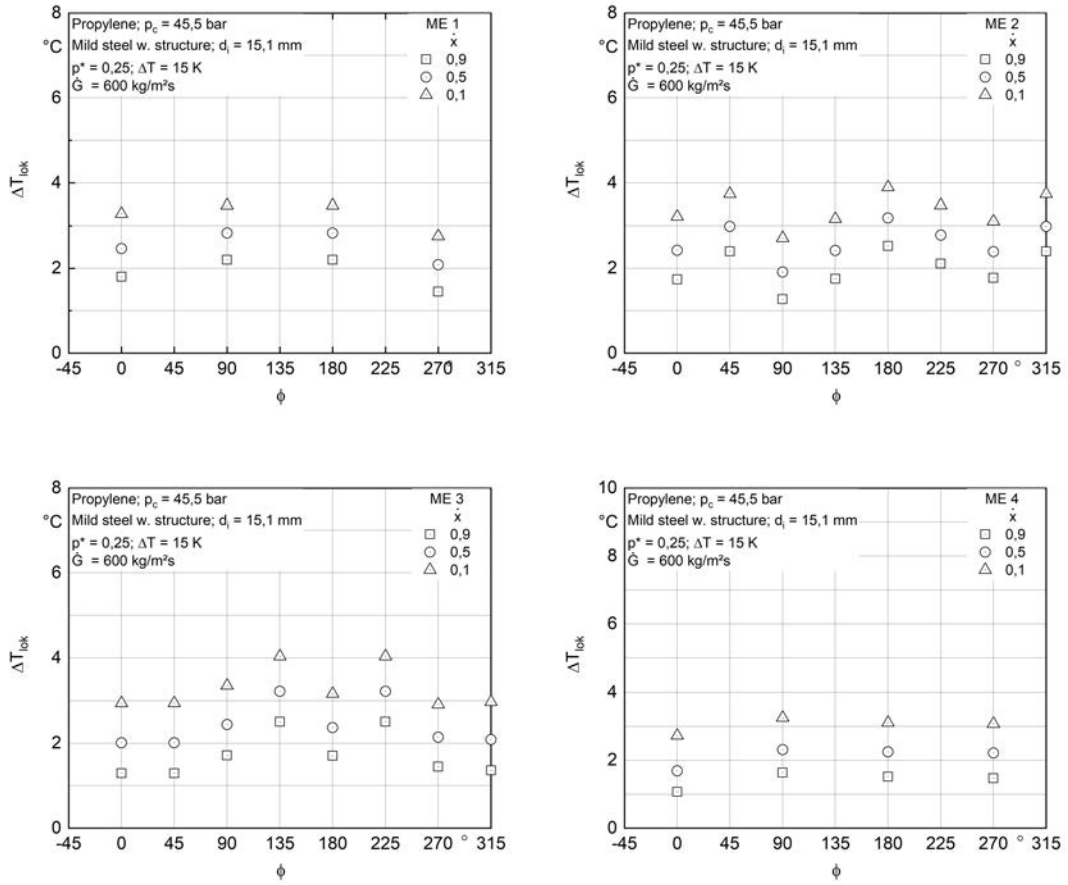


Figure 5.25: Local temperature difference measurement for propylene with specific mass flux $\dot{G} = 600kg/(m^2s)$ for 3 different vapour quality measured in every measuring section as a function of the radial positions $\phi$

From Figure 5.24 is observable that, in every measurement section, the local heat transfer coefficient increase with the increment of the vapour quality. This behaviour confirms the trend observable for the mean heat transfer coefficient in Figure 5.22 and Figure 5.23. The increasing trend of the heat transfer coefficient can be attributed, among other factors explained before, to the change of flow forms at different vapour quality. It is also possible to observe that, for every vapour quality measurement series, moving from one measuring section to the following one, an increase of the heat transfer coefficient is observable. This can be explained considering that moving from inlet to the outlet of the tube, the vapour title decrease so the gas phase velocity increases resulting in higher values of heat transfer coefficient. In both figure 5.24 and 5.25, data are presented for tests performed with different vapour quality to cover the entire range of variability of the steam

content and so of the possible flow forms. In Figure 5.25 is observable that, in every measurement section, the temperature difference between the wall temperature and the saturation temperature of the propylene decrease with the increase of the vapour quality. Analyzing the series of graphs relate to the temperature difference, from measuring section 1 to measuring section 4, is possible to notice the decreasing trend of the temperature difference $\Delta T$ as the fluid condenses for every vapour quality measurement series. This is because for every test carried out, the vapour quality difference between the inlet and the outlet of the test section is limited for having more reliable data regarding the mean values but as the condensation proceeds, more liquid phase is presents and so there is an effect on the values of temperature difference. Also, this confirms the precedent affirmation regarding the decreasing of temperature difference with the increasing vapour quality. It is also possible to notice that, in every measurement section, the temperature difference values in every radial position have the same offset and the same trend between values with different vapour quality. Regarding the heat transfer coefficient. it is instead noticeable a bigger offset between the values of the measuring series of vapour quality $x = 0{,}9$ and $x = 0{,}5$ compared to the offset between the measurement series of vapour quality $x = 0{,}5$ and $x = 0{,}1$. This could be due to a change of flow pattern inside the tube, changing between a stratified flow with low values of vapour quality like $x = 0{,}1$, to an annular flow with values of vapour quality of $x = 0{,}3 - 0{,}7$ and finally to a fog flow with high values of vapour quality like $x = 0{,}8 - 0{,}9$. This hypothesis can not be verified since in the test section there isn't the possibility to visualize the flow patterns.

### Comparison with the correlations for smooth tubes

As reported in the section related to the flow pattern maps, the manufacturer did not provide data on the geometric characteristics of the internal structure of the tubes such as fin height or winding angle. This makes it not possible to apply the correlations and the models for the calculation of pressure losses for structured tubes and consequently it is not possible to make a comparison between the experimental data and the models obtained from the studies found in the literature. For the reasons just presented, an analysis of the increase in heat transfer coefficient for the tested structured tube compared to an equivalent smooth tube is then performed. To do this, the heat transfer coefficients relative to the smooth tube are calculated through the application of correlations developed for smooth tubes obtainable from the literature related to this topic.

Figure 5.26 presents the ratio between the experimental heat transfer coefficient and those calculated for the equivalent smooth pipe using Cavallini et al. correlation [10] with propylene at the reduced pressure of $p_r = 0{,}25$ for different specific mass flux $\dot{G}$ values In Figure 5.26 it can be observed how the ratio between the

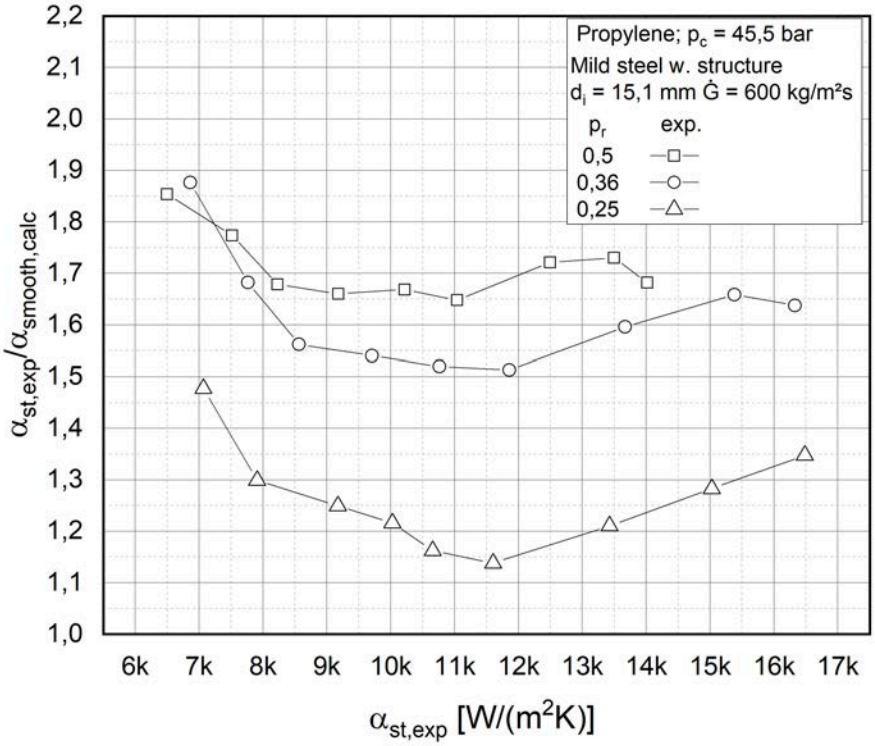


Figure 5.26: Ratio between experimental heat transfer coefficient and smooth tube's heat transfer coefficient calculated with Cavallini et al. correlation [10] for different reduced pressure $p_r$

experimental heat transfer coefficient and that calculated for an equivalent smooth tube through the correlation developed by Cavallini et al. [10] for smooth tubes, presents a trend with a minimum observable for intermediate heat transfer coefficient values. It is also possible to observe that higher values of the ratio are calculated with higher values of reduced pressure.

Figure 5.27 presents the ratio between the experimental heat transfer coefficient and those calculated for the equivalent smooth pipe using Shah et al. correlation [39] with propylene at the reduced pressure of $p_r = 0{,}25$ for different specific mass flux $\dot{G}$ values In Figure 5.27 it can be observed that the trend of the curves is similar to

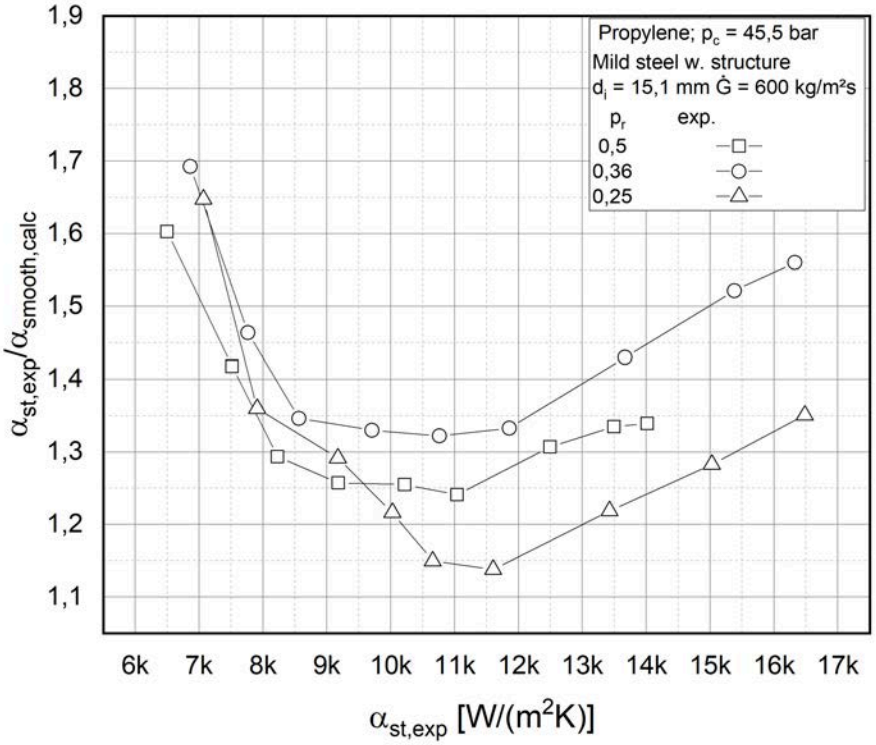


Figure 5.27: Ratio between experimental heat transfer coefficient and smooth tube's heat transfer coefficient calculated with Shah et al. correlation [39] for different reduced pressure $p_r$

the curves presented in Figure 5.26. It is also possible to notice that, unlike the others correlations, using the model developed by Shah et al. [39] for smooth tube, the highest values of ratio between the experimental heat transfer coefficient and that calculated for an equivalent smooth tube, are obtained with intermediate reduced pressure values. This is due to the fact that using the correlation of Shah, the curves related to the reduced pressure $p_r = 0{,}5$ presents lower values of the ratio between heat transfer coefficient compared to the case presented in Figure 5.26. The values obtained regarding the ratio of heat transfer coefficients using the correlations of Cavallini et al. or Shaha et al. for calculating the heat transfer coefficients in the equivalent smooth tube, are similar for the curves of reduced pressure $p_r = 0{,}25$ and $p_r = 0{,}36$. In the case of reduced pressure $p_r = 0{,}25$ and experimental heat transfer coefficient $\alpha_{st,calc} = 10025\ W/(m^2K)$, the value of the ratio between the experimental heat transfer coefficient and the heat transfer coefficient calculated with the correlation of Shah et al. [39] is $\alpha_{st,calc}/\alpha_{smooth,exp} = 1{,}216$ while using

the correlation of Cavallini et al. [10] the value is $\alpha_{st,calc}/\alpha_{smooth,exp} = 1{,}221$.

Figure 5.28 presents the ratio between the experimental heat transfer coefficient and those calculated for the equivalent smooth pipe using Thome et al. correlation [46] with propylene at the reduced pressure of $p_r = 0{,}25$ for different specific mass flux $\dot{G}$ values In Figure 5.28 it can be observed that the trend of the curves is

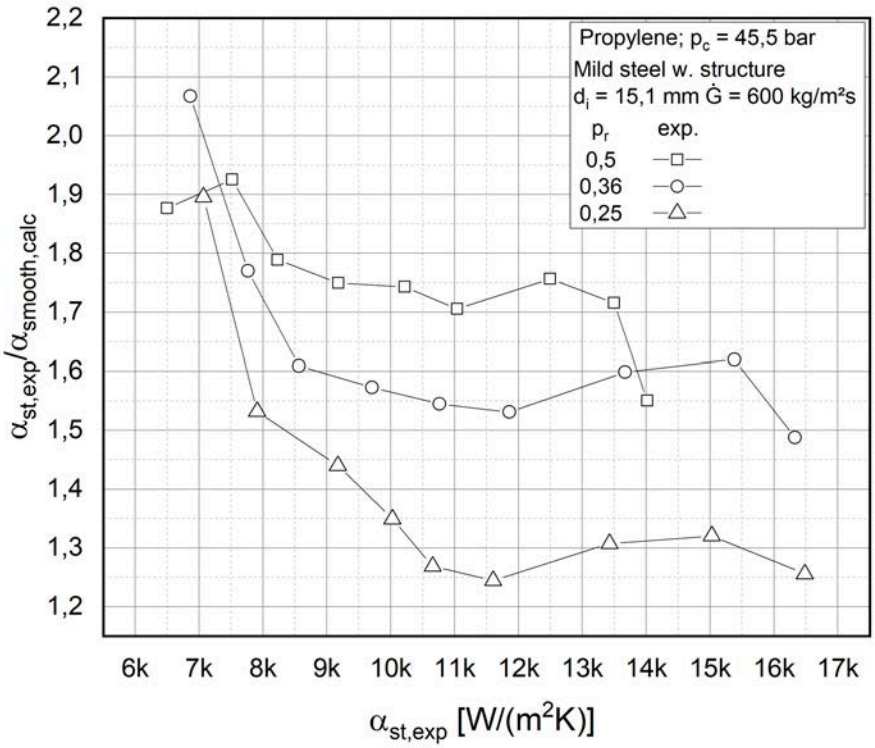


Figure 5.28: Ratio between experimental heat transfer coefficient and smooth tube's heat transfer coefficient calculated with Thome et al. correlation [46] for different reduced pressure $p_r$

similar to the curves presented in Figure 5.26 and Figure 5.27. The values obtained regarding the ratio of heat transfer coefficients using the correlations of Thome et al. [46] for calculating the heat transfer coefficients in the equivalent smooth tube are slightly bigger compared to the values presented in the previous two figures. In the case of reduced pressure $p_r = 0{,}25$ and experimental heat transfer coefficient $\alpha_{st,calc} = 10025\ W/(m^2K)$, the value of the ratio between the experimental heat transfer coefficient and the heat transfer coefficient calculated with the correlation of Thome et al. [46] is $\alpha_{st,calc}/\alpha_{smooth,exp} = 1{,}349$ while using the correlation of

Cavallini et al. [10] the value is $\alpha_{st,calc}/\alpha_{smooth,exp} = 1{,}221$.

Figure 5.29 shows the trend of the ratio between the experimental heat transfer coefficient drop and the heat transfer coefficient for an equivalent smooth pipe, calculated using the Cavallini et al. [10] correlation, as a function of vapor quality for for different values of reduced pressure $p_r$. In Figure 5.29 it can be observed

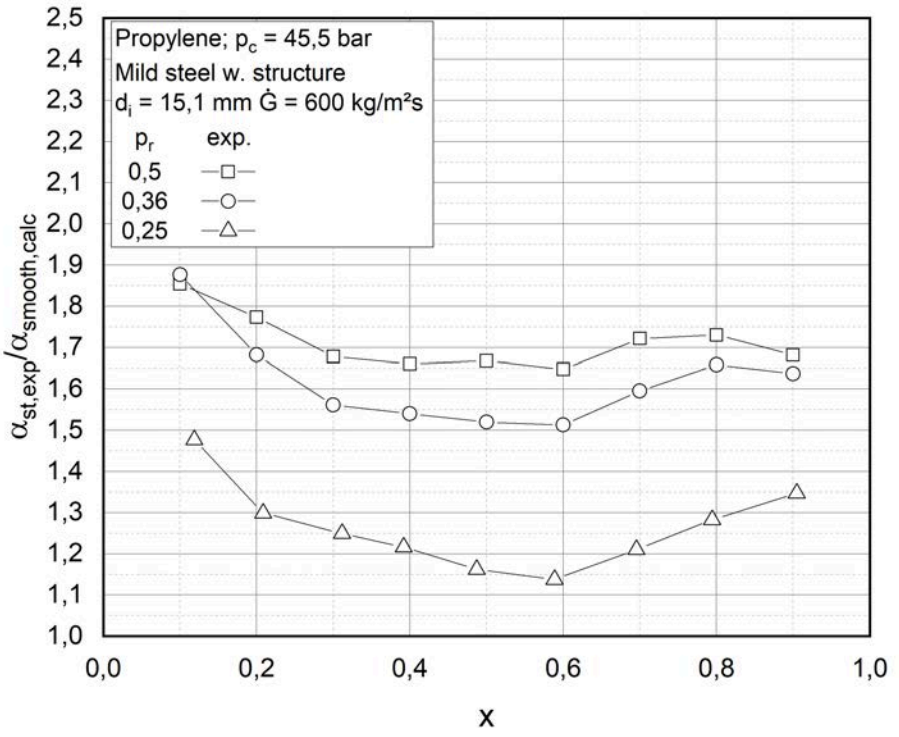


Figure 5.29: Ratio between experimental pressure losses and smooth tube's pressure drop calculated with Shah et al. correlation [39] for different reduced pressure $p_r$ as a function of vapour quality

that all the curves show a trend with a minimum at intermediate vapour quality, between $x = 0{,}4$ and $x = 0{,}6$. It can also be noted how the curves for lower reduced pressure values correspond to higher values of the ratio of the experimental heat transfer coefficient to the heat transfer coefficient calculated for an equivalent smooth tube through the correlation of Cavallini et al. [10]. The enhancement of heat transfer at high vapour quality, and the consequently increase of ratio values, is due to the fact that with a thin liquid film on the surface of the tube, the fins are very effective at mixing the liquid-vapour interface due to their proximity tot

he liquid-vapour interface. Another additional enhancement factor at high vapour quality is the surface-tension drainage forces on the fins top [26]. At low vapor counts, the increase in heat transfer for the structured tube is due to the increased heat transfer surface resulting from the presence of the fins.

Figure 5.30 shows the trend of the ratio between the experimental heat transfer coefficient drop and the heat transfer coefficient for an equivalent smooth pipe, calculated using the Cavallini et al. [10] correlation, as a function of vapor quality for for different values of mass flux $\dot{G}$. In Figure 5.30 is possible to observed a similar trend of the curves as the ones presented in Figure5.29 with the exception of the specific mass flux curve of $\dot{G} = 300\ kg/(m^2K)$.

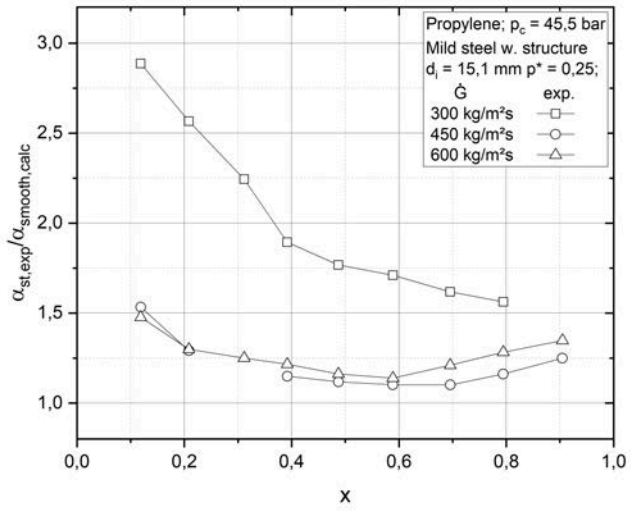


Figure 5.30: Ratio between experimental pressure losses and smooth tube's pressure drop calculated with Shah et al. correlation [39] for different specific mass flux $\dot{G}$ as a function of vapour quality

# Chapter 6

# CONCLUSIONS

In the present work, the single-phase and two-phase pressure loss and heat transfer during flow condensation with propylene as test substance in a horizontal micro-fin pipe were experimentally investigated. The work aim was to investigate the performance of a micro-fin tube in terms of pressure loss and heat transfer during single-phase gas cooling flow and two-phase condensing flow. A counterflow double-tube heat exchanger was used as a measuring section. An extensive review of the literature regarding single-phase and two-phase flow was compiled. Regarding the two-phase flow, the flow patterns of Taitel and Duckler [45], Breber et al. [3], Steiner et al [42] and Kattan et al. [25] were presented. For the two-phase pressure loss, the models of Friedel [20], Müller- Steinhagen and Heck [32], Cavallini et al. [8] and Chisholm et al. [13] were presented for smooth tubes and for structured pipes the models of Kedzierski and Goncalves [26] and Cavallini et al. [8] were described. For the calculation of the two-phase heat transfer coefficient, the correlations for smooth tubes of Cavallini et al [10], Shah et al. [39], Thome et al. [46] and Dobson and Chato [17] were explained and for the structured tubes the models of Cavallini et al. [5], Kedzierski and Goncalves [26] and Shikazono et al. [40]were presented. The test section was equipped with sensors to measure pressure and temperature and integrated into a test rig that precisely adjusted parameters such as the steam content and the volume flow. In the single-phase tests, superheated propylene steam with pressures between 11,4 $bar$ and 27 $bar$, inlet temperatures between 70 $°C$ and 74 $°C$ and Reynolds numbers of 500,000-800,000 was investigated. Measurements for two-phase heat transfer were carried out at pressures between 11,38 and 22,75 $bar$, mass flow densities of $300 - 600\ kg/(m^2 s)$ and a flow steam content of $0.1 - 0.9$. Regarding the single-phase experimental results pressure loss, heat transfer coefficient, penalty factor and enhancement factor were presented as a function of the reduced pressure $p_r$. The results confirm the trend reported in the

studies found in the open literature such as the one of Celen et al. [12] and Li et al. [29]. For the two-phase tests, the pressure loss and heat transfer were reported as a function of the reduced pressure $p_r$ and the specific mass flux $\dot{G}$ via the vapour quality $x$. Increasing the steam content and the mass flow density causes more friction at the phase boundary and on the pipe wall due to higher fluid velocities. The reduced pressure influence the two-phase pressure loss in that an increase in pressure drop was observed for smaller reduced pressure. Due to the increasing density or viscosity difference between vapour and liquid, turbulence occurs at a lower pressure, more interactions take place at the phase boundary so that the friction pressure loss increases as a result. Due to the fact that the information regarding the geometrical characteristics of the internal structure of the tested pipes was not available, no comparison with the previously presented models was possible. An analysis regarding the increase of pressure losses for the tested pipes compared to a smooth pipe was performed by calculating the pressure losses of the latter through the models developed for smooth pipes. The analysis showed an increase in pressure drop for the tested pipe compared to an equivalent smooth pipe, varying depending on the test conditions, but with a minimum ratio of 1,31 to a maximum of 3,42. The two-phase heat transfer coefficient was shown for different reduced pressure and mass flux as a function of the vapour quality. An enhanced heat transfer when increasing vapour quality was observed. An analysis regarding the increase in heat transfer coefficient of the tested tube compared to an equivalent smooth tube was performed. Calculation of the heat transfer coefficient for the smooth tube was performed using the correlations developed for smooth tubes. The analysis resulted in an increase in heat transfer coefficient with respect to an equivalent smooth tube varying according to test conditions but with a minimum ratio of 1,1 to a maximum of 2,88. Further investigations may compare the experimental results with models developed for micro-fin tubes and execute a research on the actual flow pattern inside the pipe verifying it through the use of a glass tube and an integrated special camera.

# Bibliography


[1] Bonacina C.; Cavallini A.; Mattarolo L.;. *Trasmissione del calore*. Padua, 1992.

[2] B.Pierre. No Flow resistance with boiling refrigerants. *ASHRAE Journal*, 6:58–65, 1964.

[3] G. Breber, J. W. Palen, and J. Taborek. Prediction of horizontal tube-side condensation of pure components using flow regime criteria. 102(August 1980):471–476, 1979.

[4] A. Cavallini, G. Censi, D. Del Col, L. Doretti, G. A. Longo, L. Rossetto, and C. Zilio. Condensation inside and outside smooth and enhanced tubes -a review of recent research. *International Journal of Refrigeration*, 26(4):373–392, 2003.

[5] A. Cavallini, D. Del Col, L. Doretti, G. A. Longo, and L. Rossetto. New computational procedure for heat transfer and pressure drop during refrigerant condensation inside enhanced tubes. *Journal of Enhanced Heat Transfer*, 6(6), 1999.

[6] A. Cavallini, D. Del Col, L. Doretti, G. A. Longo, and L. Rossetto. Heat transfer and pressure drop during condensation of refrigerants inside horizontal enhanced tubes. *International Journal of Refrigeration*, 23(1):4–25, 2000.

[7] A. Cavallini, D. Del Col, M. Matkovic, and L. Rossetto. Frictional pressure drop during vapour-liquid flow in minichannels: Modelling and experimental evaluation. *International Journal of Heat and Fluid Flow*, 30(1):131–139, 2009.

[8] Alberto Cavallini, Giuseppe Censi, Davide Del Col, Luca Doretti, Giovanni A. Longo, and Luisa Rossetto. Condensation of halogenated refrigerants inside smooth tubes. *HVAC and R Research*, 8(4):429–451, 2002.

[9] Alberto Cavallini, Giuseppe Censi, Davide Del Col, Luca Doretti, Giovanni Antonio Longo, Luisa Rossetto, and Claudio Zilio. Experimental heat transfer coefficient and pressure drop during condensation of R22 and R407C inside a horizontal microfin tube. 2019.

[10] Alberto Cavallini, Davide Del Col, Luca Doretti, Marko Matkovic, Luisa Rossetto, Claudio Zilio, and Giuseppe Censi. Condensation in horizontal smooth tubes: A new heat transfer model for heat exchanger design. *Heat Transfer*

*Engineering*, 27(8):31–38, 2006.

[11] R. Cavallini, A., Zecchin. A dimensionless correlation for heat transfer in force convection condensation. *Int. Heat. Transf. Confer.*, 2:309–313, 1974.

[12] Ali Celen, Ahmet Selim Dalkilic, and Somchai Wongwises. Experimental analysis of the single phase pressure drop characteristics of smooth and microfin tubes. *International Communications in Heat and Mass Transfer*, 46:58–66, 2013.

[13] D. Chisholm. Pressure gradients due to friction during the flow of evaporating two-phase mixtures in smooth tubes and channels. *International Journal of Heat and Mass Transfer*, 16(2):347–358, 1973.

[14] Jacqueline Biancon Copetti, Mario Henrique Macagnan, Daiana De Souza, and Rejane De Césaro Oliveski. Experiments with micro-fin tube in single phase. *International Journal of Refrigeration*, 27(8):876–883, 2004.

[15] A. S. Dalkilic and S. Wongwises. Intensive literature review of condensation inside smooth and enhanced tubes. *International Journal of Heat and Mass Transfer*, 52(15-16):3409–3426, 2009.

[16] F. W. Dittus and L. M.K. K Boelter. Heat transfer in automobile radiators of the tubular type. *International Communications in Heat and Mass Transfer*, 12(1):3–22, 1985.

[17] M. K. Dobson and J. C. Chato. Condensation in smooth horizontal tubes. *Journal of Heat Transfer*, 120(1):193–213, 1998.

[18] L. Doretti, C. Zilio, S. Mancin, and A. Cavallini. Condensation flow patterns inside plain and microfin tubes: A review. *International Journal of Refrigeration*, 36(2):567–587, 2013.

[19] J. El Hajal, J. R. Thome, and A. Cavallini. Condensation in horizontal tubes, part 1: Two-phase flow pattern map. *International Journal of Heat and Mass Transfer*, 46(18):3349–3363, 2003.

[20] L Friedel. Improved friction pressure drop correlations for horizontal and vertical two phase pipe flow. *3R international,*, 18:485–491, 1979.

[21] Volker Gnielinski. Neue Gleichungen für den Wärme- und den Stoffübergang in turbulent durchströmten Rohren und Kanälen. *Forschung im Ingenieurwesen*, 41(1):8–16, 1975.

[22] Kimura H. Ito M. Boiling heat transfer and pressure drop in internal spiral-grooved tubes. *Bull JSME*, 22:1251–1257, 1979.

[23] H. Jaster and P. G. Kosky. Condensation heat transfer in a mixed flow regime. *International Journal of Heat and Mass Transfer*, 19(1):95–99, 1976.

[24] Michael K. Jensen and Alex Vlakancic. Experimental investigation of turbulent heat transfer and fluid flow in internally finned tubes. *International Journal of Heat and Mass Transfer*, 42(7):1343–1351, 1999.

[25] N. Kattan, J. R. Thome, and D. Favrat. Flow boiling in horizontal tubes: Part 1-development of a diabatic two-phase flow pattern map. *Journal of Heat Transfer*, 120(1):140–147, 1998.

[26] M. A. Kedzierski and J. M. Goncalves. Horizontal convective condensation of alternative refrigerants within a micro-fin tube. *Journal of Enhanced Heat Transfer*, 6(2):161–178, 1999.

[27] P. K. Konakov. New Correlation fort he Friction Coefficient in Smooth Tubes. *Berichte der Akademie der Wissenschaften der UdSSR*, Band LI, 5:503–506, 1946.

[28] Philip G. Kosky and Fred W. Staub. Local condensing heat transfer coefficients in the annular flow regime. *AIChE Journal*, 17(5), 1971.

[29] Xiao Wei Li, Ji An Meng, and Zhi Xin Li. Experimental study of single-phase pressure drop and heat transfer in a micro-fin tube. *Experimental Thermal and Fluid Science*, 32(2):641–648, 2007.

[30] R. C Lockhart, R. W., Martinelli. Proposed correlation of data for isothermal two-phase, two-component flow in pipes. *Chemical Engineering Progress*, 45:39–48, 1949.

[31] Jesús Moreno Quibén and John R. Thome. Flow pattern based two-phase frictional pressure drop model for horizontal tubes. Part I: Diabatic and adiabatic experimental study. *International Journal of Heat and Fluid Flow*, 28(5):1049–1059, 2007.

[32] H. Müller-Steinhagen and K. Heck. A simple friction pressure drop correlation for two-phase flow in pipes. *Chemical Engineering and Processing*, 20(6):297–308, 1986.

[33] M. B. Ould Didi, N. Kattan, and J. R. Thome. Prediction of two-phase pressure gradients of refrigerants in horizontal tubes. *International Journal of Refrigeration*, 25(7):935–947, 2002.

[34] J. W. Palen, G. Breber, and J. Taborek. Prediction of flow regimes in horizontal tube-side condensation. *Heat Transfer Engineering*, 1(2):47–57, 1979.

[35] B. S. Petukhov. Heat Transfer and Friction in Turbulent Pipe Flow with Variable Physical Properties. *Advances in Heat Transfer*, 6(C), 1970.

[36] L. Rossetto. Dispense di trasmissione del calore e termofluidodinamica. 2018.

[37] Ioan Sarbu. A review on substitution strategy of non-ecological refrigerants from vapour compression-based refrigeration, air-conditioning and heat pump systems. *International Journal of Refrigeration*, 46:123–141, 2014.

[38] R. G. Sardesai, R. G. Owen, and D. J. Pulling. Flow regimes for condensation of a vapour inside a horizontal tube. *Chemical Engineering Science*, 36(7):1173–1180, 1981.

[39] MM. M. Shah. A general correlation for heat transfer during film condensation

inside pipes. *International Journal Heat Mass Transfer*, 22(4):547–556, 1979.

[40] N. Shikazono, M. Itoh, M. Uchida, T. Fukushima, T. Hatada, and Haruko OGAWA Munekazu IINUMA, Toshiyuki TANAKA, Mizuo MIZUNO, Tomoyuki KATSUZAKI. NII-Electronic Library Service. *Chemical Pharmaceutical Bulletin*, 104(43):2091, 2002.

[41] F.A. McClintock S.J. Kline. Describing uncertainties in single samle experiments. *Mechanical Engineering*, 75:3–8, 1953.

[42] D. Steiner. Heat transfer to boiling saturated liquids. In *VDI-Wär meatlas (VDI Heat Atlas)*. 1993.

[43] Yehuda Taitel. Flow pattern transition in rough pipes. *International Journal of Multiphase Flow*, 3(6):597–601, 1977.

[44] Yehudah Taitel, Naugab Lee, and A. E. Dukler. Transient gas-liquid flow in horizontal pipes: Modeling the flow pattern transitions. *AIChE Journal*, 24(5):920–934, 1978.

[45] Yemada Taitel and A. E. Dukler. A model for predicting flow regime transitions in horizontal and near horizontal gas-liquid flow. *AIChE Journal*, 22(1):47–55, 1976.

[46] J. R. Thome, J. El Hajal, and A. Cavallini. Condensation in horizontal tubes, part 2: New heat transfer model based on flow regimes. *International Journal of Heat and Mass Transfer*, 46(18):3365–3387, 2003.

[47] Baron AB Traviss DP, Rohsenow WM. Forced convection inside tubes: A heat transfer equation for condenser design. *ASHRAE Trans.*, 79:157–165, 1972.

[48] R. L. Webb. A predictive model for condensation in small hydraulic diameter tubes having axial micro-fins. *Journal of Heat Transfer*, 119(4):776–782, 1997.

[49] J Yu and S Koyama. Condensation heat transfer of pure refrigerants in microfin tubes. *International Refrigeration and Air Conditioning Conference*, 1998.